University of Alberta

LABORATORY INVESTIGATION OF NATURAL AIR CONVECTION IN A POROUS MEDIUM IN A CYLINDRICAL TANK

by

JIANFENG CHEN

A thesis submitted to the Faculty of Graduate Studies and Research
in partial fulfillment of the requirements for the degree of

Master of Science
in
Geotechnical Engineering

Department of Civil and Environmental Engineering

Fall 2010
Edmonton, Alberta

Examining Committee

Dr. David C. Sego Department of Civil and Environmental Engineering
University of Alberta

Dr. Ward Wilson Department of Civil and Environmental Engineering
University of Alberta

Dr. N. Rajaratnam Department of Civil and Environmental Engineering
University of Alberta

Dr. Morris Flynn Department of Mechanical Engineering
University of Alberta

ABSTRACT

Natural convection with high cooling effects is of increasing interest in cold region geotechnical engineering. To study natural air convection in a highly-permeable porous medium, convective and conductive heat transfer experiments were carried out using an insulated cylindrical tank filled with styrofoam chips. Convection and conduction were caused by controlling the temperatures at the top and bottom of the tank, and a series of cross-sectional conductive and convective isotherms were generated from collected temperature data. Additional convective patterns were obtained from tests by centrally localized heating below or cooling above. Flow velocities were measured at the center of the tank. Results showed that convective heat transfer rate was higher than thermal conduction. Convective isothermal patterns varied with various boundary conditions and could be influenced by small temperature perturbation. Given appropriate environmental conditions, efficient convective cooling effects can be used to enhance ground freezing or to protect permafrost from degradation.

ACKNOWLEDGEMENTS

I would like to express my deep gratitude to my research supervisor, Dr. David C. Sego, for providing me the opportunity of this research project and his guidance, support and encouragement throughout the research and preparation of this thesis. I wish to extend my sincere thanks to Dr. Lukas Arenson for his valuable instruction, help and discussion on planning this research and carrying out the experiments.

I greatly appreciate the assistant from the two laboratory technicians, Christine Hereygers and Steve Gamble, at the Geotechnical Centre of the University of Alberta.

Special gratitude goes to Mr. Hoang-Nam Pham for all inspirational discussion we had on this unconventional geotechnical research topic. Sincere thanks also go to Mr. Chenxi Zhang for his help on my preparation for the thesis examination. Thanks extend to all student colleagues who I have worked, studied and discussed with.

Finally, I am greatly indebted to my parents, my sister and my wife Yanyan. Their constant support, faithful encouragement and unwavering trust made this thesis possible. To them and my son Aaron, who was born during the thesis writing stage, I dedicate this thesis.

TABLE OF CONTENTS

LIST OF TABLES

LIST OF FIGURES

1 INTRODUCTION AND LITERATURE REVIEW

1.1 General

Spurred by economic globalization, huge demand for natural resources has caused rapid development of mining and petroleum in cold regions. The need for facilities such as roads, railways, dams and pipelines in those areas increases interest in research on cold region engineering. Either prevention of ground freezing that leads to frost heave or protection of permafrost from thaw is a critical design consideration for these facilities. The literature shows that air convection in porous media, extensively studied through experiment and numerical simulation in mechanical and thermodynamical engineering, is gradually becoming an important consideration in geotechnical engineering because of the potential for high heat transfer rates.

In areas associated with extremely low seasonal temperatures, structures often suffered from frost heave that can cause differential heave and foundation damage. If porous materials are placed above the foundation soils, air convection can occur in winter, enhancing the heat loss from the ground surface, and increasing the chance of frost heave as the soil freezes. This must be taken into account during design, using not only conductive thermal analysis, but also convective heat transfer analysis. The purpose of the study by Goering et al. (2000) was to examine the impact of natural convection within railway embankment ballast that caused extensive frost penetration and heave of the tracks for high speed rail lines. A sufficient thickness of these embankments along with an insulation layer is required to prevent detrimental frost penetration.

It may not be well understood by the public and even civil engineering professionals that 20-25% of the land surface of the earth is underlain by permafrost. Most of this frozen ground has properties of high strength and low permeability, which are normally beneficial for engineering purposes unless the permafrost is close to 0°C. Structures constructed on permafrost need to be protected from warming temperatures and especially thawing due to surface condition modification or global warming. Goering and Kumar (1996) pointed out that previous techniques, such as insulation, air duct systems and thermosyphons have limited efficiency and high capital cost. After performing a numerical study, they concluded that natural winter air convection occurring within high-permeability embankments would have an important influence on the subsurface soil temperatures. Their convection modelling cases for a highway embankment with a height of 2.5 m show that average annual temperatures of the foundation can be reduced by up to 5°C, which is sufficient to protect most permafrost from thawing (Figure 1.1). Harris and Pedersen (1998) performed a temperature monitoring study at Plateau Mountain in Alberta and found that the mean annual ground temperatures in the blocky materials of that area are 4 to 7°C cooler than nearby mineral soils because of convective cooling effect.

Natural convection of ground water is generally not considered in engineering practice (though hot springs are an exception). Since soils are normally saturated and the hydraulic conductivities are relatively low, little to no convective ground water movement can occur. Thermal conduction is the dominant heat transfer mechanism for soils. Andersland and Ladanyi (2004) provided a series of design methods to account for heat flow in frozen ground, where thermal conduction is the focus of thermal analyses for frozen soil, water or ice combinations along with latent heat considerations. Natural air convection is not possible to occur in low-permeability mineral soils as well as surface organic with low Rayleigh numbers (a convection parameter reflecting the potential or strength of air convection). This is the conclusion drawn by Kane et al. (2001), who examined seasonal temperature data focusing on the non-conductive heat transfer in frozen soils. In recent years, however, convection from the surface has gradually developed as an interesting subject for geotechnical research following initial work by Goering and Kumar (1996). A number of studies on the cooling effect of air convection in highly permeable embankments have been presented by Goering (2003a; 2003b; 2002; 1998), Goering and Kumar (1999) from the University of Alaska, as well as by Sun et al. (2009), Cheng et al. (2008), Ma et al. (2008), Wu et al. (2008), He et al. (2007), Wu et al. (2007), Zhang et al. (2007) Ma et al. (2006), Quan et al. (2006), Yu et al. (2006), Zhang et al. (2006), Sun et al. (2005), Zhang et al. (2005) and Yu et al. (2004) for the Qinghai-Tibet Railway in China. Arenson and Sego (2007) presented a numerical simulation showing that convection of cold winter air in a coarse mine waste rock cover for a tailings pond can be used to accelerate the freezing and thus potential stabilization of the tailings. Air permeability, boundary conditions, cover height and surface temperature are the main parameters influencing the design of a stable convection layer. Design recommendations in different situations are also presented by these authors.

Therefore, both conductive and convective heat transfer mechanisms must be fully understood when working on cold region or permafrost engineering in which poorly-graded materials are being used for construction (e.g., railway ballast embankments, rock fill dams, waste rock piles and tailings covers after mine closure). In this study, an experimental investigation of convective air heat transfer in a porous medium is presented. Laboratory tests were performed using natural air convection and conduction. A variety of isotherms were obtained by measuring cross-sectional temperatures.

From a geotechnical perspective, previous studies involving similar laboratory experiments were carried out by Goering (2000) and Yu et al. (2004), whose results can be directly compared to the work presented in this thesis.

Goering et al. (2000) studied convective heat transfer in railway embankment ballast by using both numerical modelling and experimentation. The tests were carried out with either top heating or bottom heating using a gravel-filled box (1m×1m×0.75m). Comparison of measured values of heat flux confirmed that the convective heat transfer rate was considerably greater than that of conduction. Non-linear cross-sectional temperature profiles were obtained through the three-dimensional modelling for the convective heat transfer. The model also showed that pore air moved upward at the centerline and sank at the corners due to natural convection.

Yu et al. (2004) presented an experiment using two larger rectangle open-top boxes filled with coarse and fine crushed rock, respectively. Changing the surface temperature over time in a range of -14 to 16°C caused temperature variations within the box, illustrating that conductive and convective heat transfer modes alternately developed. The variations of the bottom temperatures of the boxes are shown in Figure 1.2, which indicates that the coarse rock layer enhances cooling more than the fine rock layer. The authors recommended that the cooling effect of convection in porous rock layers can be utilized to protect permafrost from thawing. The authors also pointed out that the efficiency of this technique depends on the thickness and mean particle size of the layers, and boundary conditions such as boundary air flow significantly impact the air convection process. No convective isotherm was presented in Yu et al. (2004). The present laboratory investigation, however, involved use of sufficient temperature measurements to construct isotherms.

Ma et al. (2006), Sun et al. (2005) and Goering (1998) reported field studies on air convection embankments, constructed of coarse crushed rock, which were instrumented to observe the thermal conditions beneath and within the test embankments.

This study is presented in a traditional thesis format, with chapters consisting of Introduction and Literature Review (Chapter 1), Experimental Apparatus and Procedures (Chapter 2), Results and Discussion (Chapter 3) followed by Summary and Conclusions (Chapter 4).

1.2 Objective

The purpose of the present study is to investigate natural air convection in a porous low-conductivity medium via laboratory experiments. A relatively large testing space, a well-insulated cylindrical tank, was employed to complete a series of convection and conduction experiments.

There are many uncertainties associated with convective air heat transfer in porous media, related to boundary conditions and material properties. Since it is inadequate to study only via numerical modelling, both field and laboratory experimental studies are necessary. This research project is not intended to solve specific problems regarding convective air flow in porous media. It is focussed on a more detailed understanding of the characteristics of air convection in a porous medium within a particular enclosure, including factors that influence convective isotherms and air movement, and the transition between convection and conduction. This research study was initiated to further this understanding to assist with modelling of field studies being carried out by the Cold Region Research Group at the University of Alberta. It is of practical significance to future application of convective heat transfer in cold region geotechnical engineering.

1.3 Methodology

It was proposed that convection and conduction tests be carried out within a cylindrical enclosure with impermeable boundaries. The cylinder wall had to be adiabatic and the top and bottom temperature boundary conditions of the enclosure were controllable. Thus, an insulated cylindrical plastic tank filled with stryrofoam chips as a surrogate for porous media, was selected.

Controlled heating or cooling systems were installed at the top and bottom of the tank to create different top-to-bottom temperature boundary conditions including localized heating at the bottom or cooling at the top, capable of inducing conductive and/or convective heat transfer. Internal temperatures were measured at a number of locations on perpendicular sections within the tank, and isotherms and vertical temperature profiles were obtained. At the same time, air flow velocities were measured at selected locations. Before the styrofoam were placed, tank tests when empty were conducted to examine air convection and conduction mechanisms in the air-filled tank. The results are compared with those from the tests on the tank filled with the stryofoam particles.

Two-dimensional numerical modelling for conductive heat transfer in a cylinder was carried out using GeoStudio 2004, TEMP/W (Version 6.02) to predict the conductive behaviors prior to experiments.

Preliminary convective thermal modelling was carried out by Dr. Lukas Arenson (former PDF) using Geostudio 2007, TEMP/W and AIR/W to predict the convective behaviors in the tank, providing references for the convection tests. Nam Pham (PhD student) performed further thermal modelling of conditions within the tank using FlexPDE. The results were compared with the initial experimental data and summarized by Arenson et al. (2007).

1.4 Theoretical Background

Conduction, convection and radiation are the three main modes of energy (heat) transfer. Radiation is driven by electromagnetic waves and can be independent of the medium, whereas the other two are not. Solar radiation is the primary heat supplier to the ground surface. For embankments founded on permafrost, radiation warming can cause problems such as longitudinal cracking due to differential heat absorption along the south facing embankment slopes. However, radiation is difficult to quantitatively determine and is usually not directly considered in cold region engineering. This section includes definitions, equations and related theories concerning conduction and natural convection are presented.

1.4.1 Definitions

1.4.1.1 Conduction

Thermal conduction is an energy transfer mechanism based on particle interaction. Fourier's law is the fundamental law governing this mechanism, wherein heat flux is a function of the thermal conductivity of a material and the temperature gradient. It is expressed as:

$$Q = kA\frac{dT}{dx} \tag{1.1}$$

where

Q	=	Heat flux
k	=	Thermal conductivity of the material
T	=	Temperature
A	=	The cross-sectional area of x direction
x	=	Heat flux distance

Obviously, Fourier's law has a similar expression to Darcy's law accounting for fluid flows through porous media. When the thermal conductivity of a material is constant, heat flux is directly proportional to the temperature gradient and moves from warm to cold surfaces.

1.4.1.2 Convection

Unlike conduction and radiation, convection is associated with mass transfer such that heat is transferred through the movement of fluids caused by a temperature or pressure difference. It includes natural convection, forced convection and convection with phase change such as boiling or condensation. Turns (2006) defined convection as the heat transfer process that occurs at the interface between a solid surface and a flowing fluid. Lunardini (1981), however, defined convection as an energy transport phenomenon rather than a heat transfer process. Nevertheless, Newton's cooling law is an empirical and simplified approach using a convective heat transfer coefficient to account for all types of convective heat flows between solid surfaces and the ambient fluids. For convection in porous media, the fluid moving through the pores essentially undergoes heat exchange with the solid particles having highly irregular surfaces.

Natural convection, also named as free convection, transfers heat by fluid flow induced by density differences due to temperature variations within the given material. Temperatures inversely affect fluid density. That is, a fluid with a higher temperature has a lower density, and that with a lower temperature has a higher density. When a fluid is under an unstable density gradient due to temperature variations, to reach steady state, the higher-density portion of the fluid is attracted by the earth gravity and will move downward, and the lower density portion rises due to its buoyancy. Consequently, a mass flow coupled with heat transfer occurs.

Forced convection, however, is heat transfer induced by a pressure difference that induces mass movement of a fluid. It is not discussed in detail in this thesis, although it is more crucial in many other engineering systems. For the purpose of this thesis, the term 'convection' will represent natural convection in the remainder of this thesis unless otherwise indicated.

1.4.1.3 Rayleigh Number

The Rayleigh number (Ra) is a pivotal parameter for studying natural convection in porous media. As a function of various properties of the porous fluid system, it indicates the occurrence of convection and its strength. It is essentially a ratio of buoyancy forces to the viscous forces and is defined as:

$$Ra = \frac{C\beta gKH\Delta T}{\upsilon k} \tag{1.2}$$

where

C	=	Volumetric heat capacity of a fluid
K	=	Intrinsic permeability
β	=	Thermal expansion coefficient of a fluid
ν	=	Kinematic viscosity of a fluid
ΔT	=	Temperature difference
k	=	Thermal conductivity of a porous medium

If the Rayleigh number of a fluid contained within the porous medium exceeds a critical number, natural convection will be initiated and will increase with the increasing Rayleigh number. Below the critical number, conduction dominates the heat transfer. The critical Rayleigh number (Ra_c) for internal natural convection heated from below is $4\pi^2$ or 39.5 for planar boundaries. According to Nield and Bejan (1999), the transition between heat transfer mechanisms is summarized below in terms of the magnitudes of the Rayleigh numbers:

For $Ra<4\pi^2$, pure conduction;

For $4\pi^2 < Ra<240$ to 300, various stable convection;

For $Ra>240$ to 300, a stable regime was not reached.

However, the authors concluded that the critical Rayleigh number of convection can vary between 3 and 39.5 for different boundary conditions under a linear stability analysis, especially for internal convection occurring within porous media bounded in a finite area. In a cylindrical enclosure, the critical Rayleigh number can be less than $4\pi^2$ and is usually related to the aspect ratio (radius to height, denoted as a). Nield and Bejan (1999) suggested an equation for Ra_c as the function of the aspect ratio:

$$Ra_c = 3.390\left(\frac{H}{r}\right)^2 \tag{1.3}$$

where H and r are the height and radius of the cylinder, respectively. Sutton (1970) provided another critical Rayleigh number equation for a two-dimensional vertical channel with constant top and bottom temperatures and adiabatic walls. When the fluid is initially motionless, the equation is given as:

$$Ra_c = \frac{\pi^2\left(m^2 + 4a^2\right)^2}{4m^2a^2} \tag{1.4}$$

where m is the number of convective cells and a is the aspect ratio (r/H). Further discussions concerning Rayleigh numbers for convection in porous media are be presented in Chapter 3.

Nusselt number (Nu), is defined as the ratio of total transferred heat to heat transferred via conduction alone (Burmeister, 1983). When only conduction occurs, the Nusselt number is the minimum value, 1. When Ra is greater than the critical Rayleigh number, convection begins and Nu is an approximately linear function of Ra. Once determined experimentally or analytically, the Nusselt number is often used as a dimensionless thermal conductivity to calculate heat flux within the system (Elder, 1967a), simplifying calculations of convective heat transfer.

In addition, the equation for the Rayleigh number for pure air convection (without any porous medium, known as Rayleigh-Bénard convection), is different from that for air convection in porous media. The air Rayleigh number is given as (Getling, 1998):

$$Ra = \frac{c\rho\beta g H^3 \Delta T}{\upsilon k_f} \tag{1.5}$$

Where

c	=	Heat capacity of air
β	=	Thermal expansion coefficient of air
ν	=	Kinematic viscosity of air
ΔT	=	Temperature difference
k_f	=	Thermal conductivity of air
ρ	=	Density of air
H	=	Height
g	=	Acceleration due to gravity

The critical Raleigh number is 1707 for infinite horizontal fluid layers with two rigid boundaries (Getling, 1998). It is worth noting that the critical Rayleigh number for fluids in a vertical cylindrical enclosure largely relies on the aspect ratio as a result of the impact from the cylinder wall. The number is around 7180 for the tank used in this study according to Rohsenow et al. (1998).

1.4.1.4 Permeability

According to Equation 1.2, the intrinsic permeability of a porous medium has a critical influence on the degree of natural convection. The higher the permeability, the larger Rayleigh number a convection problem will have. Goering and Kumar (1999) used numerical modelling to discuss the effect of permeability on the winter natural convection within a gravel embankment using, and found that the model embankment with higher permeability has larger cooling effect and thus greater decreases in ground temperatures below the embankment.

The intrinsic permeability changes with the characteristics of a porous medium and is independent of the viscosity and density of the pore fluid. However, the intrinsic permeability can be obtained based on the properties of the fluid in a porous medium. The equation is given as follows (Carman, 1956):

$$K = \frac{k\,\mu}{\rho\,g} \tag{1.6}$$

where k is the coefficient of permeability of a fluid, and μ and ρ are the dynamic viscosity and density of the fluid, respectively. It is difficult to measure hydraulic conductivity accurately for a highly porous medium such as the styrofoam chips used in this project. Therefore, the permeability was estimated using Kozeny-Carman equation presented by Bear (1972):

$$K = \frac{d_m^2}{180}\frac{n^3}{(1-n)^2} \tag{1. 7}$$

where d_m is the average diameter of medium grains and n is the porosity of the medium. However, this equation is limited by grain shapes as the validity of Darcy's law is uncertain when flow is not laminar. The correlation between K (cm^2) and mean grain diameter d_m (micron) was also used. It is given by (Bear, 1972):

$$K = 0.617 \times 10^{-11} d_m^2 \tag{1.8}$$

This is based on experimental data and independent of the porosity. The results from the two equations are averaged to predict values of K for calculation of the onset Rayleigh numbers of the convection tests reported in this thesis.

In the modelling phase of this study, the overall thermal conductivity of the combination of air and a porous medium needs to be taken into account by using the effective thermal conductivity (Bear, 1972). That is:

$$k_e = (1-n)k_s + nk_f \tag{1.9}$$

where k_s and k_f are the thermal conductivities of the porous medium and the fluid, respectively. Similarly, the effective heat capacity to account for the material heat capacity is expressed as:

$$c_e = (1-n)c_s + nc_f \tag{1.10}$$

where c_s and c_f are the heat capacities of the matrix and of the fluid, respectively.

1.4.2 Governing Equations and Assumptions

Nield and Bejan (1999) present an all-around theoretical review of convection in porous media. According to the authors, numerical modelling of natural convection in porous media should use mass, momentum and energy equations to solve for the Darcy velocity and pressure of the fluid, and streamlines and isotherms can be obtained. Those governing equations include:

Continuity equation:

$$\nabla \cdot \vec{v} = 0 \tag{1.11}$$

Momentum equation (Darcy's Law):

$$\frac{\mu}{\mathrm{K}} \vec{v} = -\nabla P' + \rho \vec{g} \tag{1.12}$$

Energy equation:

$$C_m \cdot \frac{\partial T}{\partial t} + C_f \vec{v} \cdot \nabla T = k \nabla^2 T \tag{1.13}$$

where

$\vec{v}$	=	Fluid velocity in the pores
K	=	Intrinsic permeability of a porous medium
k	=	Thermal conductivity of a porous medium
C_m	=	Volumetric heat capacity of a porous medium
C_f	=	Volumetric heat capacity of a fluid
μ	=	Dynamic viscosity of a fluid
P'	=	Pressure
ρ	=	Density of a fluid
t	=	Time

Solving those equations gives the flow velocity:

$$\vec{v} = -\frac{\mathrm{K}}{\mu} \left(\nabla P + \rho_0 \beta \left(T - T_0 \right) \vec{g} \right) \tag{1.14}$$

where ρ_0 is initial density of air, T_0 is the initial temperature, and β is the thermal expansion coefficient of air. The first assumption is that Darcy's law is valid to relate pore air velocity and pressure. When it is invalid, a non-Darcy term should be added to Equation 1.12. The Boussinesq approximation is employed to simplify the analysis and is used to couple the momentum and energy equation. This approximation is valid when the density of the fluid changes slightly so that:

$$\rho_f = \rho_0 \left[1 - \beta \left(T - T_0\right)\right] \tag{1.15}$$

Heat release due to viscous dissipation is negligible. Furthermore, when the fluid is air, it is assumed that the pore air is incompressible and in thermal equilibrium with the solid matrix (i.e. an instantaneous change of temperature of the medium particle to match the air temperature) (Goering et al. 2000).

1.5 Additional Literature Review

Natural convection in porous media has been an absorbing subject for a long time because of its application in many areas, such as porous insulation, energy production and storage, agricultural storage and geothermal reservoirs. Studies using experiments and numerical simulations have covered almost every aspect of the subject (boundary conditions, medium types, Rayleigh numbers, oscillation, etc.), and new papers continue to be published. Some of the previous studies, particularly those using cylindrical enclosures or cavities, are reviewed. Topics such as critical Rayleigh numbers localized heating, convective patterns and cooling effect are of interest in this study.

Bau and Torrance (1982) performed an experimental study on low Rayleigh number (R<500) thermal convection in a vertical cylinder, heated from below and filled with saturated silica sand, Ottawa sand or glass beads. Critical Rayleigh numbers and four theoretical connective modes within the cylinder were presented in the paper. Figure 1.3 shows the relationship between the critical Rayleigh number and the aspect ratio, with the ranges of preferred convective modes (numbers in parentheses). The dash line shows that the critical Rayleigh number is 27.1 for an infinite horizontal layer. The convective pattern in the cylinder was found to be non-axisymmetric (1, 1), i.e. one convective cell occurs in the tank. Asymmetric convection is also preferred by Zebib (1978), who analyzed the onset of convection for a cylinder of water-saturated porous media with impermeable boundaries and found that the critical Ra tends towards $4\pi^2$ as the aspect ratio of the cylinder increases. Stewart and Dona (1988) performed numerical modelling on natural convection in a heat-generating porous medium contained in a finite vertical cylinder. Single-cell flow occurred as Rayleigh number reached 7000. Prasad and Chui (1989) presented a numerical study on natural convection in a cylindrical porous enclosure with internal heat generation under three different boundary conditions. The results based on a range of the Rayleigh numbers and aspect ratios indicated that the convective flow is unicellular in the half-cavity with insulated top and bottom. However, multicellular patterns occurred when the top was cooled. Furthermore, Prasad and Tian (1990) completed an experimental study of thermal convection in fluid-superposed layers in a cylindrical cavity with heating from below. A highly complex asymmetric multi-cellular flow structure was observed in the upper fluid layer, which also interacted with the porous layer beneath, sharply decreasing its critical Rayleigh number to as low as unity. It was concluded that the flow intensity and the number of convective rolls are strong functions of both the fluid Rayleigh number and the thickness and particle size of the porous layer.

Most previous studies on localized heating using convection in porous media were carried out using rectangular cavities. The ratio (denoted as s) of the length of heated portion to the bottom length is often defined. Elder (1967b) performed the first numerical and experimental study on this issue for a homogeneous isotropic slab of a porous medium where all temperature boundaries were constant except for a partly heated bottom. At steady state, only one convective cell formed in the half-cavity for s=0.5 (Figure 1.4) whereas more than one cell existed for s>1.5. Horne and O'Sullivan (1974) considered the localized heating problems for a rectangular cross section with adiabatic sides. For a case in which half of the bottom surface is heated, oscillation occurred when Rayleigh numbers exceeded 500. Figure 1.5 shows the oscillation for a localized heating problem with Ra=750, s=0.5 and aspect ratio a=1. Prasad and Kulacki (1985) studied the effects of centrally-located heat source with different sizes at the bottom of a cavity and different aspect ratios. The top surface was at a constant temperature and other boundaries were adiabatic. Both flow rates and flow structures were discussed. The numerical modelling showed that a fluid flow is unicellular in the half cavity if the length of the heated segment is not larger than the height of the layer. The axial symmetry of the convection patterns was assumed. There exists an aspect ratio (width to height) as a function of Rayleigh number for the maximum heat transfer rate for a heated segment. Under the same boundary conditions, Prasad and Kulacki (1987) then performed an additional numerical study for natural convection in a horizontal porous layer with a larger aspect ratio and localized heating from below. From a sensitivity analysis, they found multi-cell convection occurs when the length of the heating portion is greater than the height of the layer.

In geotechnical engineering, natural convection studies have been performed for only about 15 years especially for embankments. A thermal diode effect (heat loss in winter more than heat absorption in summer) due to convection is most desirable to protect permafrost beneath embankments. Goering (1998) presented an experimental investigation for a 2.5 m high air convection embankment to support numerical results from Goering and Kumar (1996). Temperature monitoring data illustrated a large cooling influence on the foundation due to winter air convection within this embankment (Figure 1.6). The results correspond with those from the numerical simulation shown in Figure 1.1. Shown in the circles, the temperatures of the foundation soil remained stable during the summer. Goering (2003a) conducted experiments in an embankment to study the convective thermal response to the temperature fluctuations in winter. A series of temperature isotherms show that the temperatures in the embankment reacted rapidly to air temperature changes. Jørgensen et al. (2008) measured temperatures for a small open-air embankment in a cold room with a constant temperature of -17°C. The test embankment was built to a scale of 1/4 to 1/2 of a real embankment. Temperature profiles below the shoulder of the test embankment illustrated high convective cooling effects, which were also confirmed by numerical modelling performed by the authors. Additionally, Arenson et al. (2006) studied a convective heat flow model for the purpose of evaluating temperature variation in road embankments for design in northern regions.

Moreover, the cooling effect of convection to protect permafrost beneath the embankments was studied intensively during the construction of the Qinghai-Tibet Railway. Monitoring, experimental and numerical studies were undertaken to support the completion and to evaluate maintenance requirements for the project. Quan et al. (2006) presented a convective numerical simulation regarding the cooling effects of three traditional embankments constructed of sandy soil and open riprap or insulated riprap. The authors proposed a new riprap slope covered with a sunshade board, which considerably reduces summer warming, effectively raising and protecting the permafrost table within the embankment. Sun et al. (2005) completed an in-situ test in permafrost on the cooling effectiveness of an air convection embankment using two types of protective slopes. One slope consisted of small crushed rock with particle sizes of 5-8 cm, and the other consisted of large crushed rock with particle sizes of 40-50 cm. The results show that the large crushed rock layer with higher permeability has a better cooling effect due to enhanced air convection within the embankment. However, the maximum thaw depth beneath the layer increased more than that beneath the small crushed rock layer. This is probably due to the insufficient thickness of the rock layer (0.80 m) and the lower insulating ability for the large crushed rock during the summer. The results are analogous to those from an in-situ monitoring study reported by Ma et al. (2006), who studied the cooling in and beneath three types of embankments, i.e.an embankment with protective slopes, a crushed rock embankment and an embankment with ventilated ducts. The authors found that the permafrost table could be raised 1.3-2.4 m into the embankment constructed of crushed rock. Sun et al. (2004) evaluated thermal diffusivity and conductivity of porous ballast with a variety of grain sizes. The natural convective effect of the ballast specimens inside a temperature-controlled cylindrical tank was also examined. Apparent thermal conductivity for ballast specimens in an open-top tank is found to be much greater than that in a closed top due to the convective cooling effect. Wu et al. (2008) studied temperature monitoring data in a crushed-rock based embankment and indicated that convective cooling effect is more significant in colder permafrost with temperatures less than -1°C at the depth of zero amplitude. Cheng et al. (2007) summarized the results of previous convective cooling studies on crushed rock embankments including laboratory investigations, numerical simulation, and field experiments, and described crushed rocks as a “thermal semi-conductor”. The authors recommended use of this technology in engineering for its efficiency, ease of operation, cost effectiveness and less environmental impact.

In addition to natural convection studies, some forced convection studies were also performed to support the project of the Qinghai-Tibet Railway, such as a numerical analysis for a ventilated embankment with thermal insulation layers (Liu and Lai, 2005) and wind velocity experiments to study the ventilation properties of blocky stone embankments (He et al., 2007).

1.6 Chapter Summary

This is an experiment-based research project regarding natural air convection in a porous medium within an insulated tank. The purpose, methods, related rationale and literature review for this project have been presented in this chapter. It is noted in the literature that passive cooling technique based on the mechanism of natural convection in highly permeable materials is a promising method for geotechnical engineering. Governing equations and parameter definitions related to natural convection were presented. The literature relating to this topic from both theoretical and geotechnical engineering perspectives were reviewed and summarized. In the next chapter, laboratory apparatus and experimental procedures for convection and conduction tests will be presented.

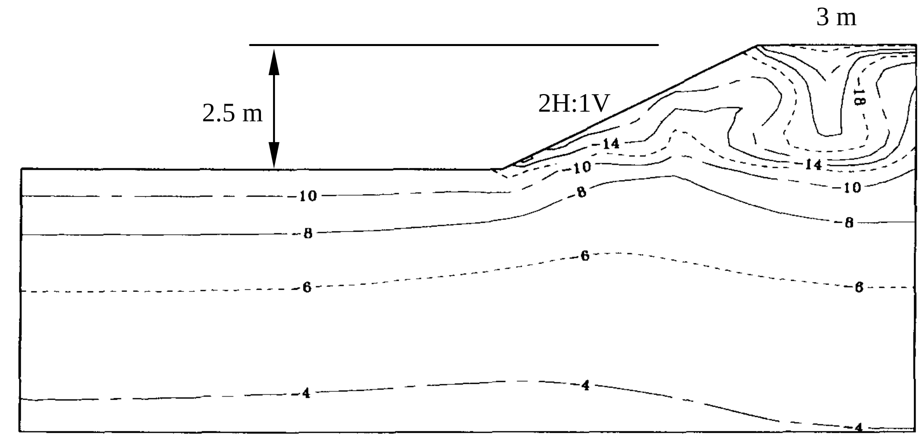

a) Convection case with enhanced frost penetration

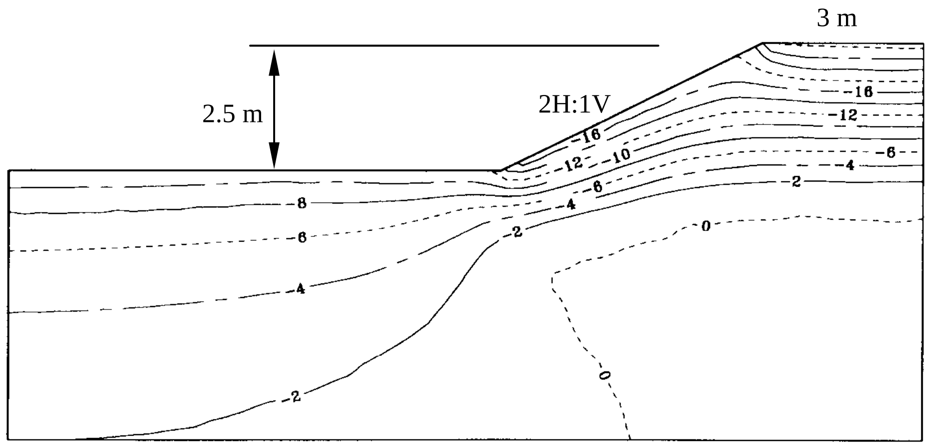

b) Conduction case with lower cooling

Figure 1.1 Numerical modelling results for convection and conduction cases (modified from Goering and Kumar, 1996)

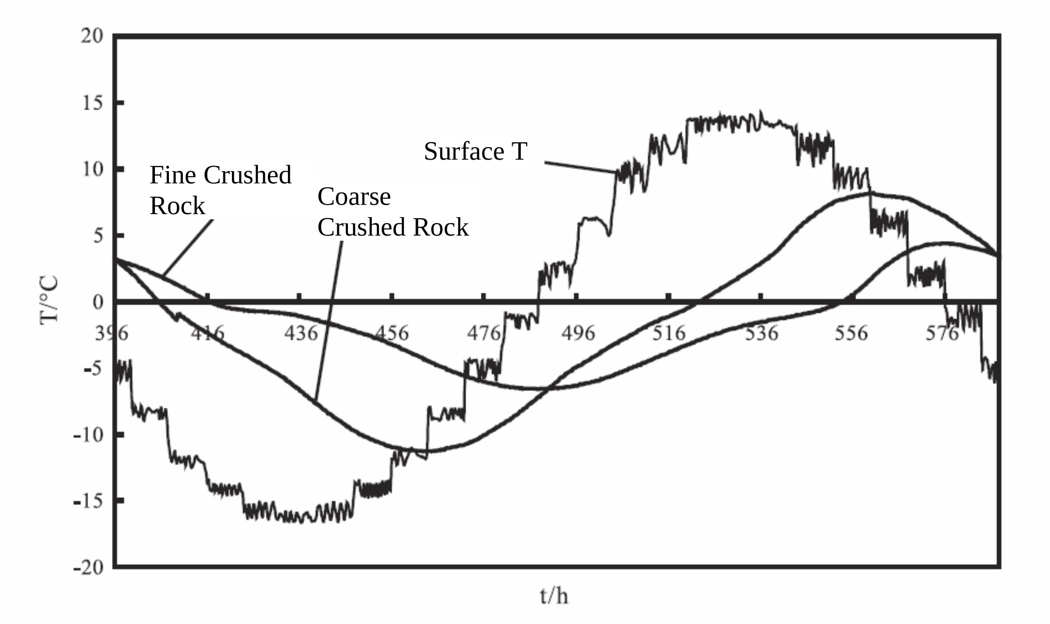

Figure 1.2 Variations of bottom temperatures in two testing boxes (modified from Yu et al., 2004)

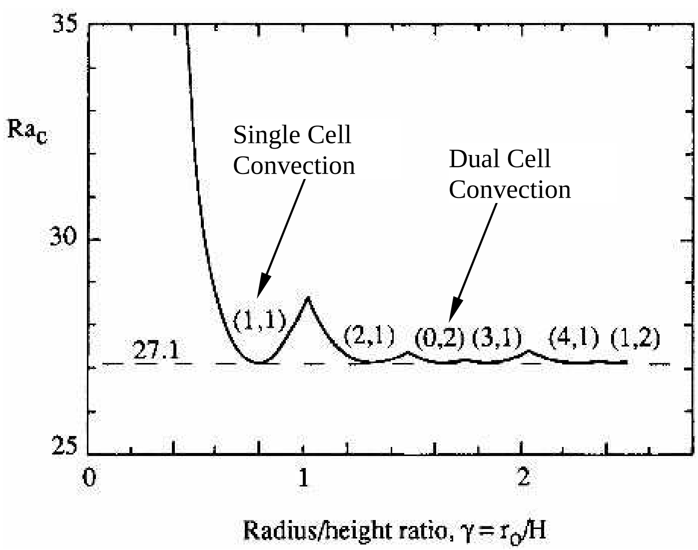

Figure 1.3 Critical Rayleigh number with respect to aspect ratio for convection in a cylinder with various convective modes (modified from Bau and Torrance, 1982)

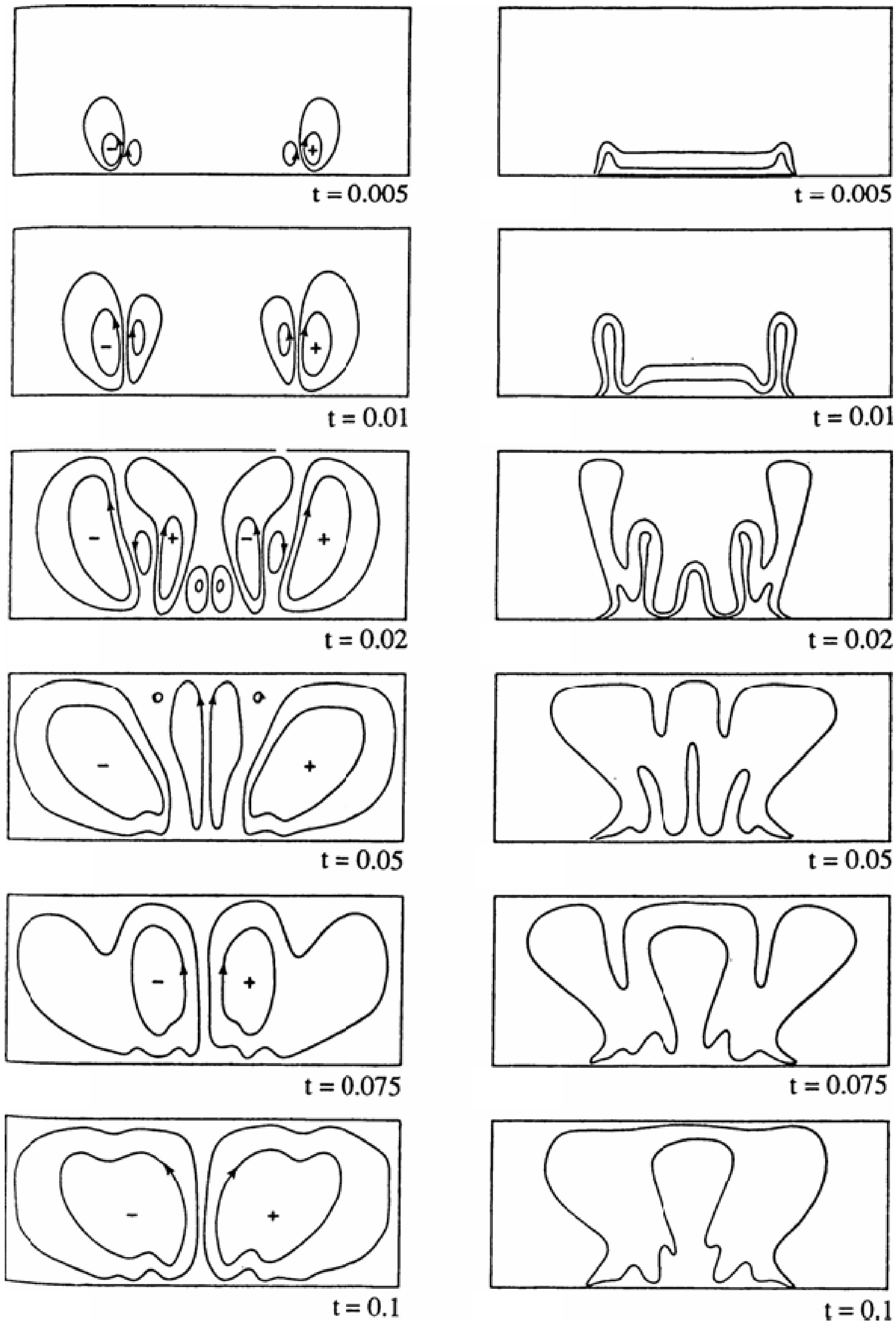

Figure 1.4 Localized heating-streamlines (left) and isotherms (right) at various time; Ra=400, a=2, s=0.5 (modified from Elder, 1967b)

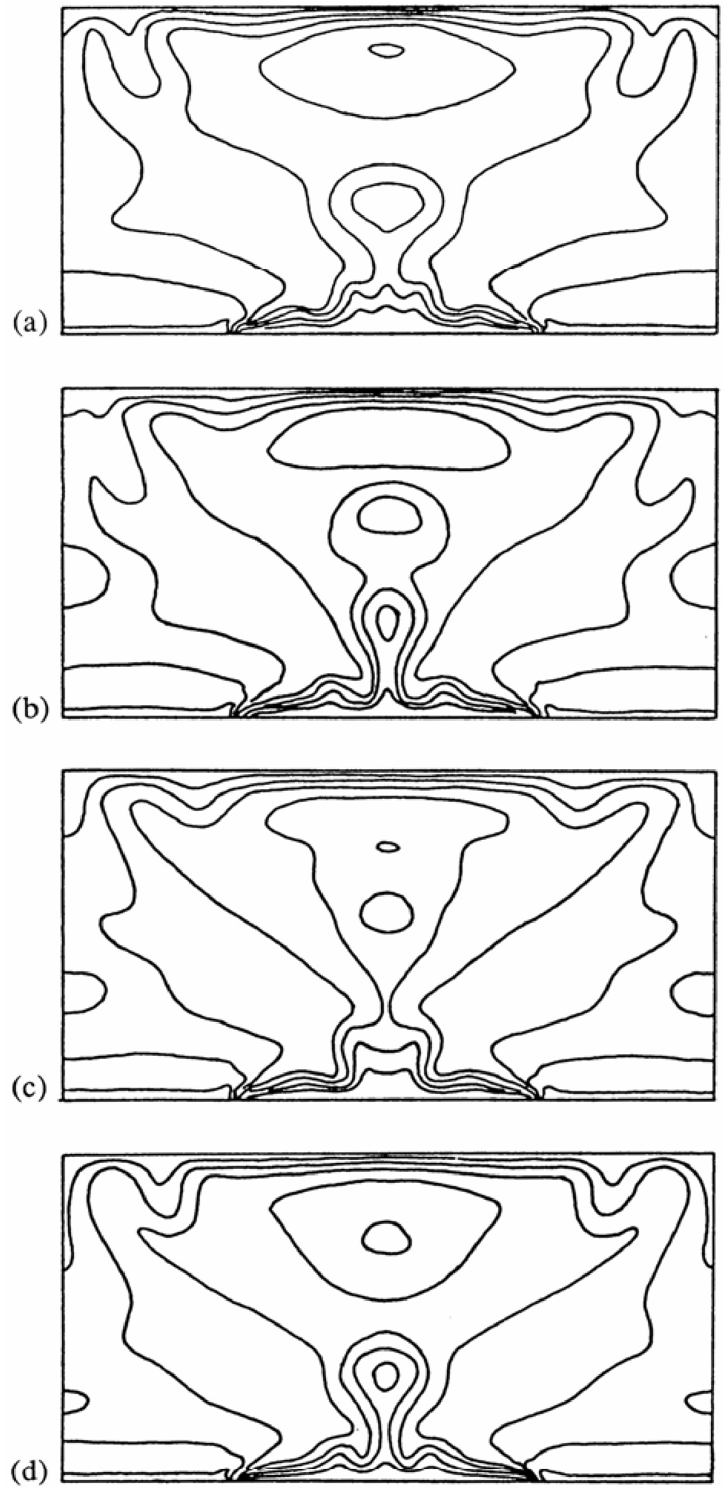

Figure 1.5 Localized heating-computed isotherms during a single oscillation; Ra=750, a = 1, s = 0.5; (a) to (d) at same time interval (modified from Horne and O'Sullivan, 1974)

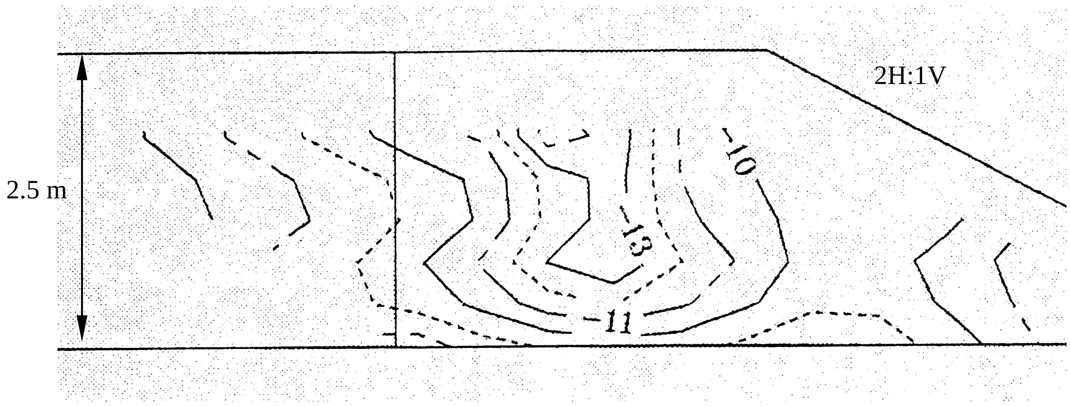

a) In February (convection)

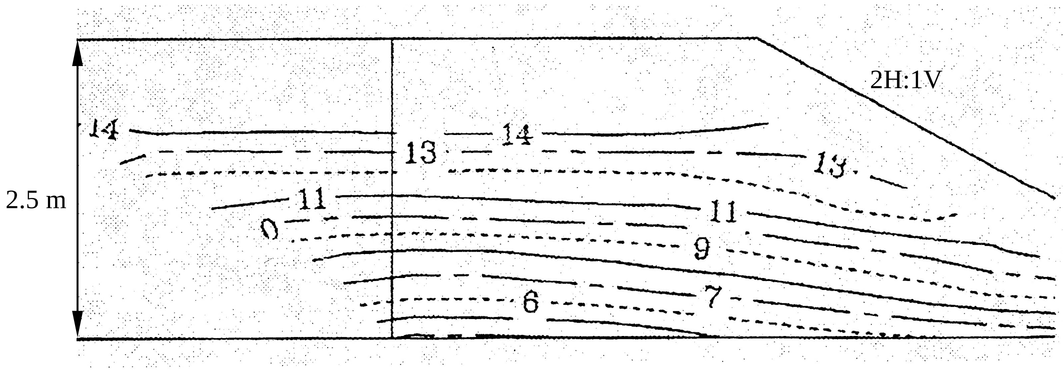

b) In August (conduction)

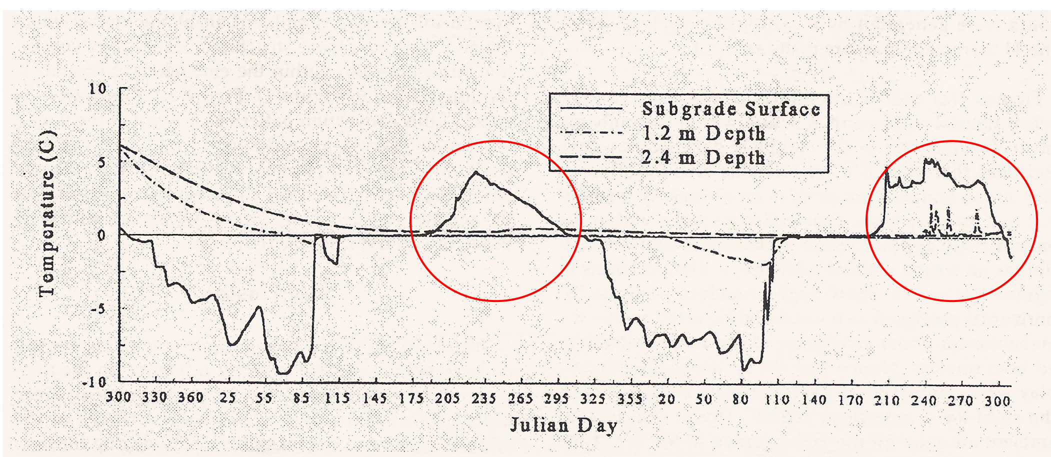

c) Variations of temperatures beneath the air convection embankment; In the circles, temperatures of the foundation soil maintain stable in the summer

Figure 1.6 Experimental results from an air convection embankment (modified from Goering, 1998)

2 EXPERIMENTAL APPARATUS AND PROCEDURES

2.1 Laboratory Apparatus

Figure 2.1 shows the cylindrical tank with an inner diameter of 120 cm and a working height of 154 cm (between the aluminum plates), which provides an aspect ratio, a=D/2H=0.39. The plastic tank wall was 1 cm thickness and was coated on the outside with spray-on polyurethane foam insulation with an average thickness of 17 cm. Four coils of 12 mm copper tubing were fixed on two wooden plates, and two sets of aluminum plates were contacted to these to transfer the heat from the copper tubing to the plates. The plates were placed at the top and bottom of the tank. Each aluminum plate consists of an inner plate (diameter 60 cm) and an outer concentric annular plate (diameter 120 cm), with different coils of the tubing attached to each plate. The tubing allowed for the localized heating or cooling during tests, i.e., different temperatures can be applied to the inner and outer plates (Figure 2.2). The two cooling/heating systems at the top and bottom were connected to constant temperature baths using plastic tubing. Water at a defined temperature flowed into the copper tubing and then back to the bath. Valves were installed between the copper tubing and the plastic tubing to control fluid flow. The tank was placed on and covered with 20 cm thick foam boards to create a space impermeable to outside air and ensure insulated boundary conditions. Figure 2.3 shows the top of the tank when filled with styrofoam chips and covered with the outside aluminum plate.

The selected porous material was Pelaspan-Pac styrofoam, S-shaped expanded polystyrene (EPS) fill, with a measured solid density of 6.5 kg/m^3 (Figure 2.4). The fill had an effective mean chip diameter of 2.6 cm based on an equivalent spherical volume. This kind of styrofoam has a characteristic of low moisture absorption, keeping the porous medium almost completely dry in the tank, (zero water saturation). The porosity of the styrofoam placed in the tank was approximately 50%.

A primary instrumentation cross section (CS1) of the tank was used to install five vertical strings of thermistors as shown in Figure 2.5 (thermistor positions for part of tests are slightly different; refer to Appendix I and II for detailed coordinates). A secondary instrumentation cross section (CS2) with 16 symmetrically distributed thermistors was perpendicular to CS1 through the centerline (Figure 2.6). The positions of the instrumentation sections are shown in Figure 2.7.

Figure 2.8 shows a photograph for the whole tank and related experimental apparatus. The baths were Fisher Scientific Isotemp 1028S and 3028D refrigerating circulators with temperature ranges of -25 to +100°C. The temperature reading displayed on the LCD has a resolution of 0.1°C.

.

The model of the thermistor sensors used during the testing program was OMEGA 44007 with resistance of 5000 ohms @25°C. The accuracy is 0.2°C over a range of 0 to 75°C. Before the thermistors were installed and connected to the data logger, each thermistor was checked and calibrated using an ice-water mixture.

The air flow meters were OMEGA FMA-904 (0-2000 sfpm) and FMA 900(0-100 sfpm) air velocity transducers, with accuracies of 3% and 1.5%, respectively. Air flow meters of the model FMA- 904 failed to record velocities due to their low sensitivity. Only one air flow meter (FMA-900) recorded data successfully. It was located approximately at the center of the tank as shown in Figure 2.1.

A Campbell Scientific AM416 Relay Multiplexer data logger system connected to a computer was used to record temperature and velocity data.

2.2 Instruments

The working rationale of the main instruments for the experiment, thermistors and air flow meters, are described in this section.

The thermistors of the type for this study were made of temperature sensitive resistors with a negative temperature coefficient, such that the resistance decreases with increasing temperature. The reading of the calibrated resistance gives a precise temperature value.

An air velocity transducer is contained on the tip of a flow meter and is composed of two RTD (Resistance Temperature Detector) elements, a velocity sensor and a temperature sensor (Figure 2.9). The RTD used as the velocity sensor is heated to maintain a constant temperature differential (30°C) above the temperature measured by the RTD used as the temperature sensor. When air flow cools the velocity sensor, an amount of compensational electricity is needed to maintain the temperature differential. This is measured and calibrated to provide readings of air velocity. It should be noted that once installed, the sensor can determine the velocity for only one direction of air flow.

2.3 Experimental Procedures

All the experiments were completed at a room temperature of 21°C. Both convection and conduction tests were carried out by setting the top and bottom temperatures of the tank by circulating fluid maintained at the required constant temperatures in the baths. Since water was used as the circulating fluid in the baths, temperatures adopted for the tests were all above 0°C, with a range of 1°C to 63°C.

In most cases, the temperatures in the tank were equalized before testing to obtain equilibrium temperature conditions. However, some of the convection tests may have been initiated from previously established steady state flow condition in order to generate a wide range of top-to-bottom temperature differences. The initial conditions for those tests will be indicated in the results presented in Chapter 3.

Temperature and velocity data were recorded at certain time intervals using the data logger program to control the data acquisition. During convection tests in the empty tank, artificial smoke was injected into the tank via an access port in the wall to observe internal air movements through a camera placed at the bottom of the tank.

Figure 2.10 shows the schematic diagrams of four major experimental scenarios of boundary conditions with respect to top and bottom temperatures. Scenario (1) in Figure 2.10 illustrates a conduction test using a vertical temperature gradient. A higher top temperature results in heat transfer from the top of the porous layer to the bottom. A typical convection test is set up as Scenario (2) with a higher temperature at the bottom. Cooling above and/or heating below for the test system can cause temperature perturbation and potentially induce convective air movements given a certain onset Ra as outlined in Chapter 2. The upper temperature control system, the wooden plate attached with the copper tubing, was rotated to a new position during a number of experiments to observe whether the inlet/outlet position affected convective patterns (especially for top-cooling conditions). The bottom temperature control system was fixed throughout all experiments. To perform localized convection tests as Scenarios (3) and (4) in Figure 2.10, the inner plate at the top was cooled, or the bottom was heated, while the other plates were maintained at a constant temperature.

2.4 Chapter Summary

In this chapter, the experimental apparatus in the laboratory and testing procedures have been described. Materials and geometries for the temperature control system in the insulated tank were introduced. Parameters for styrofoam fill were presented along with the models of the instrumentation consisting of the data logger, thermistors, air flow meters, and constant temperature baths. Four typical experimental scenarios in terms of top and bottom temperature boundary conditions were presented. In the next chapter, results from the convection and conduction experiments will be presented and discussed.

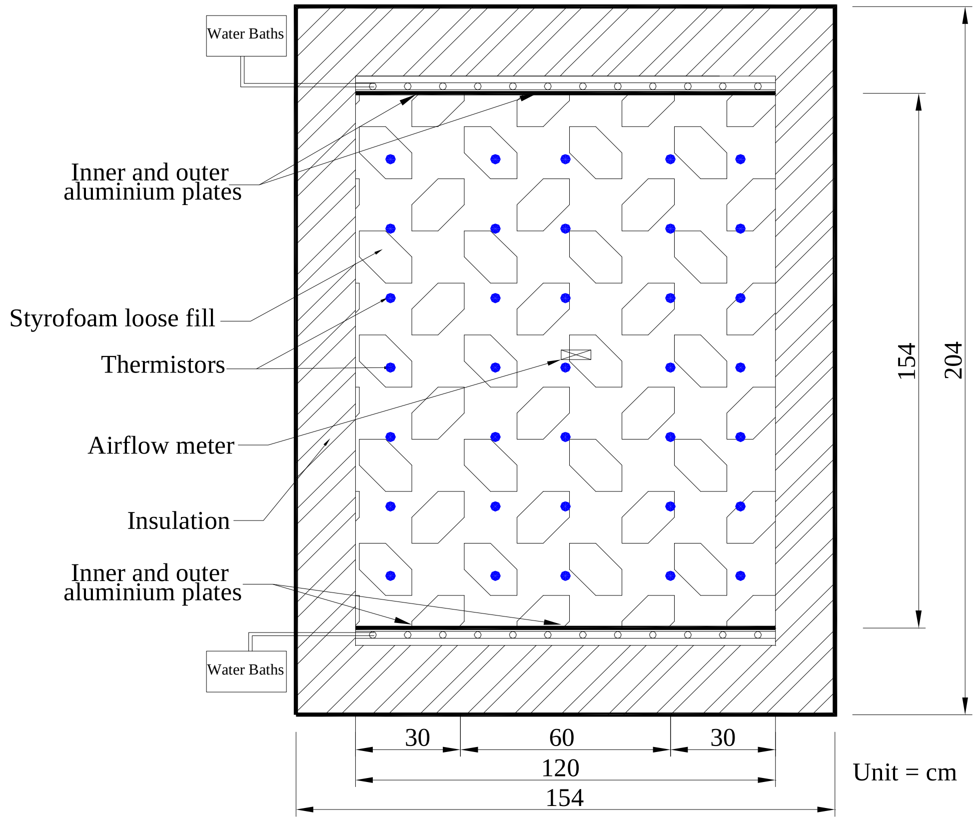

Figure 2.1 Schematic cross section of experimental system

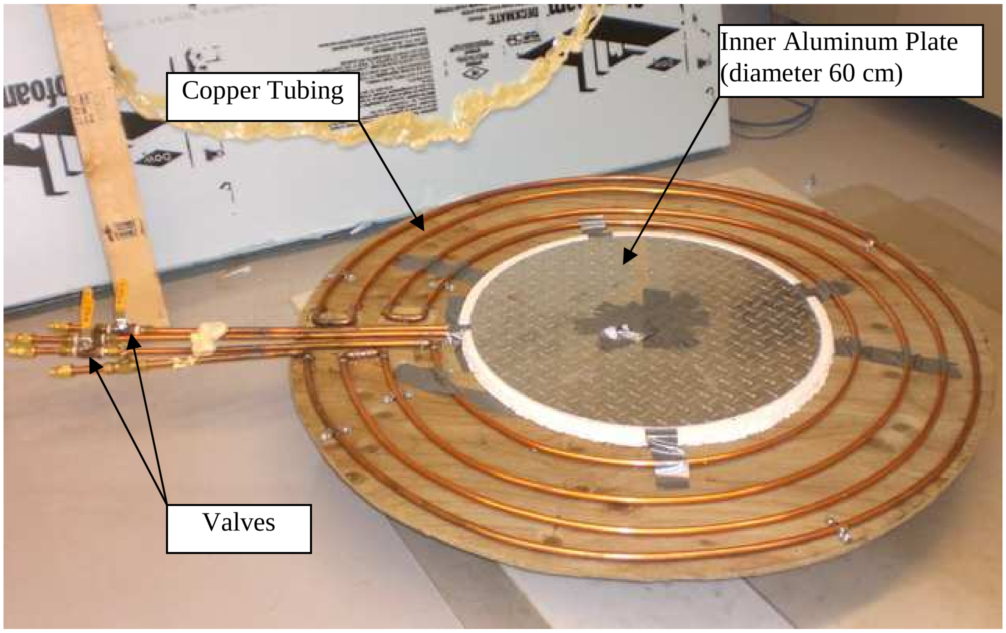

Figure 2.2 Copper tubing attached to the wood plate and covered with the inner aluminum plate. The tubing is connected to constant temperature baths with flow control valves.

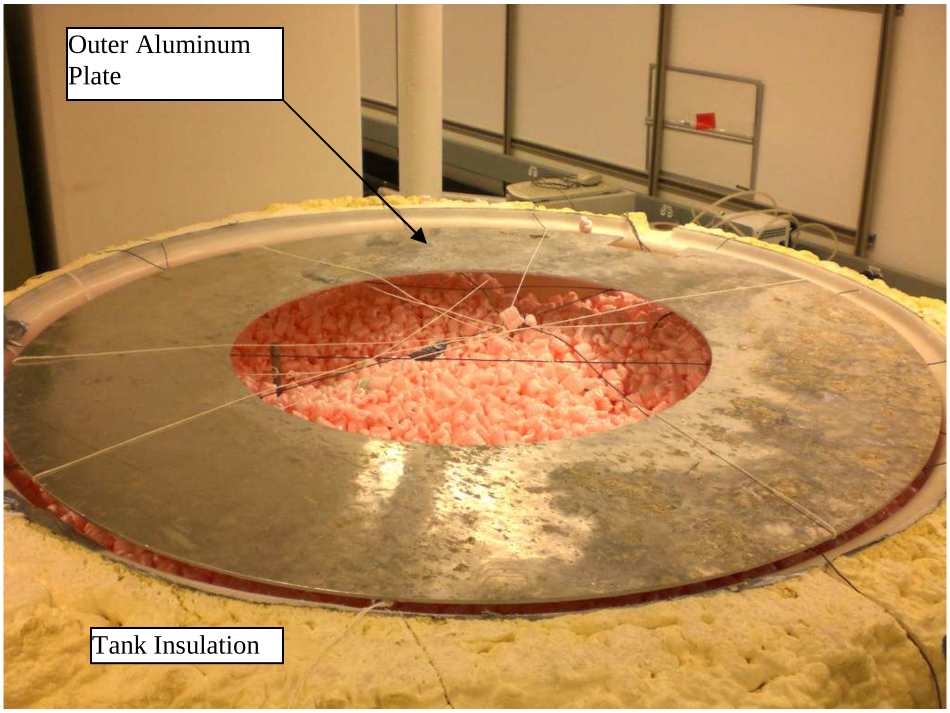

Figure 2.3 The top view of the tank filled with styrofoam chips and covered with the outer aluminum plate

Figure 2.4 S-shaped styrofoam chips with measured solids density of 6.5 kg/m^3

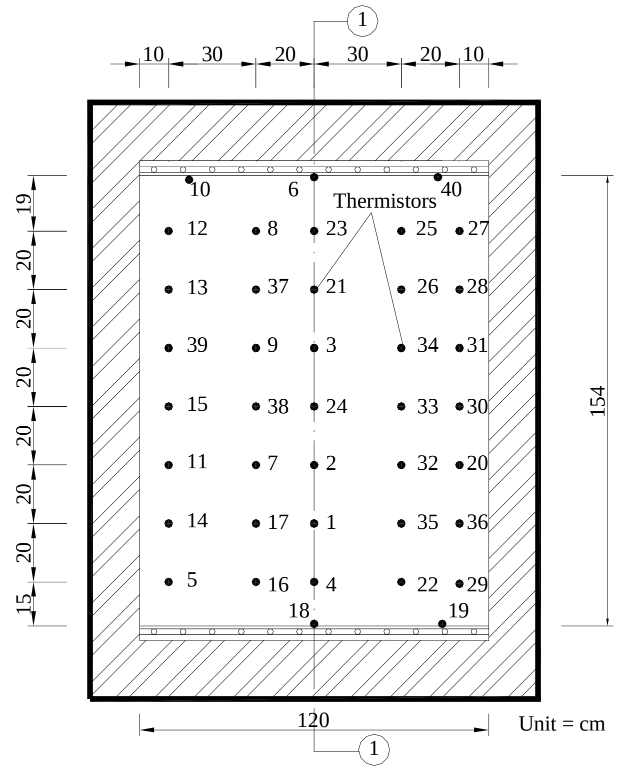

Figure 2.5 Thermistor distribution at primary instrumentation cross section (CS1): Section 1-1 shown in Figure 2.6

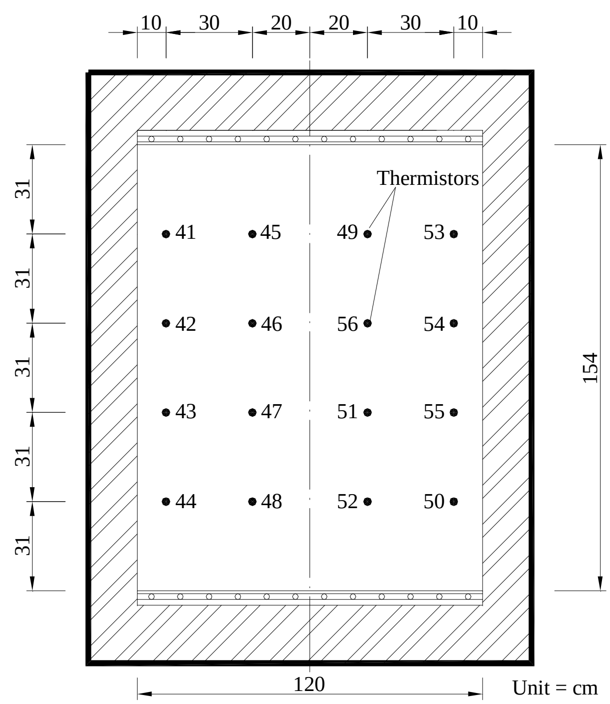

Figure 2.6 Thermistor distribution at secondary instrumentation cross section (CS2); i.e. Section 1-1 in Figure 2.5

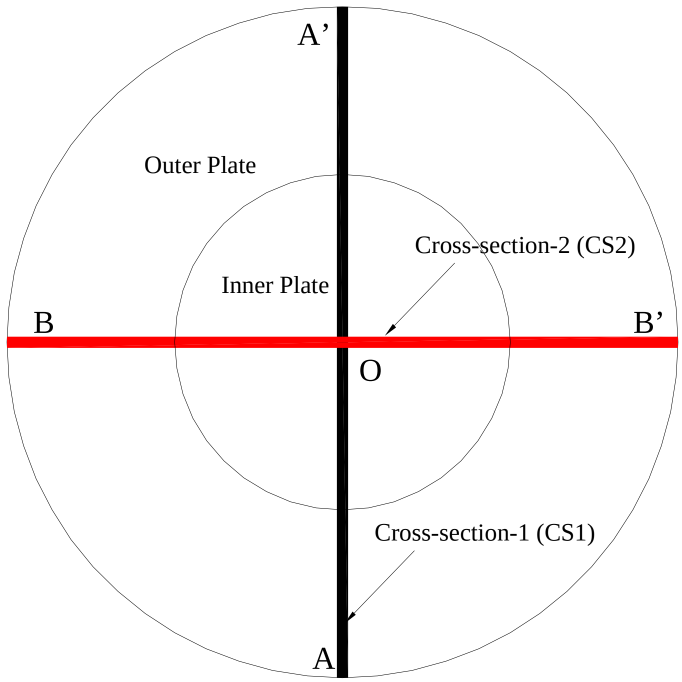

Figure 2.7 Schematic plan of the two instrumentation sections; view from top

Figure 2.8 Photograph of the insulated tank and experimental apparatus

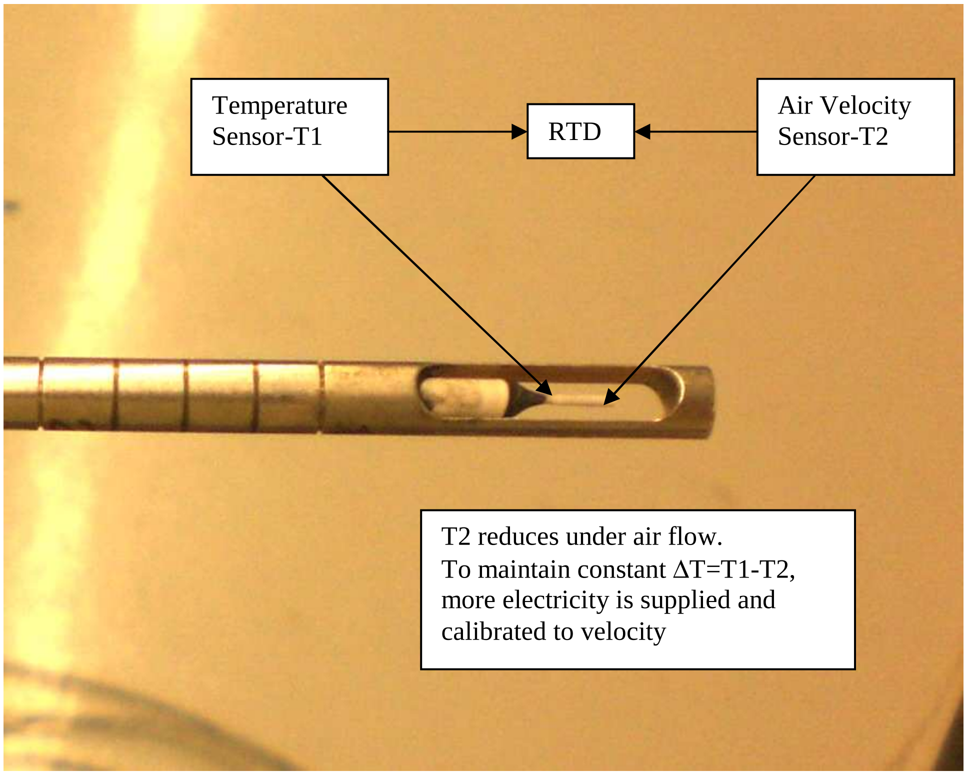

Figure 2.9 Air flow meter structure and working principle

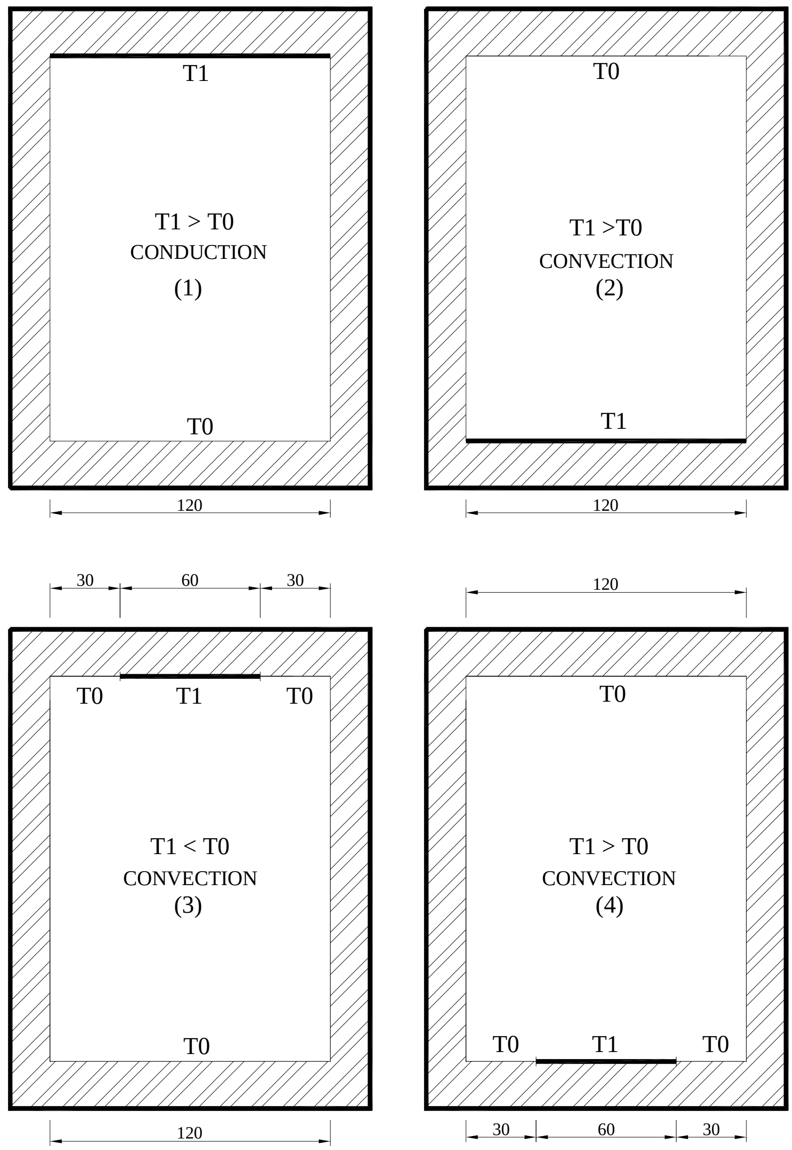

Figure 2.10 Schematic of top-to-bottom temperature boundary conditions and insulation

3 RESULTS AND DISCUSSION

Temperature and air flow velocity data were obtained from experiments of convection and conduction carried out both in empty test tank and in test tank filled with styrofoam chips. Localized heating or cooling were involved in the convection tests using styrofoam chips. Main convection and conduction tests conducted during this study are listed in the Appendix I. Measured temperature data at the two instrumentation sections CS1 and CS2 from these tests are presented in Appendix II. Temperature or normalized temperature contours presented in this chapter were constructed based on these temperature data. Once a data set consisting of coordinates and temperatures was prepared, computer software, Sigmaplot (version 10.0) was used to plot the contours based on linear interpolation between temperatures measured at the points. Temperatures profiles at the centerline of the tank may also be presented for part of the tests.

Non-dimensional temperature relationships have been used to normalize the temperature data in order to compare convection and conduction heat transfer tests with different top-to-bottom temperature boundary conditions. Near steady state, temperatures in the tank vary between the minimum and maximum applied to the top or bottom plate. Therefore, the non-dimensional temperature can be expressed as:

Convection, $$T_n = \frac{T - T_{t-\min}}{T_{b-\max} - T_{t-\min}} \tag{3.1}$$

Conduction, $$T_n = \frac{T - T_{b-\min}}{T_{t-\max} - T_{b-\min}} \tag{3.2}$$

where T_n is the non-dimensional temperature in the range of 0 to 1, T is the temperature measured at a particular location, $T_{t\text{-min}}$ and $T_{b\text{-min}}$ are the minimum temperatures measured at the top plate for convection tests and the bottom plate for conduction tests, respectively. $T_{t\text{-max}}$ and $T_{b\text{-max}}$ are the maximum temperatures measured at the top plate for conduction tests and the bottom plate for convection tests, respectively. Contours using non-dimensional temperatures were plotted using a contour interval of 0.5, and using grey intensity shading such that temperatures increase from dark to light.

As shown in Figure 2.10, only the top and bottom temperature boundary conditions are changeable while neglecting any heat flow through the insulated tank wall. Hence, some terms used in the text concerning temperature-initiating methods need to be explained. For example, heating below represents increasing the bottom temperature to a certain value while the top temperature is maintained constant. Likewise, cooling from above refers to decreasing the top temperature to a certain value while the bottom temperature is kept constant. During localized heating on the bottom or cooling on the top of the tank, only the temperature of the inner circular plate is changed while that of the outer plate is maintained constant. In addition, a temperature setting on the bath is not identical to that recorded at the plate. Reasons for this could include one or more of the following:

- the heating and cooling capacity of the baths is limited;
- heat may lose to or gain from the environment during the flow of fluids from the baths to the circulating tubing attached to the plates; and
- internal air temperatures affect the plate temperatures during tests.

Table 3.1 presents a summary of material properties used in the calculation of onset Rayleigh numbers for convection tests and the conductive thermal model for the air and styrofoam combination in the tank.

It should be noted that temperatures measured near tank wall from the sections of CS1 and CS2 were used as boundaries for the contour plots, neglecting the distances between these themistor strings and the tank wall. Temperatures measured on the top and bottom plates were averaged for contour construction except for localized heating and cooling tests where inner and outer plate temperatures were different. Averages of adjacent temperatures at a point were used to fill the data gaps existing in the section CS1 for part of the tests.

3.1 Convection and Conduction in Empty Test Tank

Results for the tests on convective and conductive heat transfer of air in the empty tank are first presented, and they will be followed by similar tests with the styrofoam chips filling the tank. Experiments in the empty test tank were briefly conducted only for comparison purposes with those tests in the styrofoam-filled tank. No detailed air flow patterns were investigated, no flow velocity measurements were made and no localized heating or cooling tests were conducted.

3.1.1 Convection in Test Tank

Five convection tests were carried out to obtain temperature contours at or close to steady state within the empty tank. Temperature differences (ΔT) of (B30-T25), 10°C (B30-T20), 20°C (B35-T15), 25°C (B35-T10), and 30°C (B40-T10) (where T and B denote the top and bottom) were used. The temperatures in the tank changed at nearly the same rate as that of the top and bottom plates, as shown in Figure 3.1 for test with ΔT=5°C. In other words, most of the air in the tank rapidly changed temperatures to achieve steady state. This is due to the fact that the Rayleigh number for each case, calculated using Equation 1.5, is much greater than the theoretical critical Ra of 1707 (Getling, 1998), or specifically 7180 for a vertical cylinder (Rohsenow et al., 1998). Therefore, the convective air movement inside the tank rapidly transfers the heat throughout the tank. An illustrative example of this scenario is a heater that rapidly increases the temperature in a room. The onset air Rayleigh numbers for the convection tests were calculated using material properties presented in Table 3.1. The results are summarized in Table 3.2, showing that the calculated magnitudes of Ra exceed 10^9, which is much greater than the critical Rayleigh number (Ra_c) of 7180.

Figure 3.2 shows the axial temperature profile of a convection test with a temperature difference of 5°C, indicating that temperatures change synchronously from about 24.5 to 26.5°C while the shapes of the temperature curves remain similar as the changes occur. Note that at steady state, the temperatures of the top and bottom plates are 25.8°C and 28.2°C, respectively, which are different from the applied boundary temperatures of 25°C and 30°C. The isotherms using non-dimensional temperatures for the primary cross section are presented in Figure 3.3 (contours for the case of ΔT=25°C are not shown due to similarity to the case of ΔT=30°C). Most of the normalized temperatures in the tank are between 0.3 and 0.4 for ΔT=5°C, while for ΔT=10°C, 20°C, 25°C and 30°C, most normalized temperatures are between 0.4 and 0.5, i.e. 40~50% of the measured top-to-bottom temperature difference (Equation 3.1). Therefore, average air temperatures in the tank are slightly less than the average of the top and bottom temperatures. It reflects that the convective air movement strengthens with increasing temperature difference or Rayleigh numbers. Figure 3.4 shows a scatter plot for a relationship between an average temperature ratio and top-to-bottom ΔT from each convection test. This average temperature ratio was defined as the average of measured internal air temperatures (thermistors in the space) to the average of measured top and bottom plate temperatures. The plot shows that the ratios are all close to unity. It reflects that most of the thermitors measurements are close to the average temperatures of the top and bottom plates, as a result of rapid convective air movement in the tank.

The four isothermal patterns are distinct from each other and temperature stratifications within the tank are irregular. Artificial smoke was injected into the tank through an access port in the tank wall to observe the air movement during the convection tests. Flow movement was observed through internal videos recorded using a camera located at the bottom of the tank. From the qualitative observation, no clear pattern of smoke movement can be identified and the flow appeared to be turbulent although no detailed measurements of turbulent spectra were made. Figure 3.5 shows a diagram of convection regimes, which is mostly based on experimental data obtained by various investigators (Getling, 1998). This figure illustrates that convective air movement is in a completely turbulent state when the Rayleigh number is higher than approximately 9000 (The Prandtl number, Pr, for a fluid is a dimensionless number defined as the ratio of viscosity to thermal diffusivity; for air, Pr = 0.713 at 20°C). Therefore, for the current tests of Ra>>9000, the convective air movement is turbulent according to Figure 3.5 (Reynolds number may be used to study the turbulent flow in detail, which is beyond the scope of this research project). Generally, air occupying a large space is sensitive to small temperature perturbation and natural convective air movement occurs readily.

3.1.2 Conduction in Test Tank

Two conduction tests with temperature differences of 15°C (Case a) and 30°C (Case b) were part of this study for the thermal conduction characteristics of air within the tank. The isotherms shown in Figure 3.6 illustrate near horizontal temperature stratifications, differing from the convective patterns shown in Figure 3.3. Overall non-dimensional temperatures in the tank were higher in Case b than in Case a, demonstrating that Case b had higher temperature gradients that lead to more efficient conductive heat transfer. As illustrated in Figure 3.7, Case b with ΔT=30°C had a temperature gradient of 2.9°C/m, nearly twice the temperature gradient for Case a with ΔT=15°C. The temperature profiles at the center of the tank with respect to time are shown in Figure 3.8. Compared to the air convection test data for lower ΔT shown in Figure 3.2, the air conduction test took longer to achieve steady state. It demonstrates that under the same conditions, air convection is a more effective heat transfer mechanism than thermal conduction within the test apparatus.

3.2 Convection Using Styrofoam Chips in Test Tank

Convective tests for pore air within styrofoam chips were carried out in the insulated cylindrical tank with various top-to-bottom temperature boundary conditions.

3.2.1 Permeability and Onset Rayleigh Number

Since natural convection starts when a Rayleigh number is larger than the critical Rayleigh number, it is necessary to calculate the Rayleigh numbers before performing the convection tests with a porous material to ensure convection air movement will occur. According to Equation 1.3, the Rayleigh number is directly related to the intrinsic permeability, the top-to-bottom temperature difference, and the tank height, regardless of the inherent properties of air and styrofoam. Equations 1.7 and 1.8 were used to estimate the values of the intrinsic permeability of the styrofoam chips deposited in the tank (Table 3.3).

Since the height of the tank is constant, the average permeability used to estimate the Rayleigh number can be presented as a function of the top-to-bottom temperature difference (Figure 3.9). For the adopted cylindrical tank, it is necessary to determine an accurate value of the critical Rayleigh number (Ra_c) using Equations 1.3 and 1.4. The result is Ra_c = 22.3 from Equation 1.3 or 41.9 from Equation 1.4, with m assumed to be 1. The high magnitudes of Rayleigh numbers presented in Figure 3.9 imply that convective air movement can easily begin in the tank, provided the critical Rayleigh number is either 22.3 or 41.9. Parameters used to calculate the Rayleigh numbers are presented in Table 3.1.

3.2.2 Transient Convective Patterns

Transient convective patterns were reconstructed using the temperature data recorded from the primary instrumentation section CS1. The convection test using a ΔT=5°C by heating from below achieved axisymmetric isotherms, with the temperature patterns changing with time as shown in Figure 3.10. The air rose from the middle of the tank and sank along the outer sides. An onset Rayleigh number of 626 calculated for this test was probably high since no unstable convective air movement was observed.

For convection induced with a ΔT=10°C, patterns in the initial 10 hours show a similar trend to those induced with ΔT=5°C. However, the centerline of the contours eventually shifted to the right side of the section (Figure 3.11). This could be due to one or all of the following factors: 1) the convection was just in the transitional stage from stable to unstable convection; 2) three-dimensional irregular shape factors associated with the plates and tank wall caused the axis of the plume of air to shift; and 3) horizontal convection may occur as a result of horizontal temperature differences at the bottom of the tank (according to Mullarney et al., 2004, horizontal convection is due to a horizontal difference in temperature or heat flux at a single horizontal boundary of a fluid, and can lead to highly asymmetric convection). Steeper contours indicate that the temperatures change rapidly under a higher Rayleigh number. In other words, in steady state, air moves up faster in the middle, touches the top boundary and then sinks to the bottom along the outer sides. The air movement induces continuous heat exchange between the warmer base and the cooler top. These axial temperature variations for the initial 20 hours concur with the axisymmetric modelling results reported by Arenson et al. (2007).

Although the numerical modelling results showed absolute symmetric patterns for both heating below and cooling above, the convection test under a temperature difference of 10°C with cooling from above had a different temperature pattern: the cold air sank from the side instead of the middle of the tank (Figure 3.12). A unicellular convective pattern developed in the whole tank. It may be due to the conditions at the top seal were different than at the bottom. Air is sensitive to small temperature perturbation such that the convective pattern varied with minor temperature changes. Also, horizontal convection due to temperature differences at the top of the tank may be another factor that caused the asymmetric patterns of convection (Mullarney et al. 2004).

Corresponding axial temperature profiles for scenarios of heating below and cooling above are also different. The patterns for convection by heating below illustrate that the temperatures increased as the bottom temperature rose. The temperatures initially changed quickly and then slowed until steady state was reached or established. All the temperatures vary monotonically with the height of the tank (Figure 3.13). However, the curves for the case by cooling above have different shapes such that the vertical variations have non-monotonic characteristics. It demonstrates that the bottom temperatures gradually decreased and were lower than the upper part where steady state was established (Figure 3.14). This was due to the unicellular convective pattern in which colder air is sinking along the right side of the tank.

3.2.3 Steady State Convective Isotherms

Steady state contours are shown in Figures 3.15 and 3.16 for tests using temperature differences ΔT=5°C, 10°C, 20°C, 30°C and 40°C. Associated vertical temperature profiles are also shown in Figures 3.17 and 3.18.

Heating below normally leads to a dual-cell being formed during convection in the tank, i.e. air rising along an axis and sinking along the outer tank wall. For convection with higher Rayleigh numbers, the contours are steeper and the axis deflects from the centerline of the tank. The rising air flow plumes near the center of the tank also have higher values of non-dimensional temperatures (Figure 3.15).

Under current experimental conditions, it was observed that all tests by cooling from above lead to steady state unicellular convective flow patterns. Comparing the contours at the left of the sections, the non-dimensional temperatures of the sinking air flow plumes are lower for the tests with higher Rayleigh numbers (Figure 3.16). Note that the contours at the lower right corner become denser from ΔT=10°C to 40°C, illustrating that the cool air moved more effectively to the right wall and then rose (Figure 3.16). These observations demonstrate that convection with high Rayleigh numbers has higher convective heat transfer rates.

The contour plots using data from the other sections can be used to confirm the air flow patterns. The similarity of the patterns at CS1 and CS2 in Figure 3.19 confirms the occurrence of a dual-cell convective pattern. Figure 3.20 shows that the unicellular convection can be confirmed by the contours from CS2.

To investigate the convective cell orientation for a unicellular convective pattern, the top copper tubing coil was rotated approximately 45 degrees, as shown in Figure 3.21. The isotherms shown in Figures 3.22 and 3.23 illustrate that the convective air flow cell direction moved to a new position between the two cross sections, likely following the position change of the tubing inlet/outlet. This, in turn, shows that the temperature at the top initiated by the water entering the tubing may influence the direction induced in the unicellular convective cell within the tank. A convective air flow mode tends to form based on small disturbances of system inputs under the existing boundary conditions.

3.2.4 Fluctuation and Oscillation

When a convection test of $\Delta T=50°C$ (B53-T3; Ra=6200) was carried out, temperature fluctuations and oscillations occurred. This test was started by decreasing the top temperature to 3°C from the previously established steady state under $\Delta T=30°C$ (B53-T23). As shown in Figure 3.24, temperatures at particular locations fluctuated extensively. Oscillations were contained during the fluctuations and some points near the bottom underwent large amplitude variations. The plots illustrate that those oscillations were time dependent with varying amplitudes, and nearly disappeared by the end of the test.

Part of the temperature variation curves (approximately 80 minutes) is presented in Figure 3.25 to show the typical period and amplitude of the oscillation. The amplitude varies, and the largest variation is about 6 °C for the thermistor T4, which is located at the center of the bottom (see Figure 2.5). The curve of T4 shows that the time taken for the variation from point 1 to 3 is longer than that from point 3 to 4, indicating slower temperature decreases from peak to trough than increases from trough to peak in a single oscillation period (Figure 3.25). Corresponding contours at CS1 for points 1 to 4 in the oscillation period are presented in Figure 3.26, illustrating unicellular convective patterns and similarity between the temperature variation with time patterns of points 1 and 4.

It was explained by Horne and O'Sullivan (1978) that this type of oscillation is attributable to the high air flow acceleration caused by the rapid temperature changes. Kladias and Prasad (1990) performed a numerical study to examine convective fluctuation and concluded that the higher the Rayleigh number, the shorter the oscillation period.

As expected, strong fluctuation occurred during the convection test of $\Delta T=60°C$ (Figure 3.27), particularly for those points near the right side of the bottom plate. However, only minor oscillatory instability was observed from the curve of thermistor T22 (see Figure 2.5) located near the lower right corner of the measurement section CS1. The oscillations still have a time-dependent characteristic for this convection with a Rayleigh number of around 7500. More oscillations may occur in the future, given a longer testing period.

3.2.5 Localized Heating or Cooling

Localized heating induced convection tests were carried out under ΔT=10°C (LB32-T22), 20°C (LB42-T22) and 30°C (LB52-T22) (where L denotes localized heating). Contours for these tests are presented in Figures 3.28, 3.29 and 3.30. Heat plumes rose in the center of the tank with steep and more concentrated contours. Higher ΔT convection showed more compressed central isotherms, indicating higher air flow rates leading to higher heat transfer rate along the tank axis. Localized heating apparently stabilizes the symmetry of the convective air flow in the tank as warm air is well confined to the center of the tank.

Localized cooling convection isotherms for ΔT=10°C (B20.5-LT10.5), 15°C (B20.5-LT5.5) and 20°C (B21-LT1.0) are presented in Figures 3.31, 3.32 and 3.33, respectively. Dual-cell convection was observed with poor symmetry such that the thermal plume axis was situated in the A'B'O zone shown in Figure 2.7. Comparison of the various isotherms shows that the cooled air sank along the plume axis, thus reducing temperatures in lower areas under higher ΔT conditions.

Since the heating or cooling source at the boundary was smaller, heat transfer for convection with localized heating or cooling conditions were less efficient than that with a fully heated or cooled boundary. Through comparison with the magnitudes of the non-dimensional temperatures shown in Figures 3.15 and 3.16, it is demonstrated that the temperatures in the tank are generally lower for localized heating tests (Figures 3.28 to 3.30) and higher for localized cooling tests (Figures 3.31 to 3.33).

Transient convective patterns from the instrumentation section CS1 for localized heating under ΔT=10°C (LB32-22T) and localized cooling under ΔT=10°C (B20.5-LT10.5) are presented in Figures 3.34 and 3.35, respectively. It was observed that the convective patterns were established in the first several hours and the overall temperatures in the tank continued to vary until steady state was reached. The patterns are more stable than those shown Figures 3.11 and 3.12. The symmetry of the patterns from localized heating test is also better than that shown in Figure 3.11.

Temperature variations in the tank are stable for convection test with localized heating under ΔT=60°C (LB63-T3). No fluctuation and oscillation were observed as shown in Figure 3.36. This further demonstrates that localized heating can stabilize the convective air movement, compared to the temperature variations shown in Figures 3.24 and 3.27 for the tests under high temperature differences with fully heated lower tank boundary.

3.2.6 Air Velocity

According to the governing equations, air flow velocities are related to air temperatures in the tank and vary throughout the tank. However, as mentioned previously, only one air flow meter (FMA-900) at the center of the tank recorded valid velocity data in the vertical direction during the test program (Figure 2.1).

The velocity variations with time for tests with a top-to-bottom temperature difference of 10°C are shown in Figure 3.37, illustrating different velocity values and irregular fluctuations prior to establishment of stable air flow at the measurement location. As demonstrated in the figure, vertical air movement at the center of the tank for the localized heating test is the fastest. It is due to the concentration of rising warm air under centrally localized heating.

It is understood that those air flow velocities are directly related to the convective patterns. Since axial air flow for unicellular convection is unstable as observed from the contours from the tests by cooling from above, measuring vertically at the center of the tank is more suitable for axisymmetric flow with stable patterns than it is for unicellular convective flow. Therefore, convection tests with localized heating below have more stable air flow (temperature) pattern, and velocities recorded from those tests were used to illustrate that higher Rayleigh numbers result in higher flow velocity. It was observed from these tests with heating below that flow velocity normally peaks then decreases to a relatively stable value. These velocity data from tests of localized heating are summarized in Figure 3.38, showing that peak and stable values increase with increasing ΔT under localized heating conditions. In this study, a maximum velocity of 0.068 m/s was observed for convective air movement in the porous styrofoam chips. This flow velocity is a true velocity through a pore, and is distinct from the Darcy velocity used in the governing equations shown in Chapter 1 (using this maximum velocity and assuming a pore diameter of 0.005 m, a Reynolds number can be estimated to be 22.5).

3.3 Conduction Using Styrofoam Chips in Test Tank

Simplified thermal modelling under transient conditions was carried out using TEMP/W (GEO-SLOPE, 2004) to predict the conductive heat transfer behaviour of air and styrofoam chips inside the tank. The tank wall insulation was assumed to be adiabatic in the model. The isotherm results after a model run of 42 hours are presented in Figure 3.39, and the axial temperature profile with time is presented in Figure 3.40. Material properties used in the model are shown in Table 3.1.

After equalized to uniform temperatures inside the tank, conduction tests of the styrofoam chip filled tank were started by increasing the top temperature. Temperatures gradually increased vertically throughout the tank. Clear temperature stratifications were formed as shown in Figure 3.41.

Figure 3.42 shows the vertical temperature profile varying with time. It shows a slow change compared with the thermal conduction tests for air in the empty tank (Figure 3.7). Furthermore, the profile slowly approaches the theoretical steady state, that is a linear distribution through the styrofoam chips. It is understood that the thermal conductivity of styrofoam is similar to the tank wall insulation. Conductive heat transfer through the wall thus impacts the internal heat flow system during these tests. This is likely attributable to an insufficient heat supply from the constant temperature baths. If the bottom is cooled at the same time, the steady state contours will be closer to a theoretical condition (Figure 3.43). As compared with convection tests, the ability to approach steady state is lower during thermal conduction. This illustrates that high heat transfer rates can be easily obtained from convection in a low thermal conductivity medium through convective air movement. It is due to the fact that the lower thermal conductivity of the porous medium leads to the higher Rayleigh number.

3.4 Discussion

In this project, the vertical tank wall is insulated and considered to be adiabatic for convection within the enclosure. It should be noted that convective patterns will differ for other geometries or in open layered systems. However, heat transfer rates are normally higher than those for thermal conduction using the same materials.

The low-conductivity styrofoam chips increased the Rayleigh number and therefore maximized the ability of convective air movement. The conductive heat exchange through tank wall in this project is therefore negligible compared to relatively strong convective heat transfer in the tank. However, if porous media and vertical boundaries with higher thermal conductivity are used, the conductive heat exchange through the boundaries may need to be taken into consideration especially when attempting to model these scenarios. Also, if permeable rockfill is used, which has much higher thermal conductivity than styrofoam, higher temperature differences will be required to initiate convection and achieve the same convective strength.

Insulation limitations and conditions of the upper seal can cause unexpected temperature perturbation leading to unstable convective air movement that affect the test results. Since convective air movement is sensitive to small air temperature perturbation, for given test conditions, the limitations can impact the convective pattern symmetry, the convective cell number established, fluctuations and oscillations as well as the time to reach steady state heat flow conditions.

A three-dimensional effect of the top and bottom plates and the tank shape is an additional factor that may also influence the convective patterns, such that the flow directions may change when air flow contacts any uneven surface on the constant temperature plate and tank wall.

Arenson et al. (2007) presented results of two-dimensional numerical modelling of convection with $\Delta T = 5$ and 10ºC (heating from below) for this testing system and compared them with the experimental data from this study. They illustrated that small discrepancy between numerical and experimental data was shown for the convection case of $\Delta T = 5$ºC, and better agreements were obtained for convection case of $\Delta T = 10$ºC in the first 20 hours, which was modelled axisymmetrically. The authors further acknowledged that a two-dimensional model may underestimate the air flow and temperature in the tank, and recommended axisymmetrically two-dimensional or even entirely three-dimensional modelling to obtain better reproduction for this particular testing system. However, special modelling procedures and setup should be required to simulate the asymmetric characteristics of convective patterns observed in this laboratory investigation.

The capacity of the constant temperature baths is limited for warming or cooling of the plates during the tests, particularly for those with larger top-to-bottom temperature differences. Circulating water through the tubing entails heat loss or gain, further impacting temperatures. Consequently, in this experiment, the plate temperatures were not able to maintain the same temperatures as the baths. The top plate temperature is more affected due to less insulation at the top of the tank compared to the bottom plate.

Table 3.1 Properties Used in Rayleigh Number Calculation and Thermal Modelling

Material		Value	Unit	Source
Fluid (Air)				
c_f	Specific heat capacity	1.005	kJ/(kg · °C)	Henderson et al. (1997); Air at 20ºC
β	Expansion coefficient	3.42×10^{-3}	1/°C	
υ	Kinematic viscosity of air	1.511×10^{-5}	m^2/s	
ρ_f	Air density	1.205	kg/m^3	
k_f	Thermal conductivity	0.0257	W/(m · °C)	
Porous medium (Styrofoam)				
K	Intrinsic permeability	1.15×10^{-6}	m^2	Estimated for the project (see Table 3.3)
k_m	Thermal conductivity	0.035	W/(m · °C)	Andersland and Ladanyi (2004)
c_m	Specific heat capacity	1.25	kJ/(kg · °C)	Andersland and Ladanyi (2004)
ρ_s	Density (particle)	6.5	kg/m^3	Measured for the project
n	Porosity	50%		Measured for the project
Others				
H	Height	1.54	m	
ΔT	Temperature difference	varied	°C	
g	Acceleration due to gravity	9.81	N/kg	

Table 3.2 Summary of Calculated Onset Air Rayleigh Numbers

Temperature Difference, ΔT (°C)	Onset Rayleigh Number, Ra	Critical Rayleigh Number (Vertical Cylinder) Ra_c
5	1.91×10^{9}	7,180
10	3.54×10^{9}	
20	7.07×10^{9}	
25	8.84×10^{9}	
30	9.47×10^{9}	

Table 3.3 Estimate of Intrinsic Permeability for Styrofoam Chips

	Unit	The Kozeny-Carman (Equation 1.7)	The Correlation (Equation 1.8)	Average
Intrinsic permeability	m^2	1.88×10^{-6}	4.17×10^{-7}	1.15×10^{-6}
Equivalent Air Permeability (20°C)	m/s	1.2	0.3	0.7

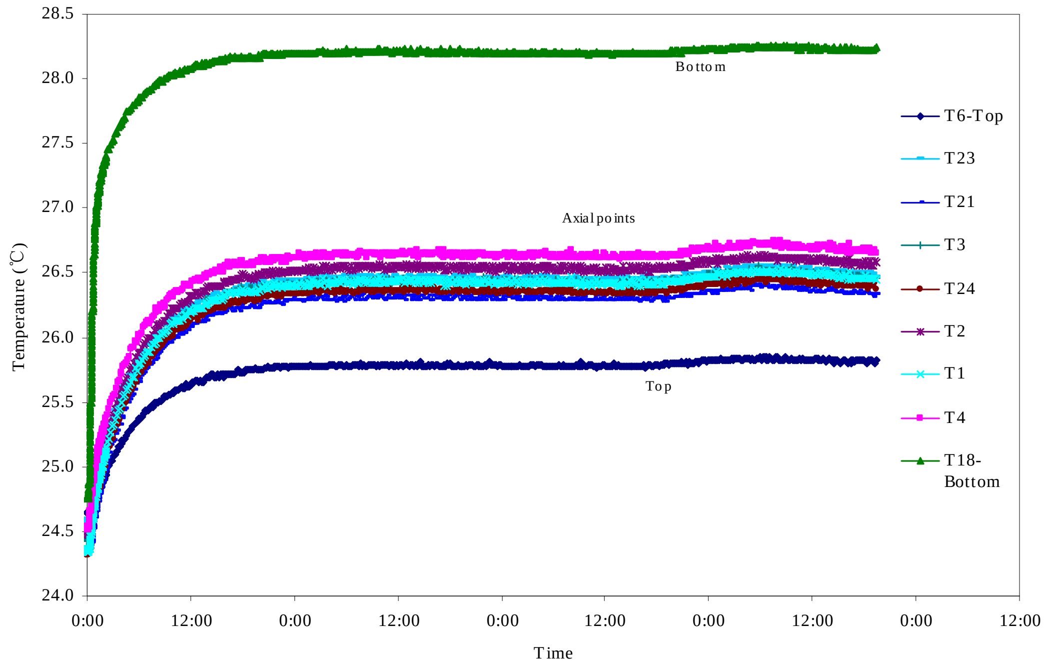

Figure 3.1 Axial temperature variation curves; convection in empty test tank - **ΔT=5°C** (B30-T25)

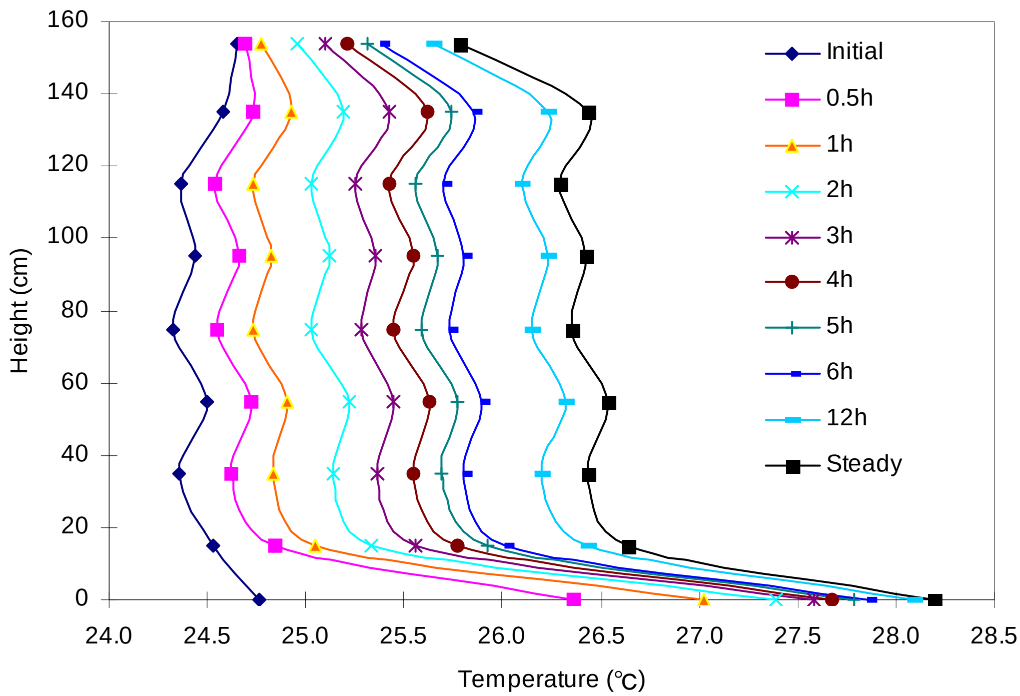

Figure 3.2 Axial temperature profile versus time; convection in empty test tank - **ΔT=5°C** (B30-T25)

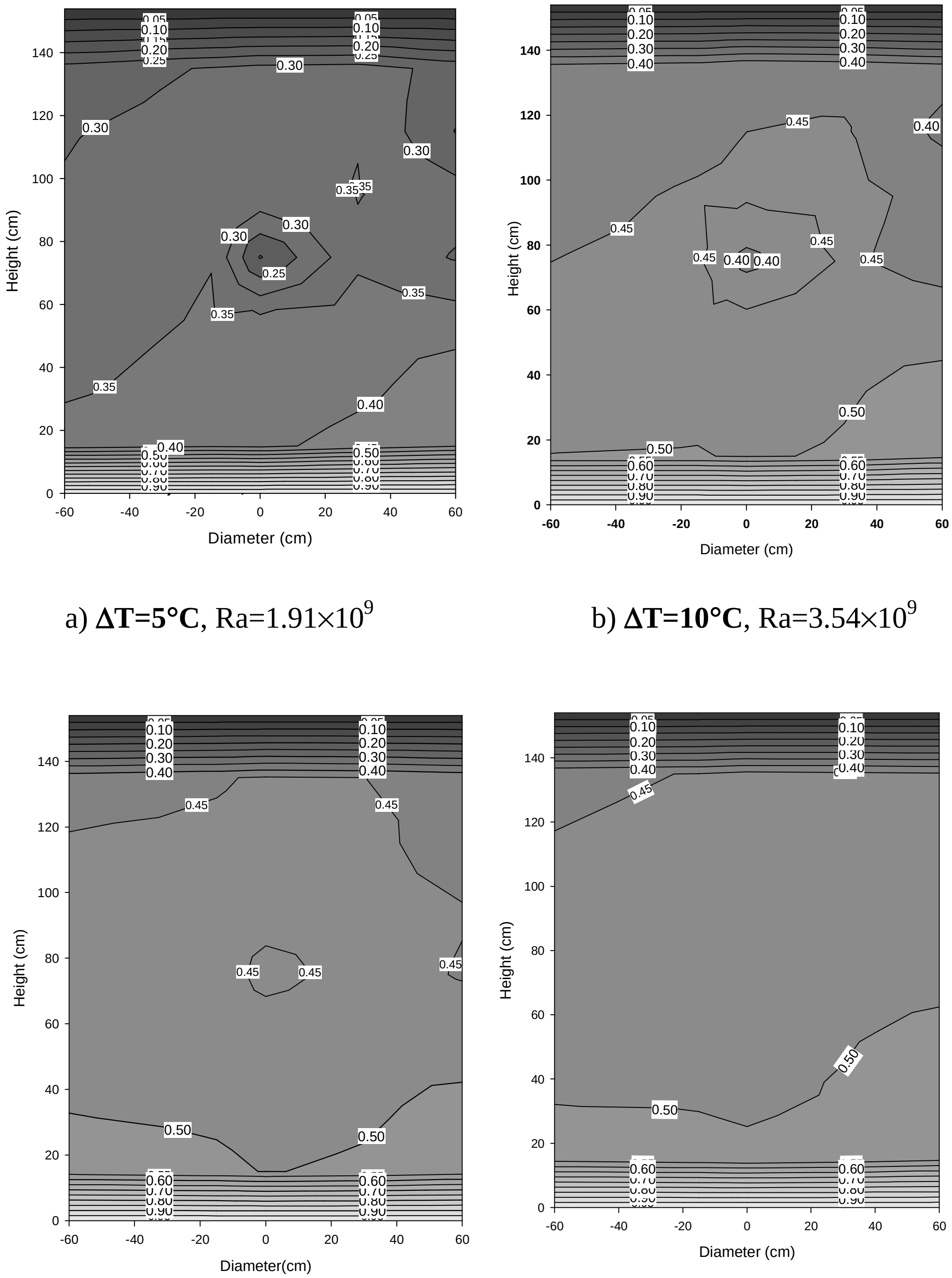

a) **ΔT=5°C**, Ra=1.91×10^9 b) **ΔT=10°C**, Ra=3.54×10^9

c) **ΔT=20°C**, Ra=7.07×10^9 d) **ΔT=30°C**, Ra= 9.47×10^9

Figure 3.3 Air convection in empty test tank steady state normalized temperature contours

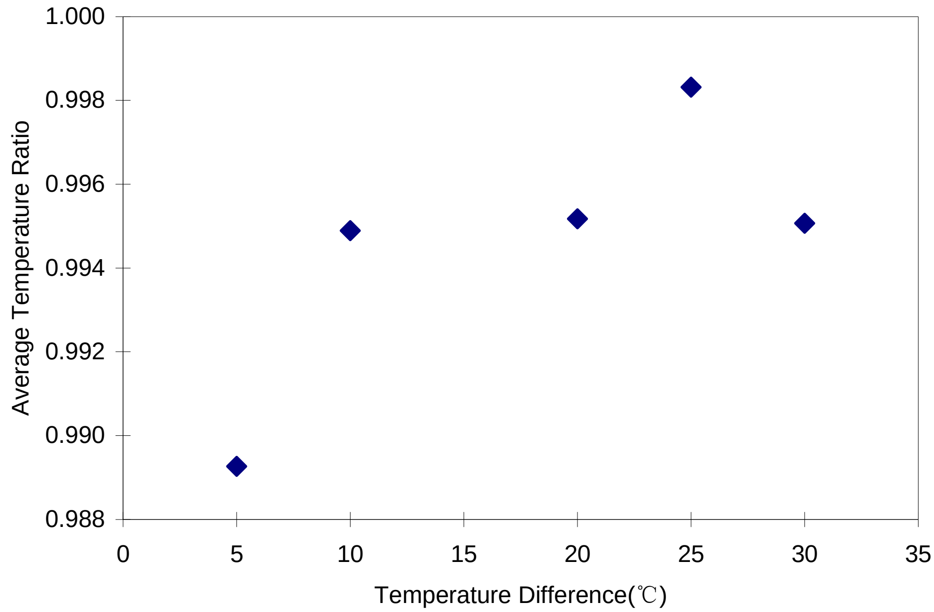

Figure 3.4 Average temperature ratio versus temperature difference (ΔT); The ratio is the average measured air temperature to the measured top and bottom temperature difference

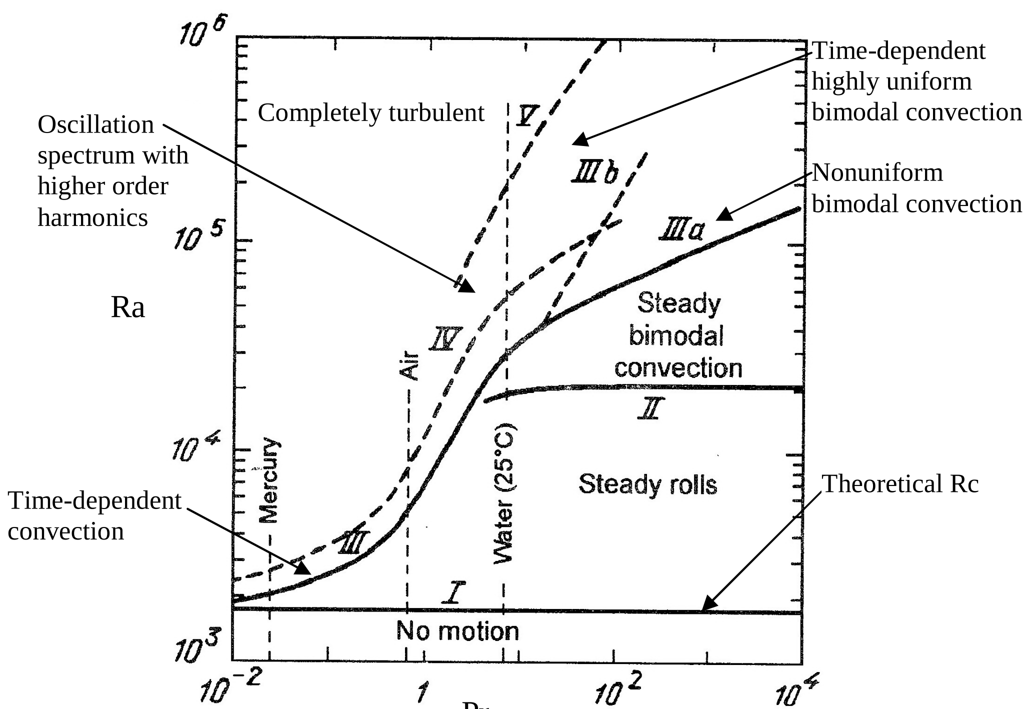

ΔT

Figure 3.5 Rayleigh-Bénard convection regimes with respect to fluid Rayleigh number (Ra) versus Prandtl number (Pr). Curves I to V represent boundaries of the convection regimes (modified from Getling, 1998).

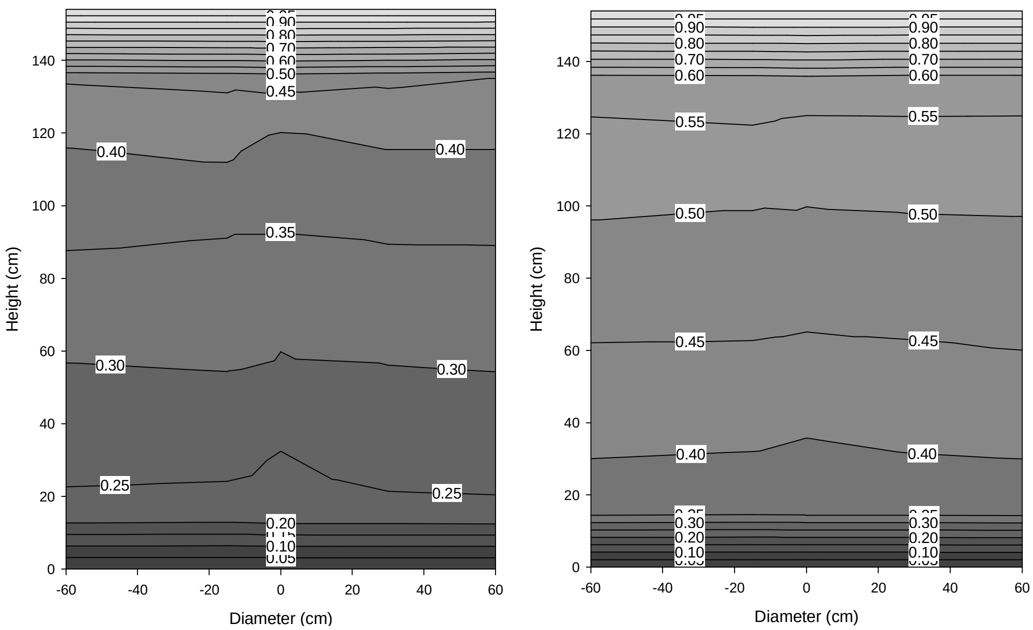

a) **ΔT=15°C** (B25-T40) b) **ΔT=30°C** (B10-T40)

Figure 3.6 Air conduction in empty test tank steady state isotherms

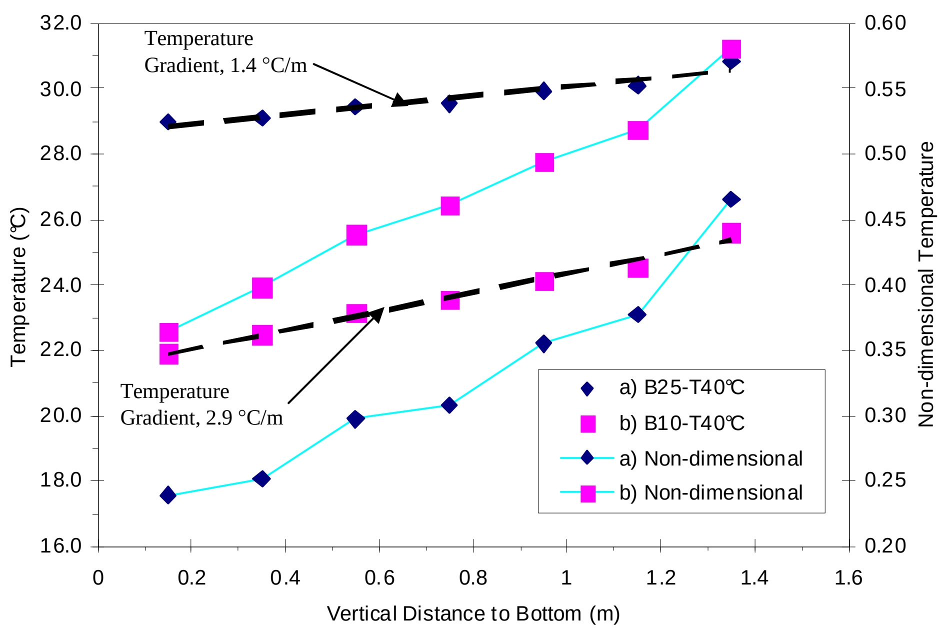

Figure 3.7 Air conduction in empty test tank vertical temperature gradients at steady state

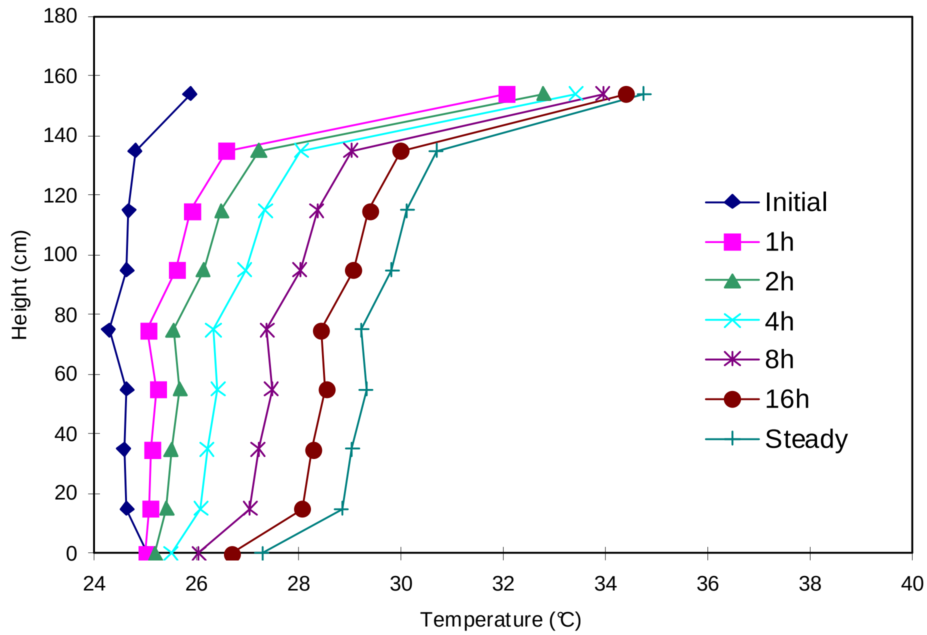

Figure 3.8 Axial temperature profile versus time; conduction in empty test tank - ΔT=15°C (B25-T40)

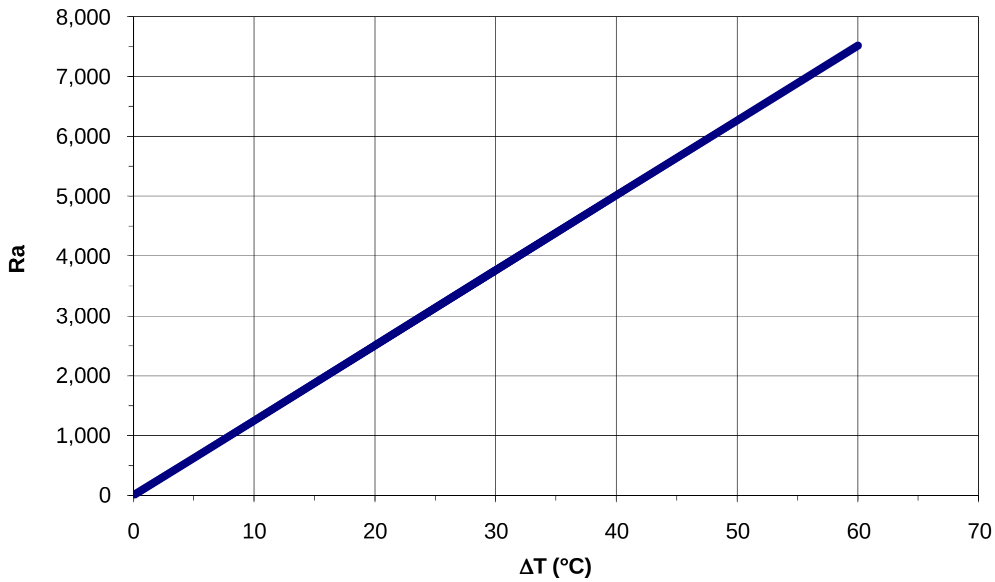

Figure 3.9 Rayleigh number versus top-to-bottom temperature difference within the test tank filled with styrofoam chips

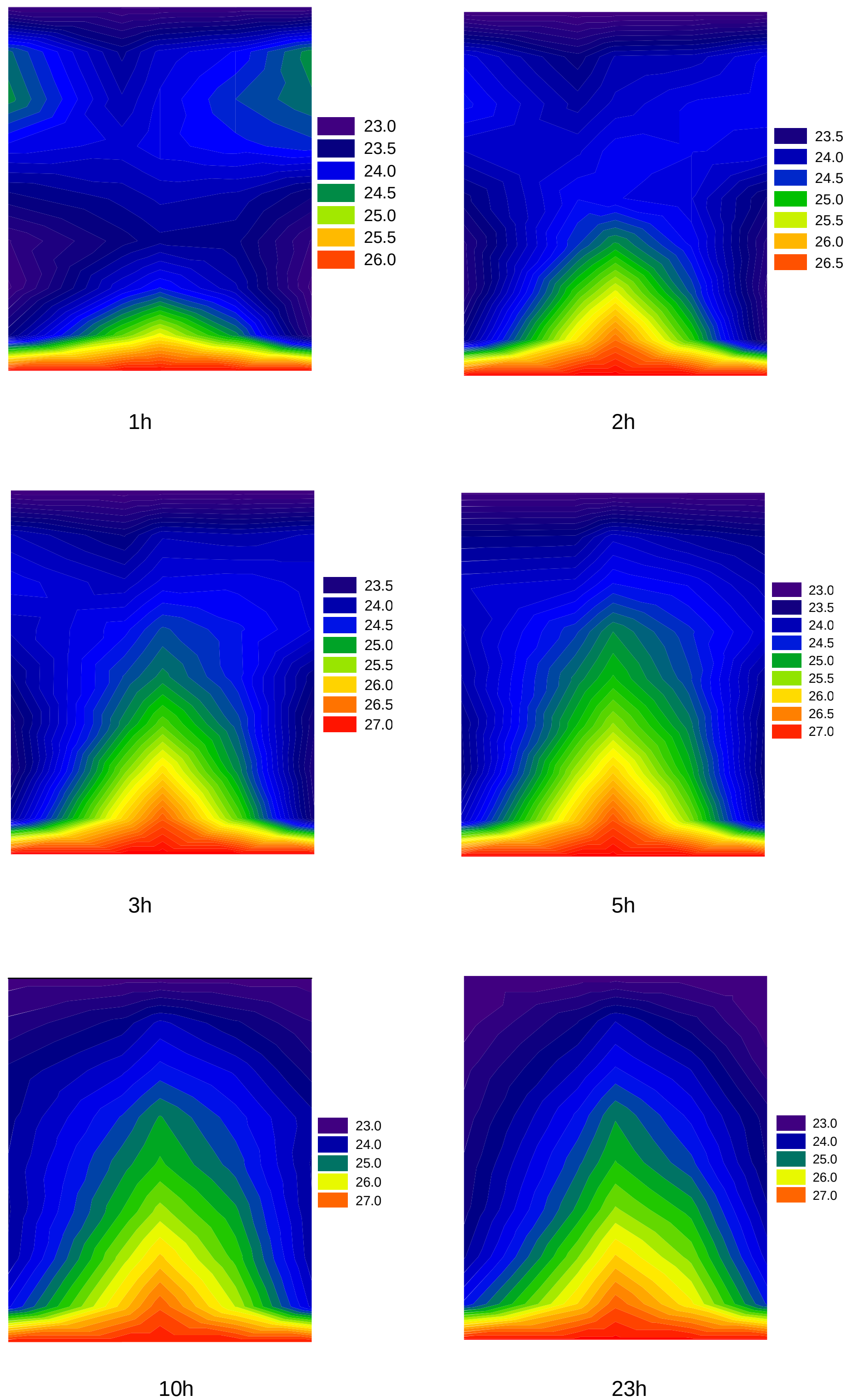

Figure 3.10 Convective isothermal contour patterns varying with time
(**ΔT=5°C**, onset Ra= 626, heating below)

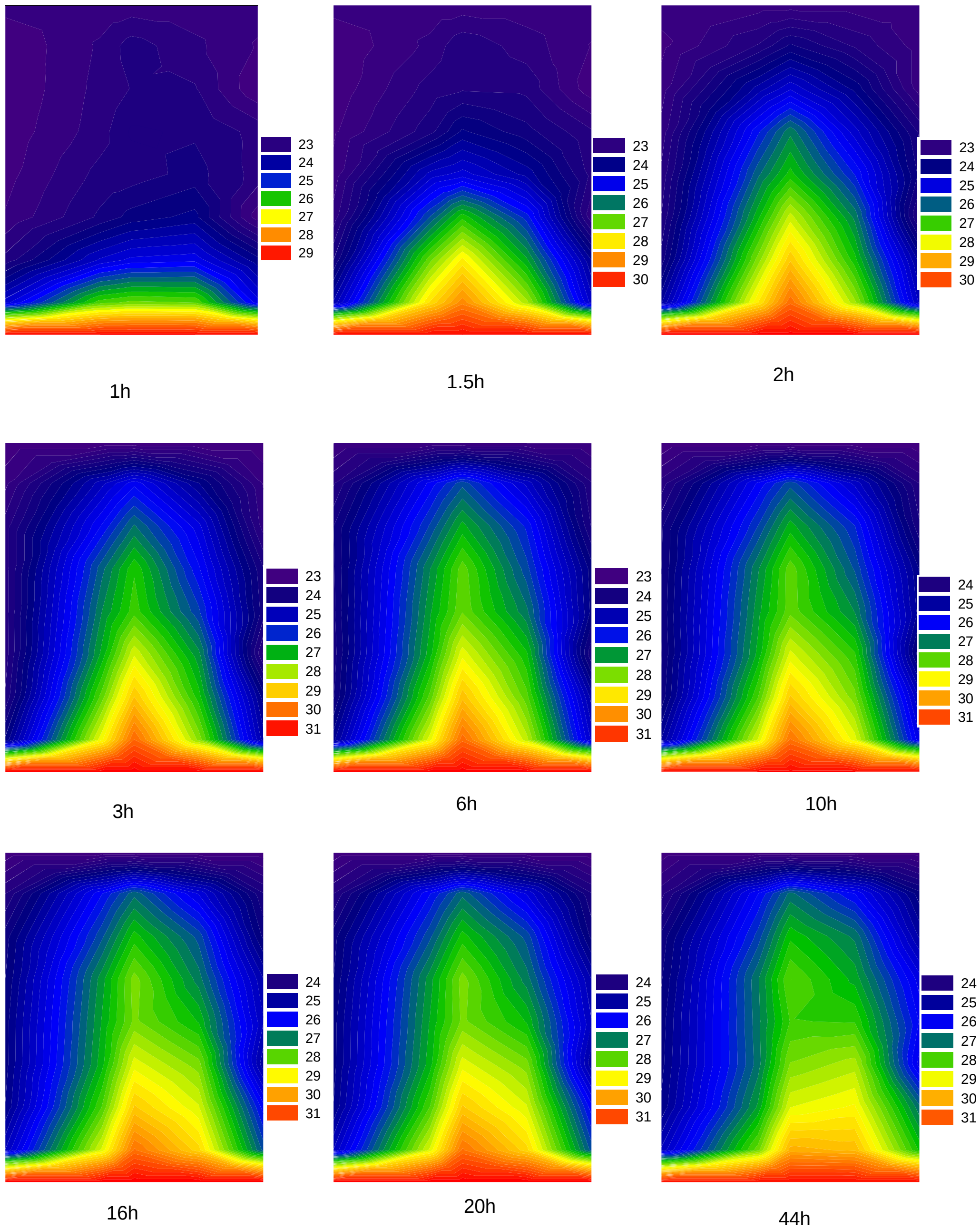

Figure 3.11 Convective isothermal contour patterns varying with time (**ΔT=10°C**, onset Ra=1253, heating below)

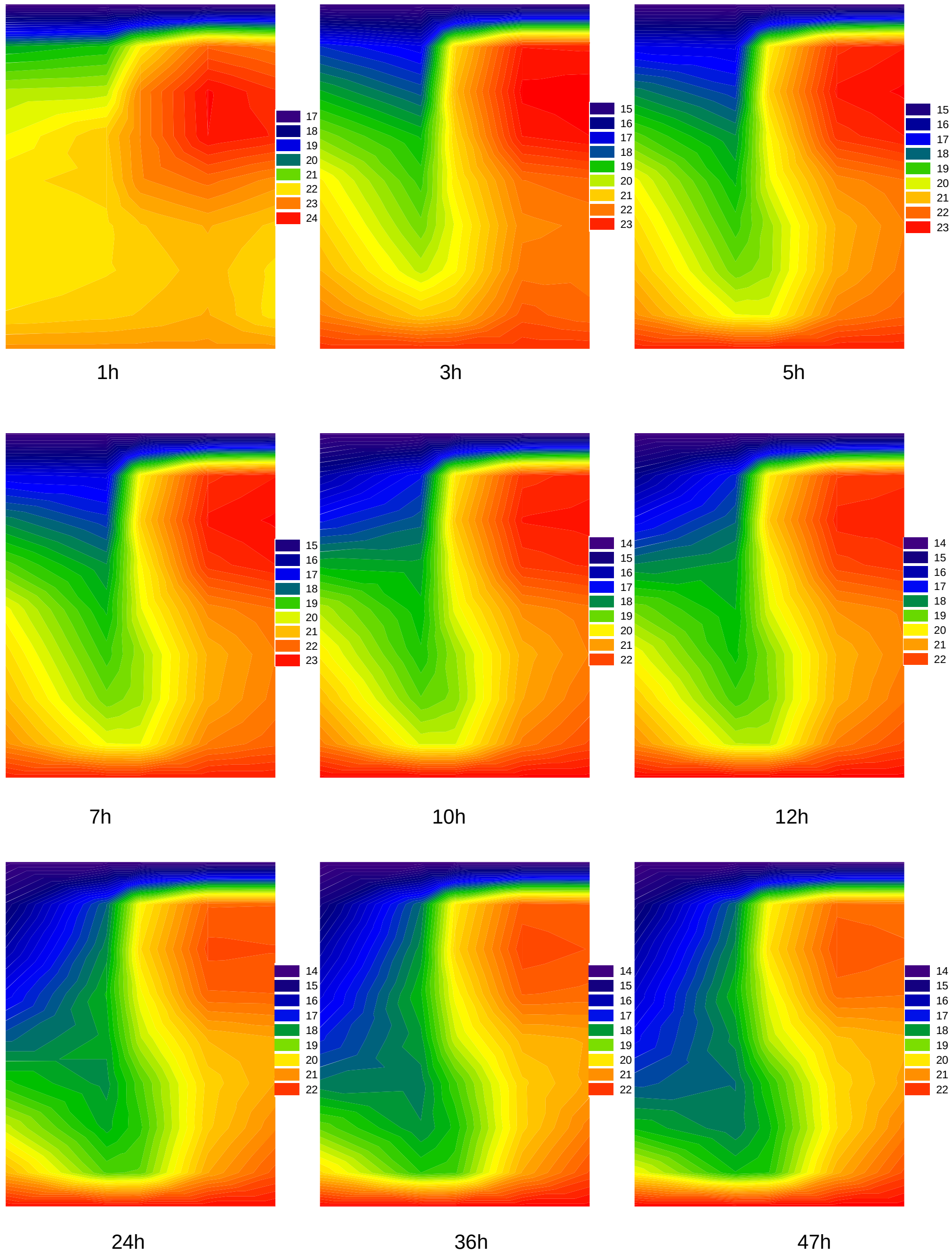

Figure 3.12 Convective isothermal contour patterns varying with time (**ΔT=10°C**, Onset Ra=1253, Cooling above)

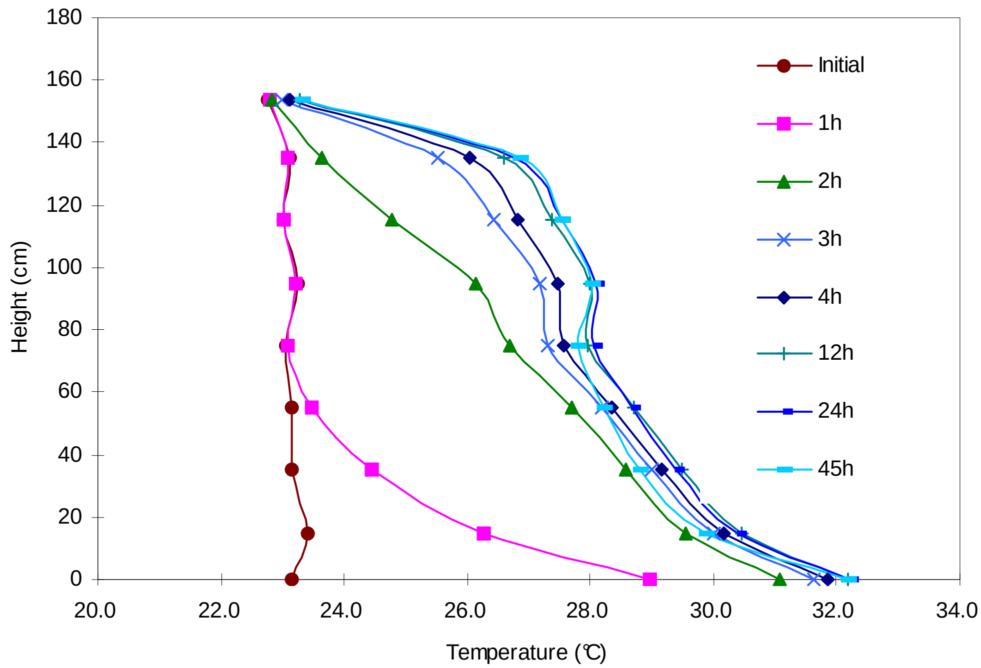

Figure 3.13 Axial temperature profile versus time; convection in styrofoam chips with heating below - **ΔT=10°C** (B33-T23)

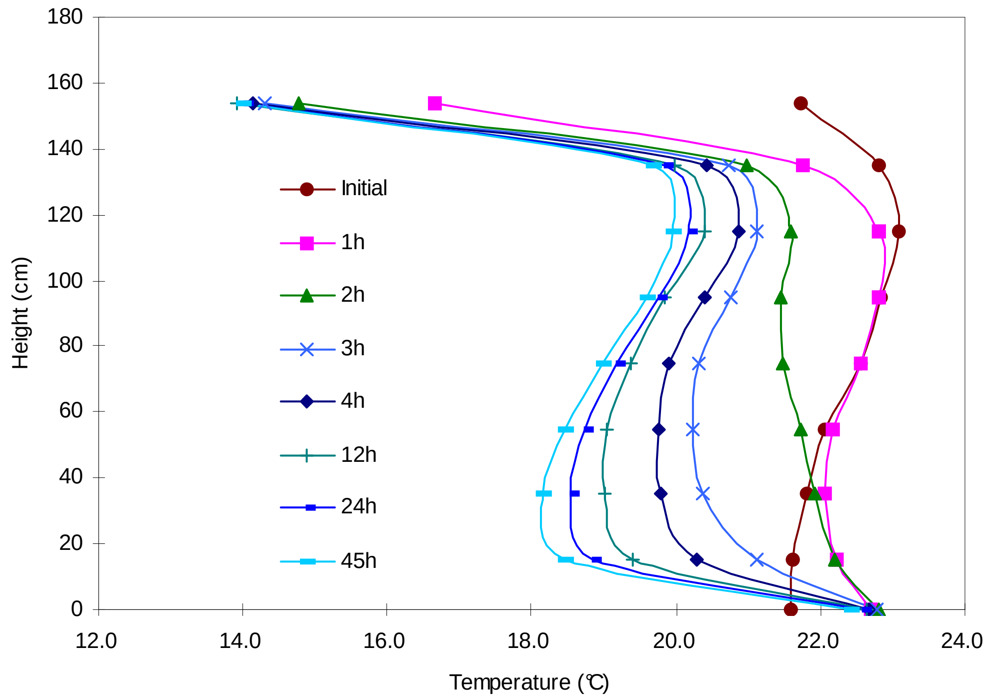

Figure 3.14 Axial temperature profile versus time; convection in styrofoam chips with cooling above - **ΔT=10°C** (B13-T23)

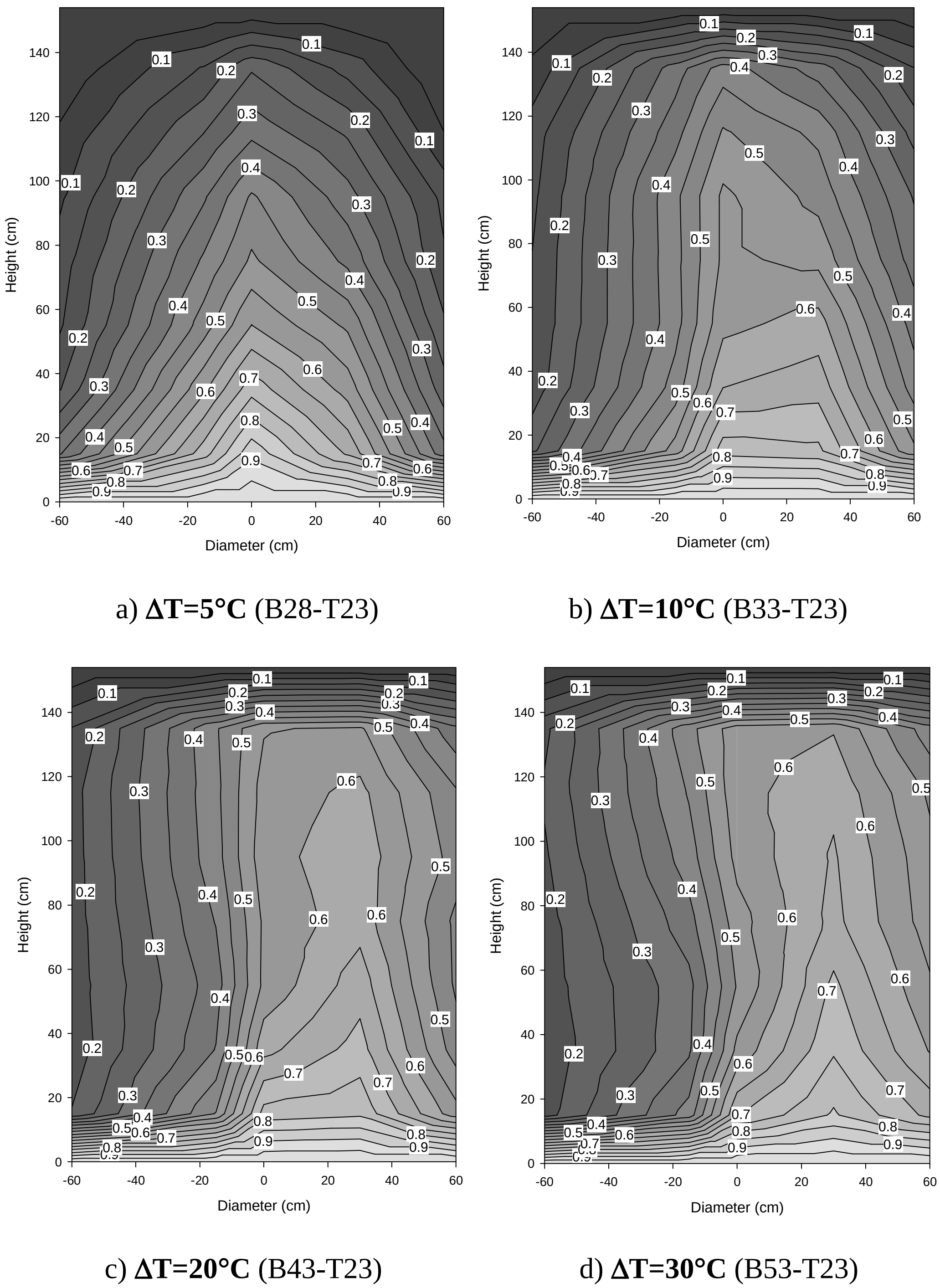

a) **ΔT=5°C** (B28-T23)

b) **ΔT=10°C** (B33-T23)

c) **ΔT=20°C** (B43-T23)

d) **ΔT=30°C** (B53-T23)

Figure 3.15 Convection in styrofoam chips steady state isotherms for instrumentation section CS1 (heating below)

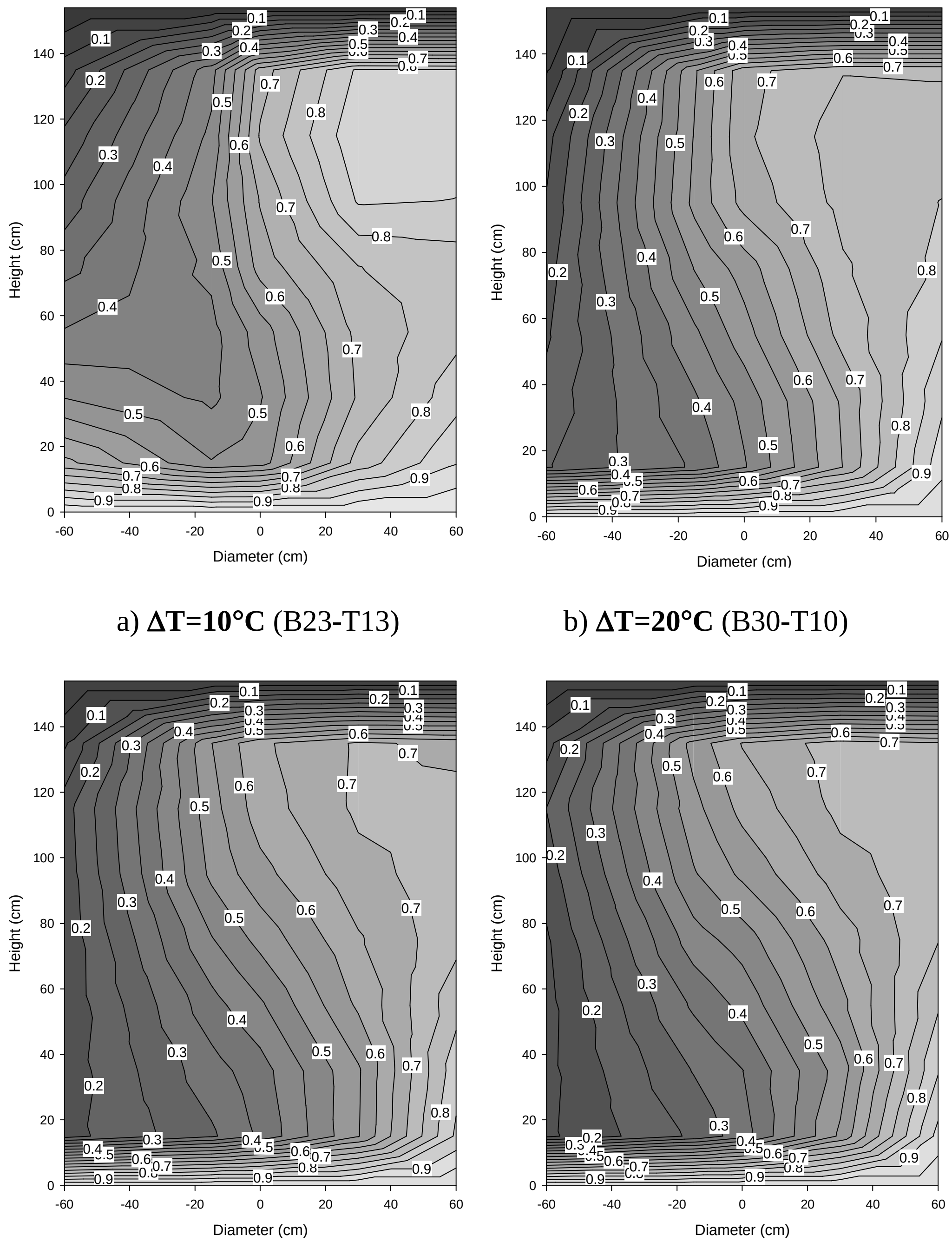

a) **ΔT=10°C** (B23-T13)

b) **ΔT=20°C** (B30-T10)

c) **ΔT=30°C** (B40-T10)

d) **ΔT=40°C** (B50-T10)

Figure 3.16 Convection in styrofoam chips steady state isotherms for instrumentation section CS1 (cooling above)

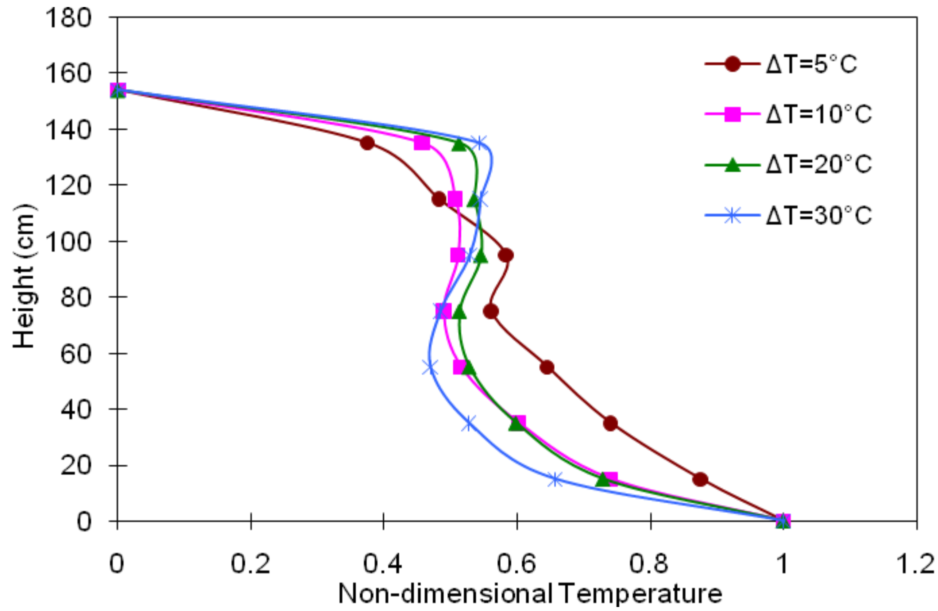

Figure 3.17 Steady state axial temperature profiles of convection in styrofoam chips by heating from below

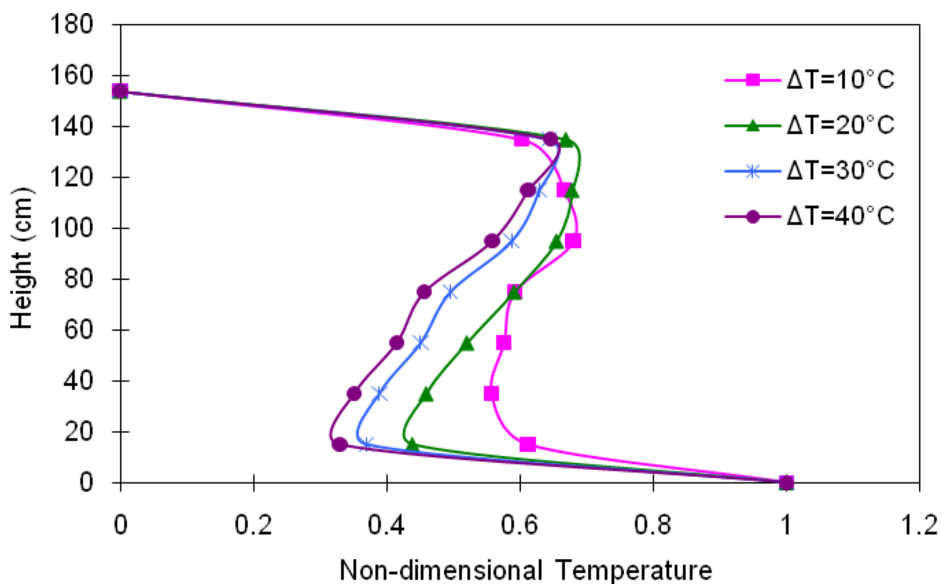

Figure 3.18 Steady state axial temperature profiles of convection in styrofoam chips by cooling from above

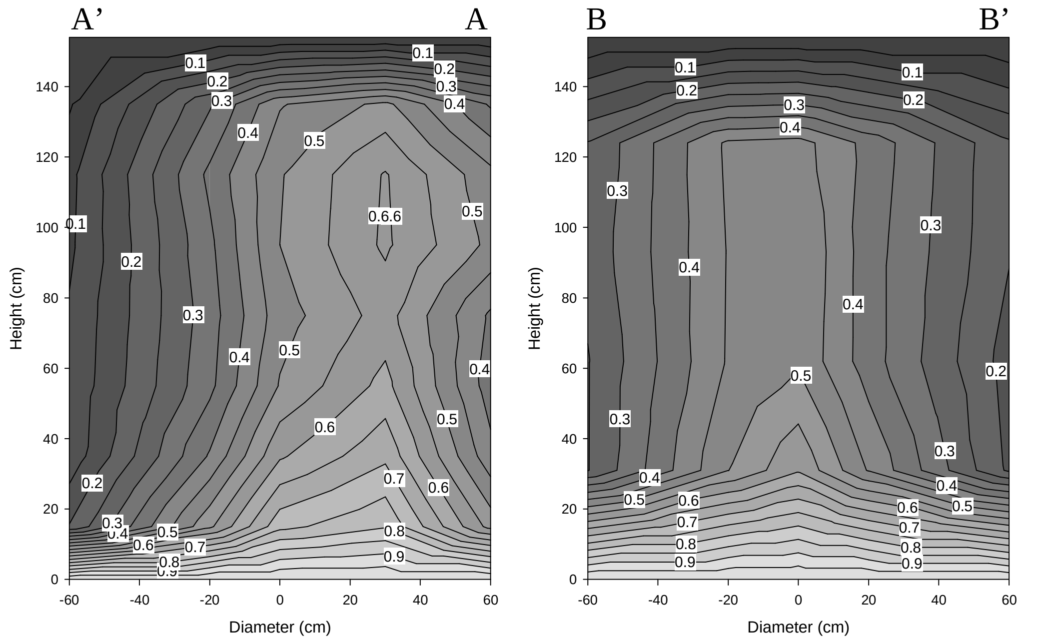

a) CS1 b) CS2

Figure 3.19 Convection in styrofoam chips steady state isotherms **ΔT=10°C** (B33-T23) for the two perpendicular instrumentation sections (heating below)

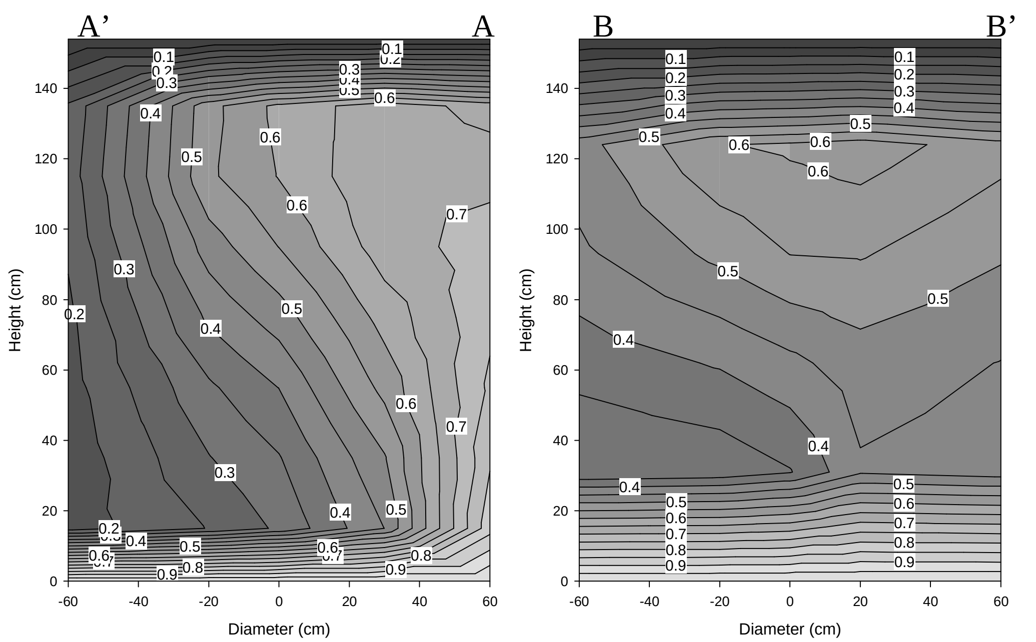

a) CS1 b) CS2

Figure 3.20 Convection in styrofoam chips steady state isotherms **ΔT=40°C** (B53-T13) for the two perpendicular instrumentation sections (cooling above and heating below)

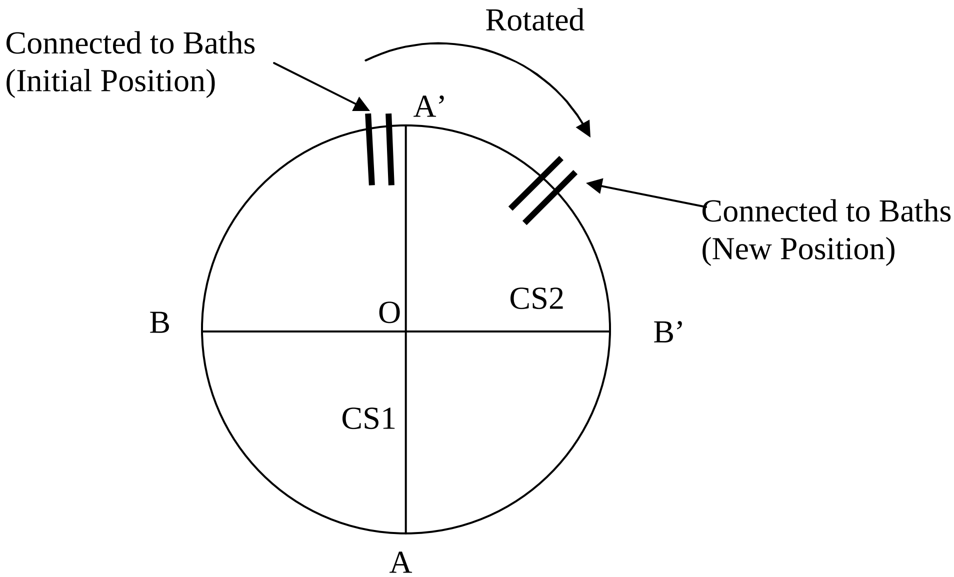

Figure 3.21 Inlet/outlet position of the top copper coil rotated about 45 degrees in order to study convective cell direction.

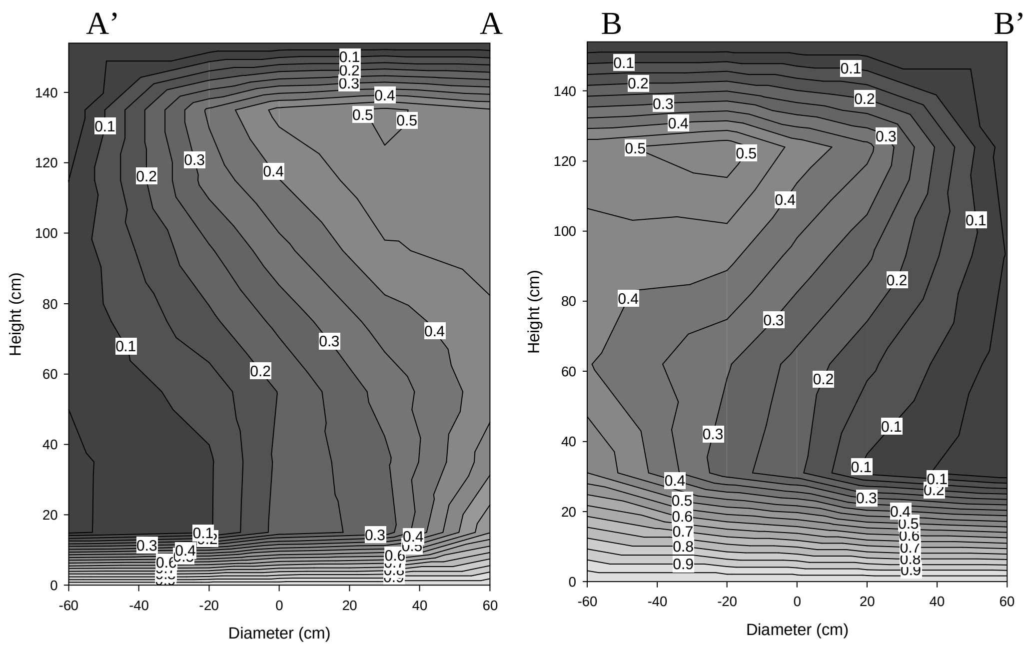

a) CS1 b) CS2

Figure 3.22 Convection in styrofoam chips steady state isotherms **ΔT=40°C** (B52.5-T12.5, cooling above and heating below) for the two perpendicular instrumentation sections (after rotation)

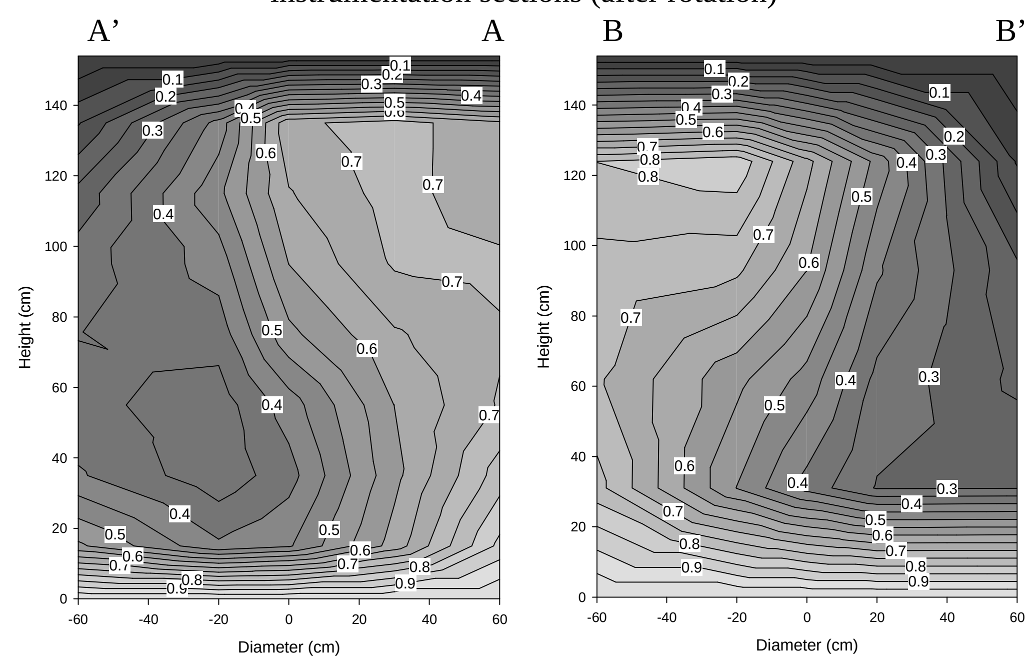

a) CS1 b) CS2

Figure 3.23 Convection in styrofoam chips steady state isotherms **ΔT=10°C** (B22.5-T12.5, cooling above) for the two perpendicular instrumentation sections (after rotation)

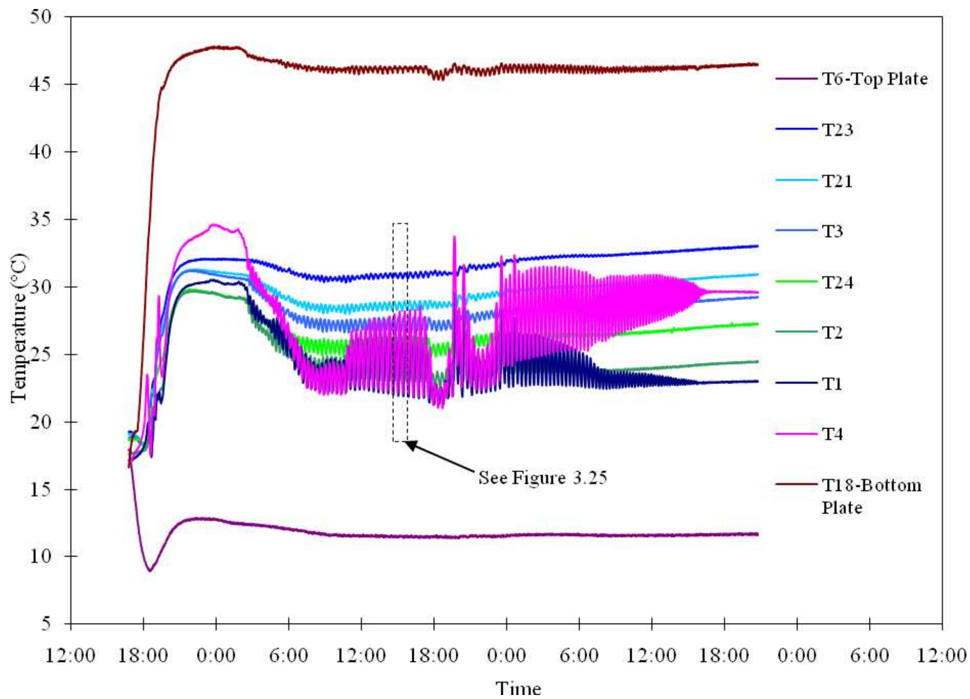

Figure 3.24 Fluctuation and oscillation observed from convection test under **ΔT=50°C** (B53-T3)

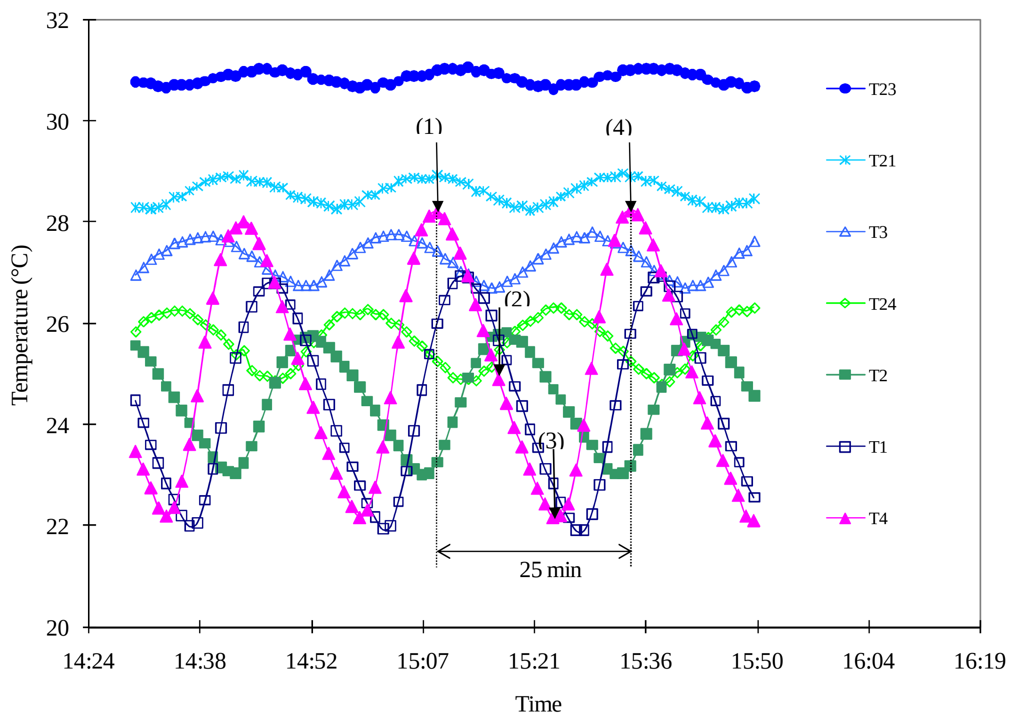

Figure 3.25 Typical oscillation period and amplitude; corresponding isothermal patterns at points 1 to 4 shown in Figure 3.26

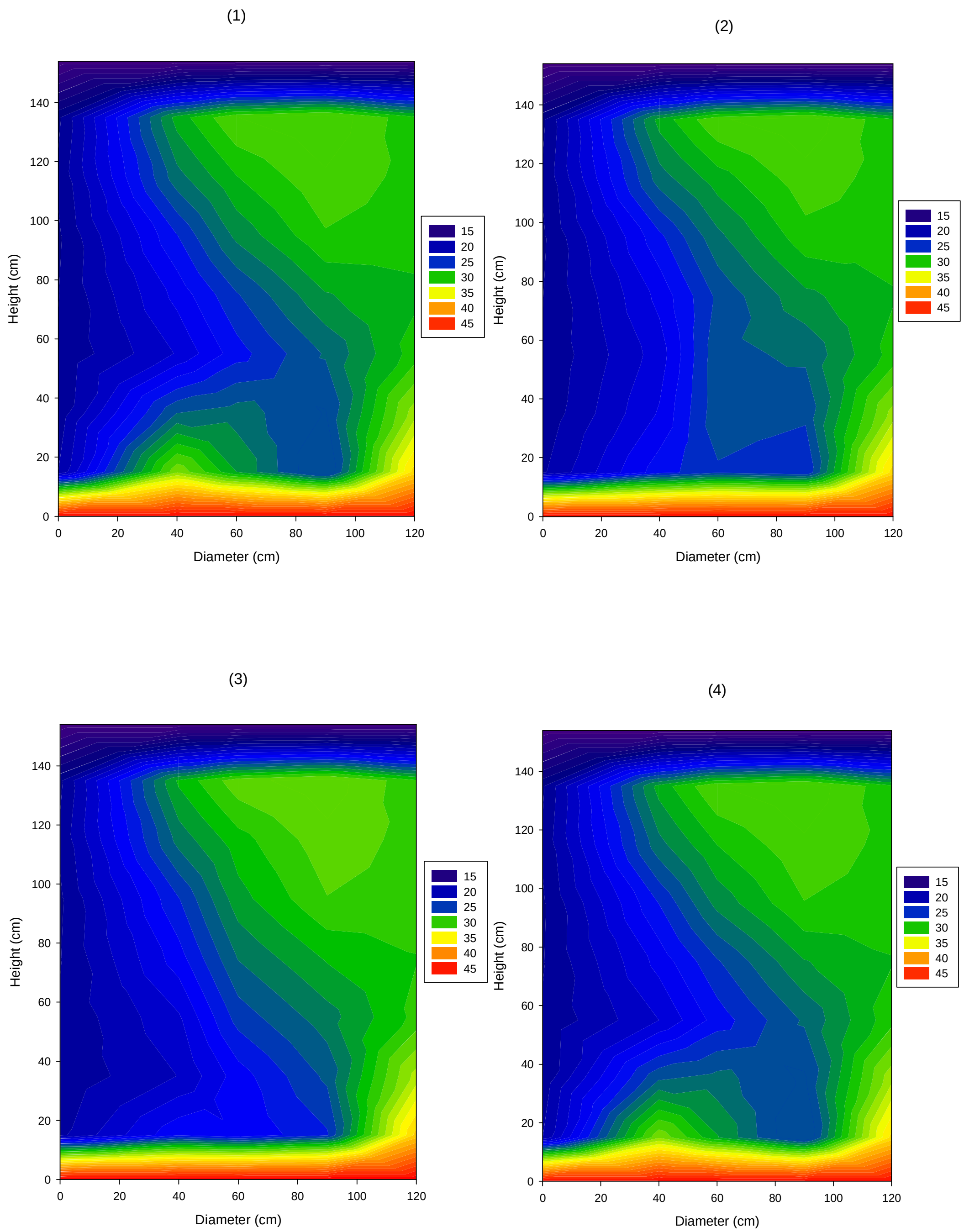

Figure 3.26 Isothermal patterns for instrumentation section CS1 in the oscillation period shown in Figure 3.25 for **ΔT=50°C** (B53-T3)

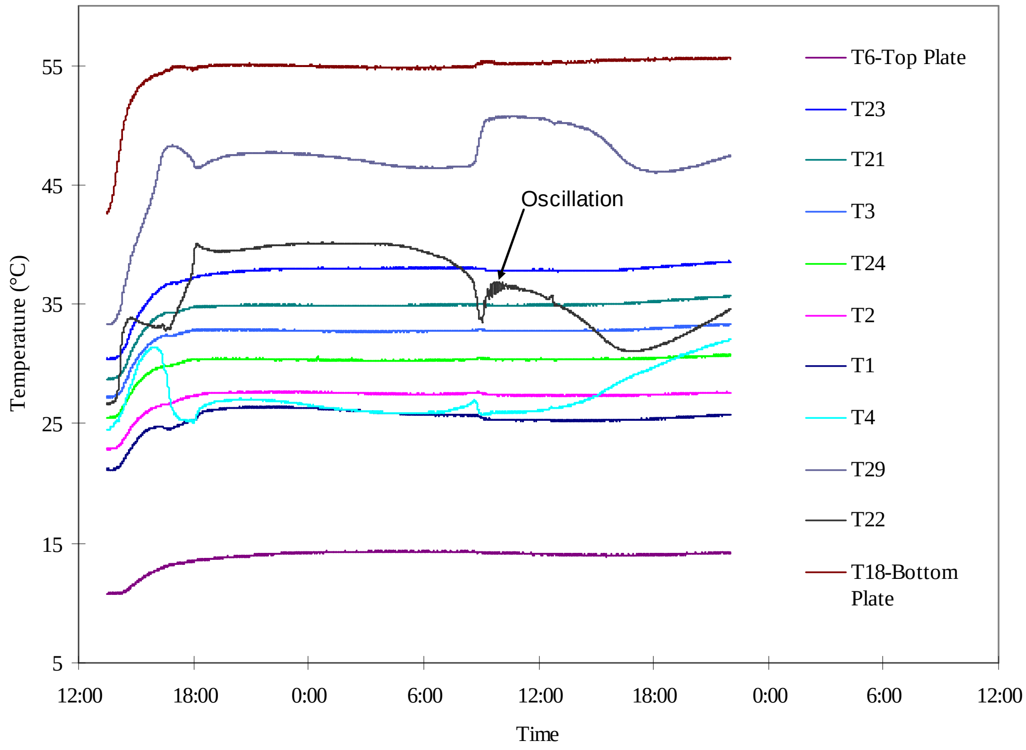

Figure 3.27 Fluctuation and oscillation observed from convection test under **ΔT=60°C** (B63-T3)

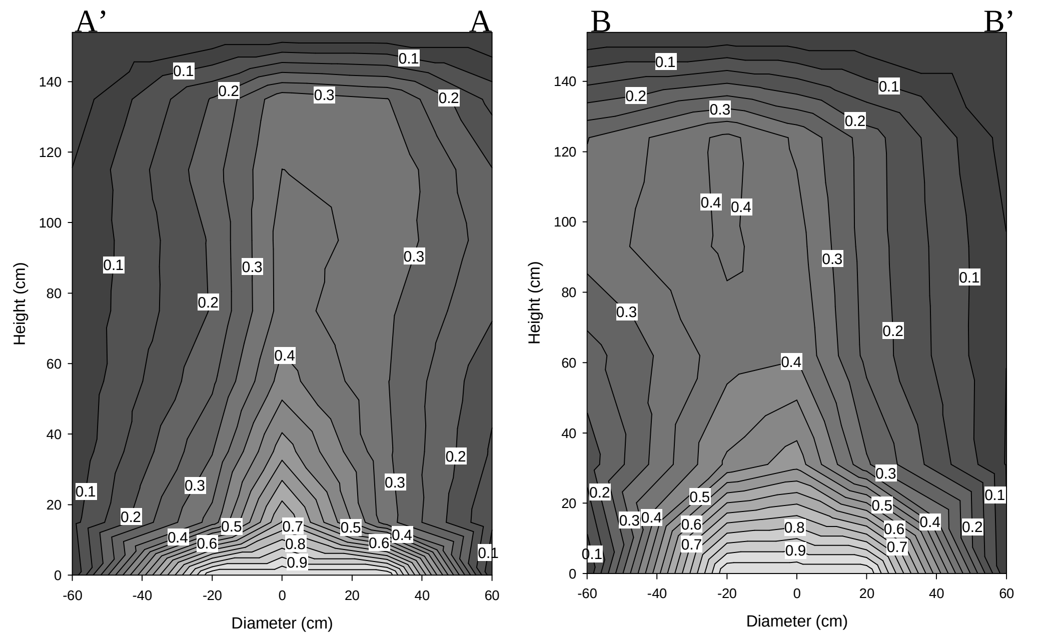

a) CS1 b) CS2

Figure 3.28 Convection by localized heating from below: steady state isotherms **ΔT=10°C** (LB32-T22) for the two perpendicular instrumentation sections

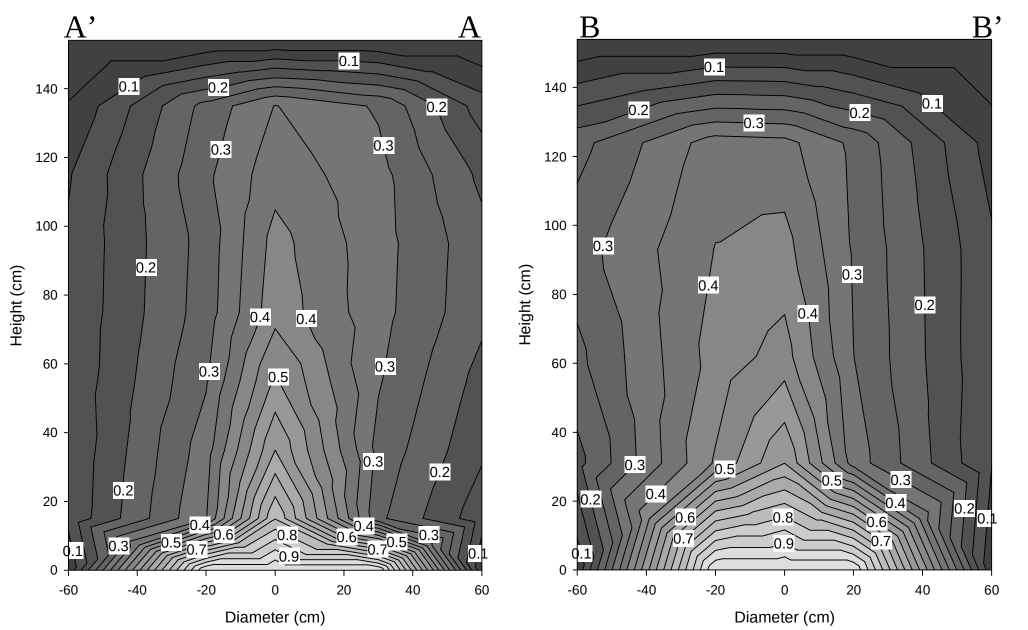

a) CS1 b) CS2

Figure 3.29 Convection by localized heating from below: steady state isotherms **ΔT=20°C** (LB42-T22) for the two perpendicular instrumentation sections

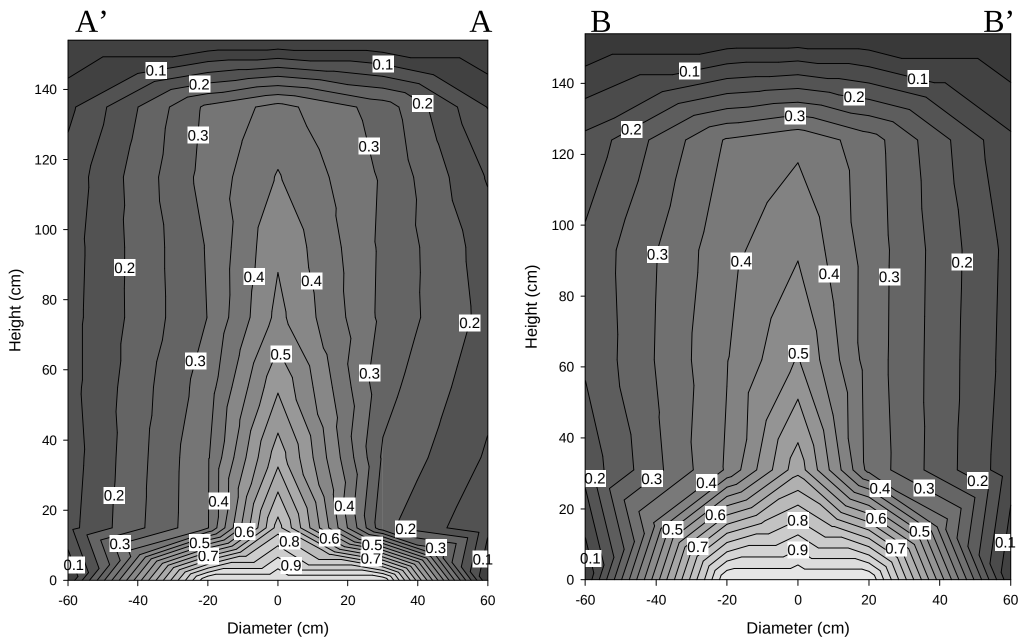

a) CS1 b) CS2

Figure 3.30 Convection by localized heating from below: steady state isotherms **ΔT=30°C** (LB52-T22) for the two perpendicular instrumentation sections

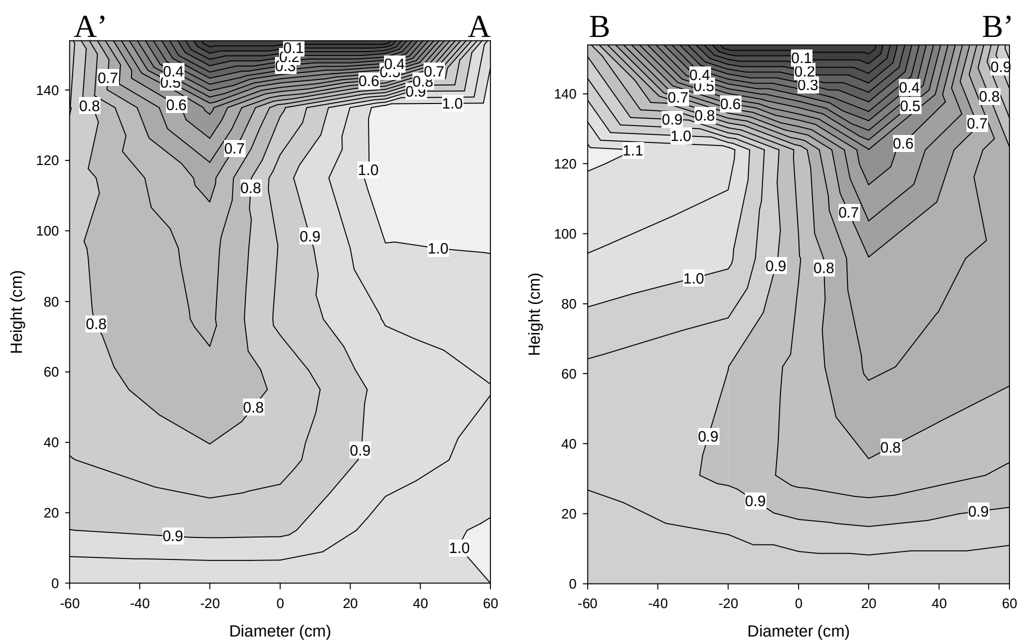

a) CS1 b) CS2

Figure 3.31 Convection by localized cooling from above: steady state isotherms **ΔT=10°C** (B20.5-LT10.5) for the two perpendicular instrumentation sections

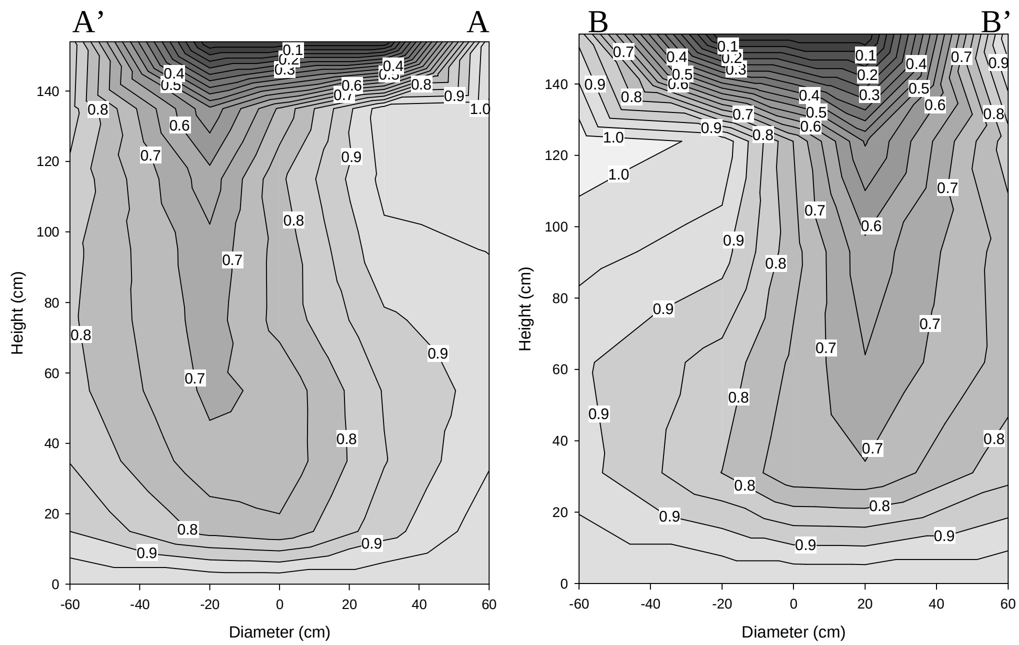

a) CS1 b) CS2

Figure 3.32 Convection by localized cooling from above: steady state isotherms **ΔT=15°C** (B20.5-LT5.5) for the two perpendicular instrumentation sections

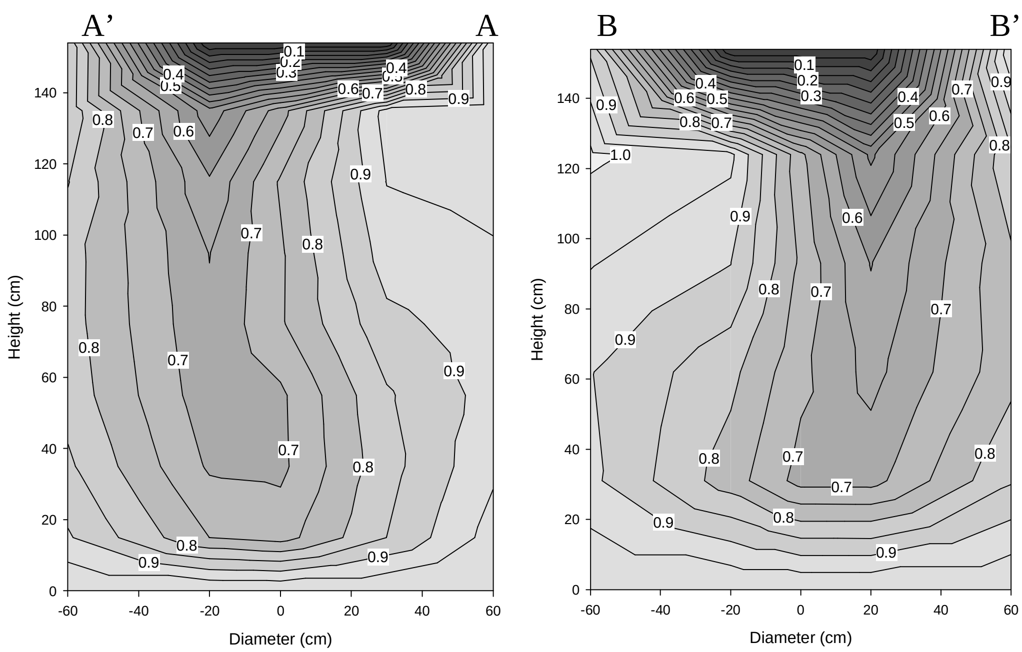

a) CS1 b) CS2

Figure 3.33 Convection by localized cooling from above: steady state isotherms **ΔT=20°C** (B21-LT1.0) for the two perpendicular instrumentation sections

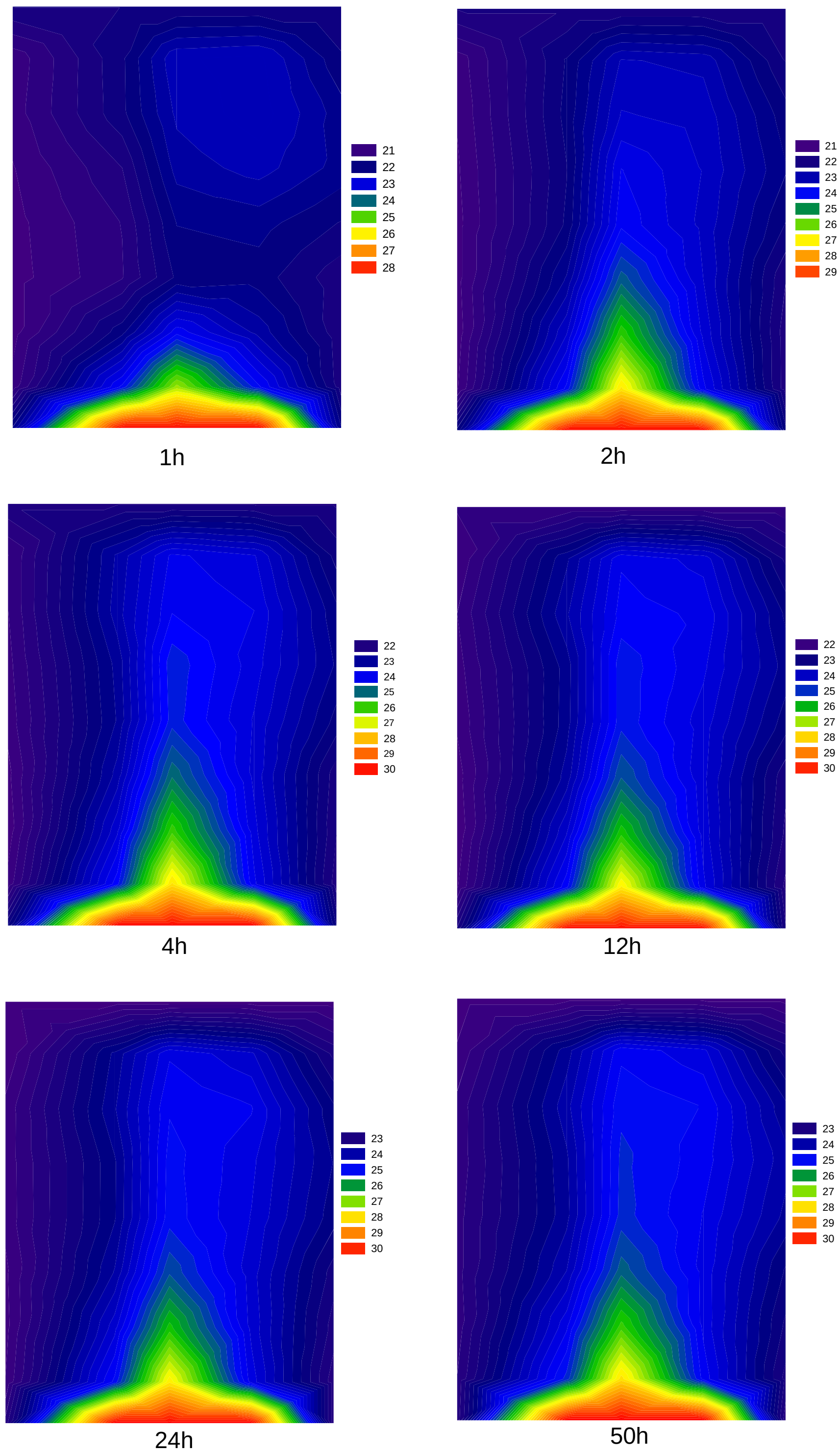

Figure 3.34 Convective isothermal contour patterns varying with time
(**ΔT=10°C**, localized heating below)

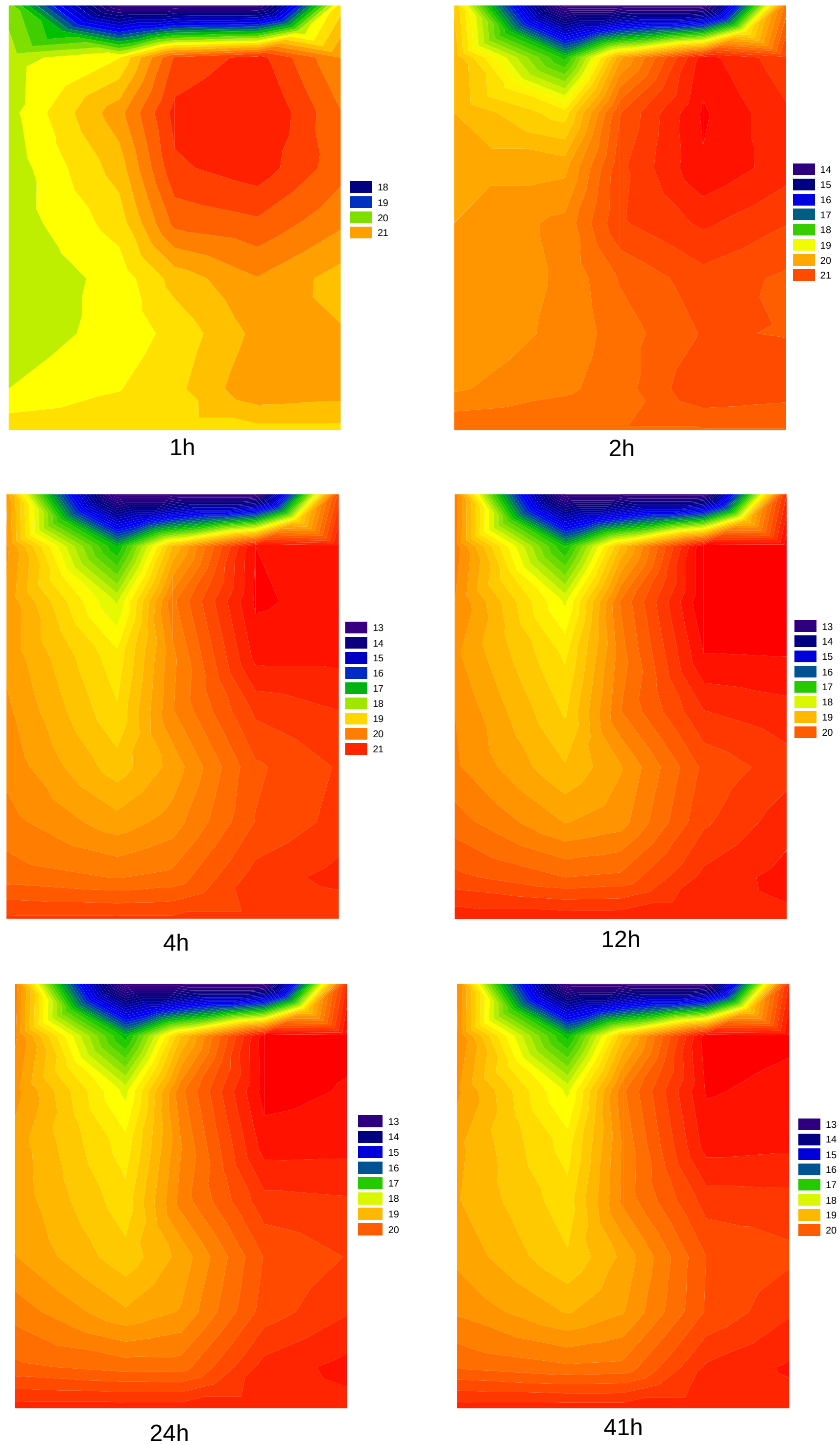

Figure 3.35 Convective isothermal contour patterns varying with time (**ΔT=10°C**, localized cooling above)

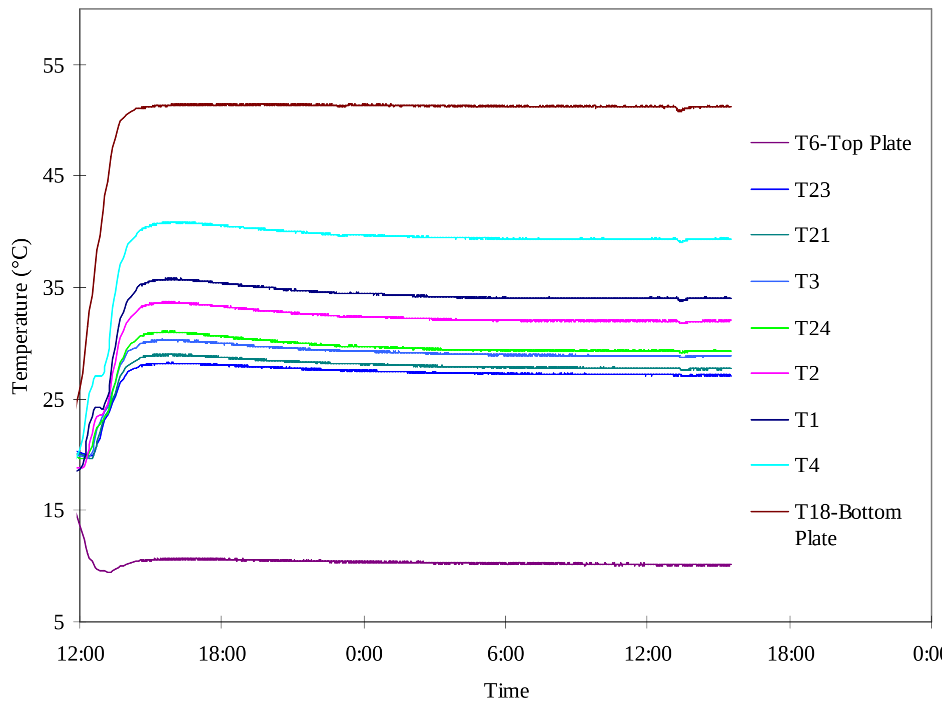

Figure 3.36 No fluctuation and oscillation observed from convection test with localized heating under **ΔT=60°C** (LB63-T3)

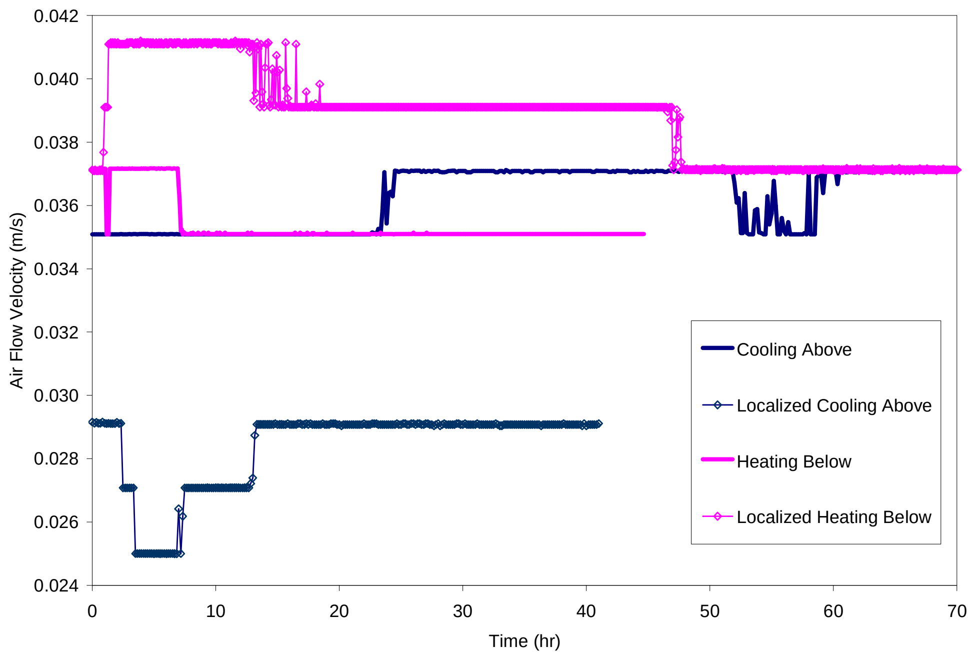

Figure 3.37 Measured air flow velocity for tests with **ΔT=10°C**

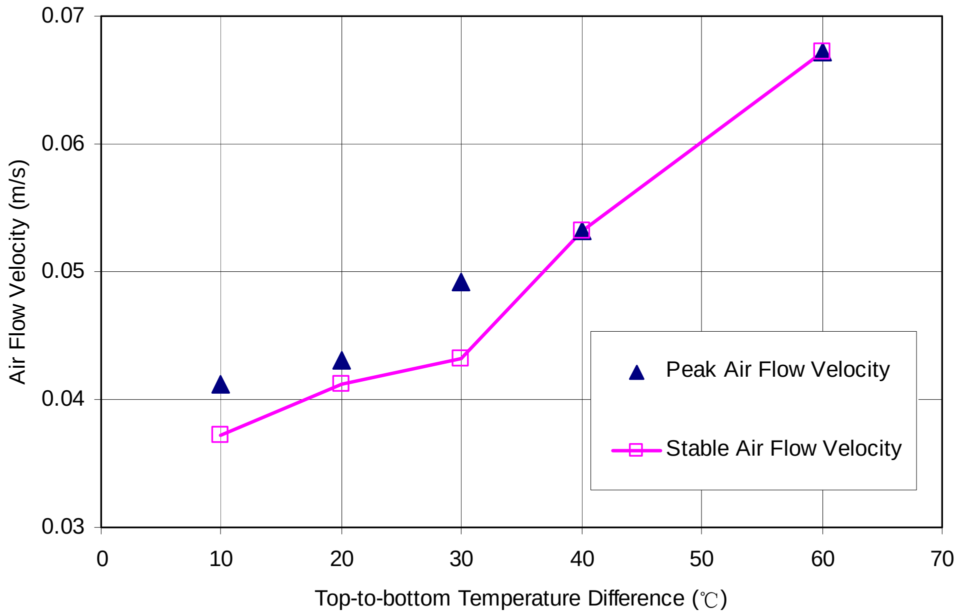

Figure 3.38 Measured air flow velocity versus temperature difference with localized heating below

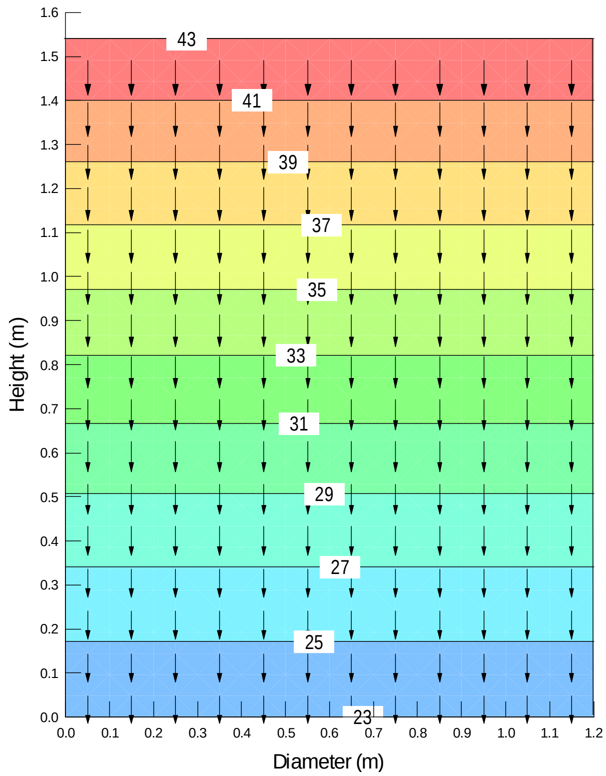

Figure 3.39 Conductive thermal model on air and styrofoam for **ΔT=20°C** (B23-T43); steady state isotherms at 42h

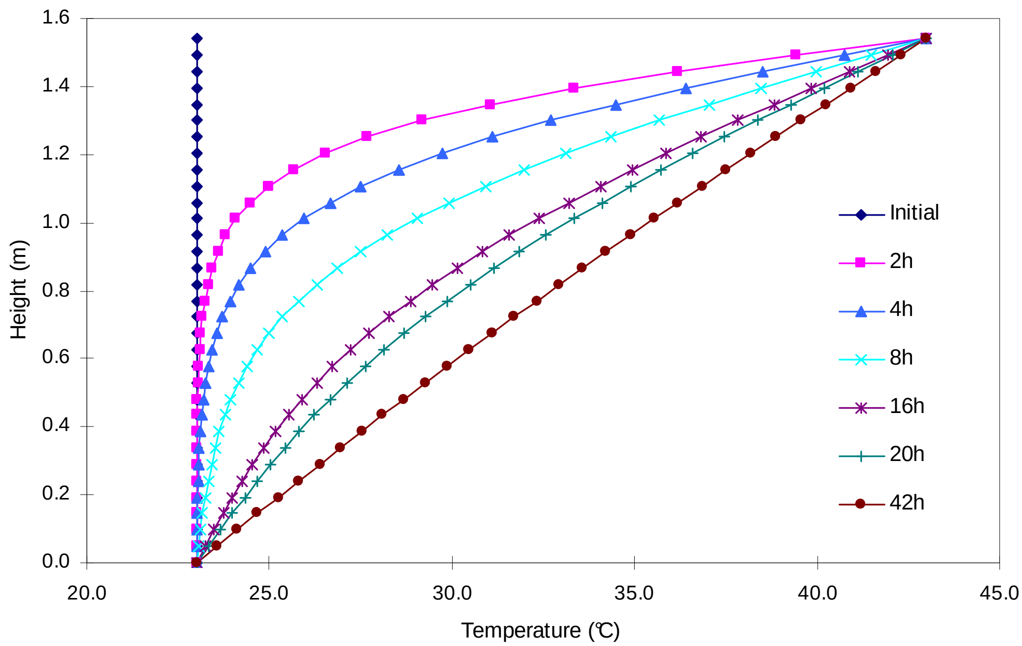

Figure 3.40 Conductive thermal model for **ΔT=20°C** (B23-T43) on air and styrofoam; axial temperature profile versus time

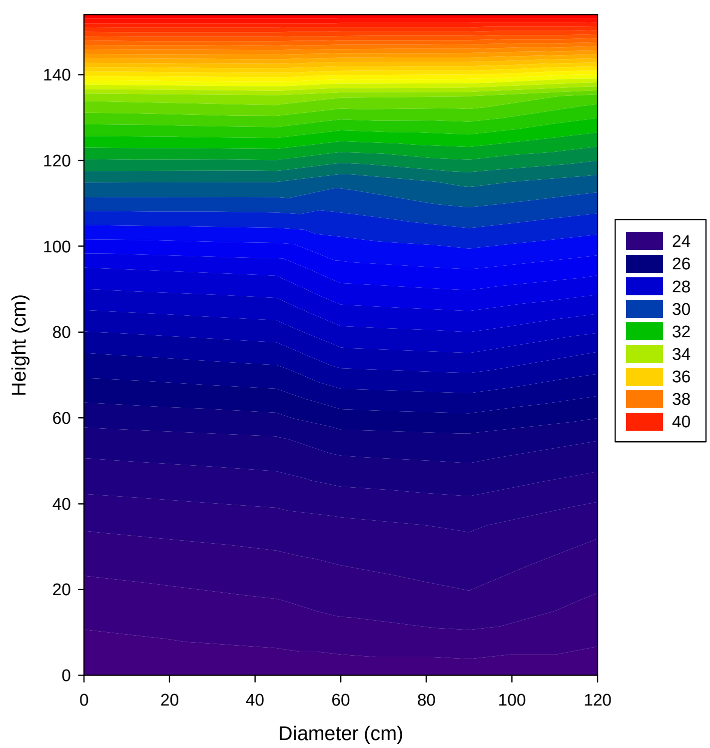

Figure 3.41 Conduction test on air and styrofoam for **ΔT=20°C** (B23-T43); steady state isotherms at 42h

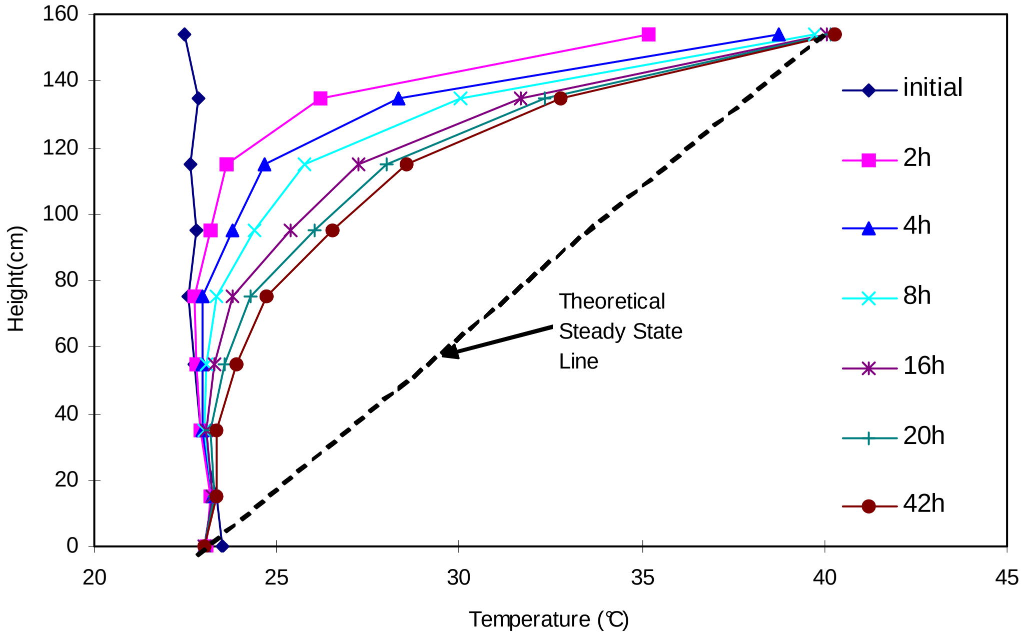

Figure 3.42 Conduction test on air and styrofoam for **ΔT=20°C** (B23-T43); axial temperature profile versus time

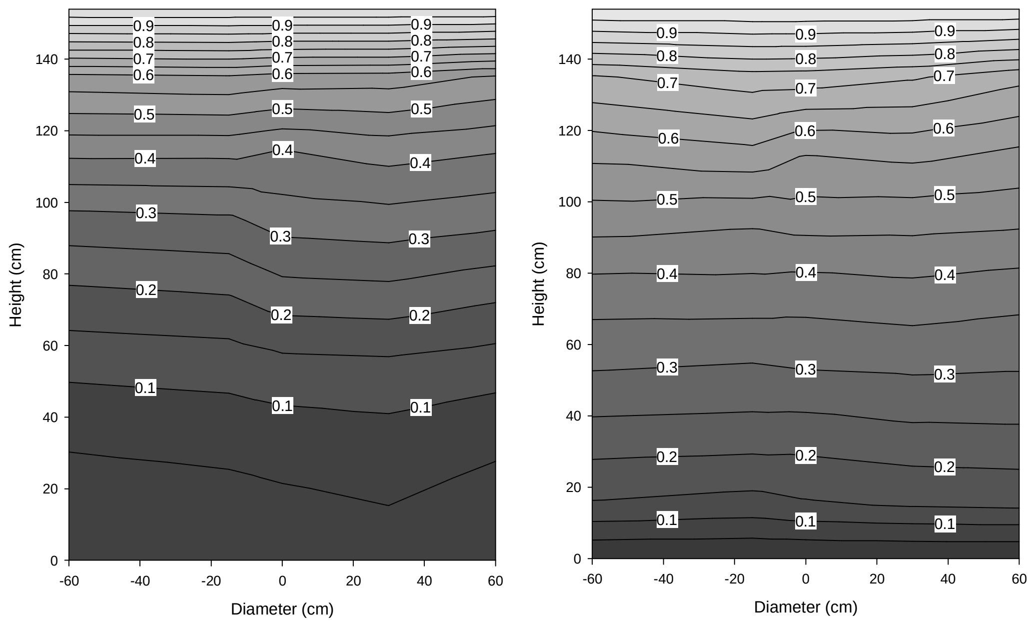

a) ΔT=20°C (B23-T43)
Heating above only

b) ΔT=20°C (B15-T35)
Cooling below and heating above

Figure 3.43 Conduction test on air and styrofoam; steady state non-dimensional isotherms with different initiation methods

4 SUMMARY AND CONCLUSIONS

Mechanisms associated with convective heat transfer in porous media have been extensively studied in the literature. However, convective cooling effects for application in cold region geotechnical engineering have only been examined for a limited number of years. Potential use of the cooling effects to reduce and/or stabilize frozen ground temperatures beneath rockfill embankments and dams, permeable tailings covers, and waste rock piles is possible. It is therefore an economical approach to take advantage of frozen soils generally with high strength and low hydraulic conductivities.

To investigate convective heat transfer in a porous medium, laboratory experiments on natural air convection and thermal conduction were carried out using a well-insulated cylindrical tank and also when it was filled with styrofoam chips with low thermal conductivity. By controlling the top and bottom temperature boundary conditions for the test tank, a series of conductive and convective thermal contours and profiles were determined from an extensive array of point measurements.

No clear patterns of air movement were observed during convection in the empty test tank. In fact, markedly large fluid Rayleigh numbers were associated with the testing system under the top-to-bottom temperatures used. As a result, convective air movement could readily approach steady state, resulting in more efficient heat transfer when compared with that for the thermal conduction of air in the tank.

As expected, convective pore air movement in the styrofoam chips filled tank easily appeared. However, the Rayleigh number values may be overestimated in terms of test results. Transient convective patterns for $\Delta T=5°C$ heated from below showed axisymmetric characteristics and stable temperature patterns. For convection under $\Delta T=10°C$ heated from below, the patterns were initially symmetric. However, the centerline of the contours eventually shifted to the right hand side of the temperature measuring section. The possible reasons include that the convection was in a transition from stable to unstable convection, it is due to the three-dimensional effects of the test, and/or horizontal convection that can cause asymmetric patterns occurred in the tank (Mullarney et al., 2004). Unlike numerical modelling results, a unicellular convective pattern occurred during the convection test at $\Delta T=10°C$ with cooling from above. This may be due to the fact that air was sensitive to small temperature perturbation causing by imperfect seal conditions of the top of the tank.

A number of steady state isotherms showed that most convective cell patterns with heating below deflected slightly from the central axis, although related numerical modelling results always show axisymmetric conditions (Arenson et al., 2007). On the other hand, cooling the top plate resulted in a single convective cell in the tank, i.e. cooler air moves down along one side and rises along the other side of the tank. The asymmetric characteristics of the patterns may be due to small temperature perturbation and/or horizontal convection at the top of the tank. Higher Rayleigh number during convection has more efficient heat transfer by comparison with the magnitudes of non-dimensional temperature from the convection tests.

When the Rayleigh number is above approximately 6200, Temperature fluctuations and oscillations appeared during the convection tests. For tests under $\Delta T=50°C$ with heating below, oscillations with varying periods and amplitudes occurred close to the bottom heating plate. Strong fluctuation also occurred in the test of $\Delta T=60°C$ with a higher Rayleigh number. However, only minor apparent oscillation was observed near lower corners of the tank. As explained by Horne and O'Sullivan (1978), these oscillations could be due to high air flow acceleration as a result of the rapid changes of air temperatures.

It was found that convection induced by localized heating stabilized the symmetry of the convective patterns and had steeper and more concentrated isotherms in the center area of the tank. Dual-cell convection with poor symmetry was observed during the convection induced by localized cooling. Heat transfer for convection by localized heating or cooling conditions were found to be less efficient than for that with a fully heated or cooled boundary in the tank. Localized heating tests also showed that air flow velocity normally peaks, then decreases to a relatively stable value, and increases with an increasing ΔT or Rayleigh number. It should be noted that the flow velocity measured in the tank reflected only the vertical component of air flow through local pore spaces of the styrofoam. A maximum air flow velocity of 0.068 m/s was observed in this study.

This study also illustrated that convective air movement was sensitive to small temperature perturbation. Consequently, the limitations of experiment apparatus in this study (such as the tank seal and insulation, the three-dimensional shape factor, and the heating or cooling system) can influence the symmetry of connective patterns, the number of convective cells, and the time required to reach steady state.

In light of the results from this laboratory investigation on natural convection in the porous medium under unique experimental conditions, the following can be concluded:

- Convective heat transfer through air movement is more efficient than thermal conduction, and requires less time to achieve steady state temperature conditions.
- Convection with a higher Rayleigh number has a higher heat transfer rate.
- Convective patterns for natural air convection in a highly permeable porous medium are sensitive to boundary conditions. Small

temperature perturbation may change the symmetry, the cell numbers and directions, and the time required to reach steady state.

- Temperature fluctuation can occur near heating sources during convection with a certain level of Rayleigh numbers. It usually involves time-dependent oscillatory instabilities that impacts development of steady state conditions.
- Localized heating or cooling can stabilize convective patterns, but reduces heat transfer rates under the same conditions. Higher Rayleigh number may be required to initiate fluctuation for convection under localized heating or cooling conditions.
- Convection with higher Rayleigh numbers has faster convective air movement. However, velocity magnitudes vary in different directions.
- Without a porous medium in a large space, natural convection for pure air can easily occur because of large fluid Rayleigh numbers; as a result, steady state can be achieved rapidly.

This laboratory study aiming at a detailed understanding of the characteristics of natural air convection in a porous medium within a cylindrical tank was completed. Principles and literature review first provided a general comprehension of convection. Then, comparisons between conduction and convection, various convective temperature patterns, factors that influence these patterns and convective air movement modes were presented and discussed to illustrate detailed variations under this mechanism, based on this specific experimental setup.

However, the limitation of this study includes that only one medium material was tested; only one type of test enclosure (geometry) was used; and only one type of boundary condition (i.e. variable top-to-bottom temperatures with adiabatic wall) was adopted. This therefore reflects that the complexity of air convection is significant, which is one of the reasons that air convection is commonly excluded from thermal studies for projects in current cold region engineering practice. This study did not solve any specific problems of convection, but is intended to provide a concept that natural air convection in porous media is applicable for cold region geotechnical engineering, and is worth studying for engineers and researchers.

As an efficient and economical passive cooling approach, convective cooling is suitable for use in relatively long-term operation of engineering projects such as embankment roads, tailings covers, and rockfill dams. It should continue to be investigated experimentally and numerically to become more widely appreciated since it is an applicable and reliable geotechnical technology. Future research may include:

- laboratory investigations using the convective heat transfer cell assembled during this study and using different types of materials and boundary conditions;
- convective thermal modelling of these varied factors such as fluid flow, radiation, wind and global warming; and
- field experiments in cold regions using highly permeable materials such as crushed rock.

5 REFERENCES

Arenson, L.U., Chen, J., Pham, H., and Sego, D.C. 2007. Laboratory investigations on air convection in porous media, In Proceedings of the 60th Canadian Geotechnical Conference, Ottawa. pp. 340.

Arenson, L.U., and Sego, D.C. 2007. Protection of mine waste tailing ponds using cold air convection. In Assessment and Remediation of Contaminated Sites in the Arctic and Cold Climates (ARCSACC). Edited by K. Biggar, G. Cotta, M. Nahir, A. Mullick, J. Buchko, A. Ho, and S. Guigard. Edmonton, AB, Canada. May 7-8, 2007, pp. 256-264.

Arenson, L.U., Sego, D.C., and Newman, G. 2006. The use of a convective heat flow model in road designs for northern regions. In Climate Change Technology Conference. Ottawa, Ontario, Canada. May 10-12, 2006, CD-Rom.

Andersland, O. B. and Ladanyi, B. 2004. Frozen ground engineering, John Wiley & Sons.

Bau, H.H., and Torrance, K. E., 1982. Low Rayleigh number thermal convection in a vertical cylinder filled with porous materials and heated from below. Journal of Heat Transfer, ASME, pp. 166-172.

Bear, J. 1972. Dynamics of fluids in porous media. New York:Elsevier.

Burmeister, L.C. 1983. Convective heat transfer. Wiley, New York.

Carman, P.C. 1956. Flow of gases through porous media. London: Butterworths Scientific Publications.

Cheng, G.D., Lai, Y., Sun, Z., and Jiang, F. 2007. The “thermal semi-conductor” effect of crushed rocks. Permafrost and Periglacial Processes, 18 (2): 151-160.

Cheng, G.D., Sun, Z.Z., and Niu, F.J. 2008. Application of the roadbed cooling approach in Qinghai-Tibet railway engineering. Cold Regions Science and Technology, 53 (3): 241-258.

Elder, J.W., 1967a. Steady free convection in a porous medium heated from below. Journal of Fluid Mechanics, 27: 29-48.

Elder, J.W., 1967b. Transient convection in a porous medium. Journal of Fluid Mechanics, 27, Part 3: 609-623.

GEO-SLOPE, 2004. Thermal modelling with TEMP/W, an engineering methodology. GEO-SLOPE International Ltd., First Edition, May 2004.

Getling, A.V. 1998. Rayleigh-Bénard convection. Singapore: World Scientific, pp. 10-20, 99-101.

Goering, D.J. 1998. Experimental investigation of air convection embankments for permafrost-resistant roadway design. In Seventh International Conference on Permafrost. Edited by A.G. Lewkowicz and M. Allard. Yellowknife, NWT, Canada. June 23-27, 1998, Collection Nordicana, 57: 319-326.

Goering, D.J. 2002. Convective cooling in open rock embankments. Proc., 11th Int. Conf. on Cold Regions Engineering, ASCE, Reston, Va., 629–644.

Goering, D.J. 2003a. Thermal response of air convection embankments to ambient temperature fluctuations. Proceedings of Eight International Conference on Permafrost[C]. Zurich, Switzerland, pp.291-296.

Goering, D.J. 2003b. Passively cooled railway embankments for use in permafrost areas. Journal of Cold Regions Engineering, 17 (3): 119-133.

Goering, D.J., Instanes, A., and Knudsen, S. 2000. Convective heat transfer in railway embankment ballast. In International Symposium on Ground Freezing and Frost Action in Soils. Louvain-la-Neuve, Belgium. pp. 31-36.

Goering, D.J. and Kumar, P. 1999. Permeability effect on winter-time natural convection in gravel embankments. Advances in Cold Regions Thermal Engineering and Sciences, Springer, Berlin. pp. 455–464.

Goering, D.J., and Kumar, P. 1996. Winter-time convection in open-graded embankments. Cold Regions Science and Technology, 24 (1): 57-74.

Harris, S.A., and Pedersen, D.E. 1998. Thermal regimes beneath coarse blocky materials. Permafrost and Periglacial Processes, 9: 107-120.

He, P., Zhang, Z., Cheng, G.D., and Bing, H. 2007. Ventilation properties of blocky stones embankments. Cold Regions Science and Technology, 47 (3): 271-275.

Henderson, S.M., Perry, R.L., and Young, J.H. 1997. Principles of process engineering. 4th Edition, ASAE Publication, 1997.

Horne, R.N., and O’Sullivan, M.J. 1974. Oscillatory convection in a porous medium heated from below. Journal of Fluid Mechanics, 66, part 2: 339-352.

Horne, R.N., O'Sullivan, M.J. 1978. Origin of oscillatory convection in a porous medium heated from below. Physics of Fluids, 21, Issue 8: 1260-1264.

Jørgensen, A.S., Doré, G., Voyer, É., Chataigner, Y., and Gosselin, L. 2008. Assessment of the effectiveness of two heat removal techniques for permafrost protection. Cold Regions Science and Technology 53 (2): 179–192.

Kane, D.L., Hinkel, K.M., Goering, D.J. Hinzman, L.D., and Outcalt, S.I. 2001. Non-conductive heat transfer associated with frozen soils. Global and Planetary Change, 29: 275-292.

Kladias, N., and Prasad, V. 1990. Flow transitions in buoyancy-induced non-darcy convection in a porous medium heated from below, ASME Journal of Heat Transfer 112: 675-684.

Liu, Z., and Lai, Y. 2005. Numerical analysis for the ventilated embankment with thermal insulation layer in Qinghai-Tibet Railway. Cold Regions Science and Technology, 42: 177-184.

Lunardini, V.J. 1981. Heat transfer in cold climates. New York: van Nostrand Reinholdt.

Ma, W., Shi, C., Wu, Q., Zhang, L., and Wu, Z. 2006. Monitoring study on technology of the cooling roadbed in permafrost region of Qinghai-Tibet plateau. Cold Regions Science and Technology, 44: 1-11.

Ma, W., Feng, G.L., Wu, Q.B., and Wu, J.J. 2008. Analyses of temperature fields under the embankment with crushed-rock structures along the Qinghai-Tibet railway. Cold Regions Science and Technology, 53 (3): 259-270.

Mullarney, J.C., Griffiths, R.W., and Hughes, G.O. 2004. Convection driven by differential heating at a horizontal boundary. Journal of Fluid Mechanics, 516: 181–209.

Nield, D.A., and Bejan, A. 1999. Convection in porous media. 2nd Edition, Springer, New York.

Prasad, V., and Kulacki, F.A. 1985. Natural convection in porous media bounded by short concentric vertical cylinders. ASME Journal of Heat Transfer, 107: 147-54.

Prasad, V., and Kulacki, F.A. 1987. Natural convection in horizontal porous layers with localized heating from below. Journal of Heat Transfer, 109: 795–798.

Prasad, V., and Chui, A. 1989. Natural convection in a cylindrical porous enclosure with internal heat generation. ASME Journal of Heat Transfer, 111: 916-925.

Prasad, V., and Tian, Q. 1990. An experimental study of thermal convection in fluid. Superposed porous layers heated from below. Heat Transfer Proc., 9th. International Heat Transfer Conference, Jerusalem, 5: 207-212.

Quan, X.J., Li, N., and Li, G.Y. 2006. A new ripraped-rock slope for high temperature permafrost regions. Cold Regions Science and Technology, 45 (1): 42-50.

Rohsenow, W.M., Hartnett, J.P., and Cho, Y.I. 1998. Handbook of heat transfer. 3rd Edition, New York: McGraw-Hill.

Stewart, W.E., and Dona, C.L.G. 1988. Free convection in a heat generating porous medium in a finite vertical cylinder. ASME Journal of Heat Transfer, 110: 517–520.

Sun, B., Yang, L., Liu, Q., Wang, W., and Xu, X. 2009. Numerical analysis for critical thickness of crushed rock revetment layer on Qinghai–Tibet Railway. Cold Regions Science and Technology, 57 (2-3): 131–138.

Sun, B., Xu, X., Lai Y., Li, D., Wang, S., and Zhang, J. 2004. Experimental researches of thermal diffusivity and conductivity in embankment ballast under periodically fluctuating temperature. Cold Regions Science and Technology, 38(2/3):219-227.

Sun, Z. Ma, W. and Li, D. 2005. In situ test on cooling effectiveness of air convection embankment with crushed rock slope protection in permafrost regions. Journal of Cold Regions Engineering, 19 (2): 38-51.

Sutton, F.M. 1970. Onset of convection in a porous channel with net through flow. Physics of Fluids, 13: 1931–1934.

Turns, S.R. 2006. Thermodynamics: Concepts and Applications. New York: Cambridge University Press.

Wu, Q., Zhao, S., and Zhang, L. 2007. Qinghai-Xizang railroad construction in permafrost regions, Journal of Cold Regions Engineering, ASCE, 21(2): 60-67.

Wu, Q., Lu, Z., Zhang, T., Ma, W., and Liu, Y. 2008. Analysis of cooling effect of crushed rock-based embankment of the Qinghai-Xizang Railway. Cold Regions Science and Technology, 53 (3): 271-282.

Yu, W.B., Lai, Y.M., and Zhang, X.F. 2004. Laboratory investigation on cooling effect of coarse rock layer and fine rock layer in permafrost regions. Cold Regions Science and Technology, 38 (1): 31-42.

Yu, W.B., Lai, Y.M., Sun, Z.Z., Jin, H.J., and Zhang, X.F. 2006. Experimental studies on the ripped-rock revetment embankment in permafrost regions of the Qinghai-Tibet railroad. Cold Regions Science and Technology, 45 (1): 1-7.

Zebib, A. 1978. Onset of natural convection in a cylinder of water saturated porous media. Physics of Fluids, 21 (4): 699-700.

Zhang, M.Y., Lai, Y.M., Yu, W.B., and Huang, Z. 2007. Experimental study on influence of particle size on cooling effect of crushed-rock layer under closed and open tops. Cold Regions Science and Technology, 48 (3): 232-238.

Zhang, M.Y., Lai, Y.M., Gao, Z.H., and Yu, W.B. 2006. Influence of boundary conditions on the cooling effect of crushed-rock embankment in permafrost regions of Qinghai-Tibetan Plateau. Cold Regions Science and Technology, 44: 225-239.

Zhang, M.Y., Zhang, J.M. and Lai, Y.M. 2005. Numerical analysis for critical height of railway embankment in permafrost regions of Qinghai–Tibetan Plateau. Cold Regions Science and Technology, 41 (2): 111–120.

6 APPENDICES

Appendix I List of Tests

Test Type	No.	Top-to-bottom Temperature Difference °C	Bottom Temperature °C	Top Temperature °C	Cooling and/or Heating Means	Notes
Convection in Empty Test Tank	1	5	30	25	Heating Below	
	2	10	30	20	Cooling Above	Continued from Test No.1
	3	20	35	15	Heating Below & Cooling Above	Continued from Test No.2
	4	25	35	10	Cooling Above	Continued from Test No.3
	5	30	40	10	Heating Below & Cooling Above	
Conduction in Empty Test Tank	6	15	25	40	Heating Above	
	7	30	10	40	Heating Above	
Convection Using Styrofoam Chips in Test Tank	8	5	28	23	Heating Below	Transient patterns
	9	10	33	23	Heating Below	Transient patterns; CS1
	10	10	33	23	Heating Below	CS1 and CS2
	11	20	43	23	Heating Below	Continued from Test No.10
	12	30	53	23	Heating Below	Continued from Test No.11
	13	50	53	3	Heating Below & Cooling Above	
	14	60	63	3	Heating Below & Cooling Above	
	15	10	23	13	Cooling Above	Transient patterns

	16	20	30	10	Cooling Above	Continued from Test No.18
	17	30	40	10	Cooling Above	
	18	40	50	10	Cooling Above	Continued from Test No.17
	19	40	53	13	Cooling Above	Continued from Test No.12
	20	10	22.5	12.5	Cooling Above	Rotation check
	21	40	52.5	12.5	Heating Below & Cooling Above	Rotation check
	22	10	32	22	Localized Heating Below	Transient patterns
	23	20	42	22	Localized Heating Below	Continued from Test No.22
	24	30	52	22	Localized Heating Below	Continued from Test No.23
	25	60	63	3	Localized Heating Below	
	26	10	20.5	10.5	Localized Cooling Above	Transient patterns
	27	15	20.5	5.5	Localized Cooling Above	Continued from Test No.26
	28	20	21	1	Localized Cooling Above	Continued from Test No.27
Conduction Using Styrofoam Chips in Test Tank	29	20	23	43	Heating Above	
	30	20	15	35	Cooling below & Heating above	

Appendix II Measured Temperature Data for Generation of Contours

The temperature data were calibrated and are presented here following the order of the test No. shown in Appendix I. Thermistor positions are shown as follows:

Thermistor positions for Tests No. 1-9, 15-18 and 30 (no CS2):

Instrumentation section: CS1

Height (cm)	0	15	45	60	90	110	120		
154				•		•		154	Top
135		•	•	•	•	•		135	
115		•		•	•	•		115	
95			•	•	•	•		95	
75		•		•	•	•		75	
55		•	•	•	•	•		55	
35		•	•	•	•	•		35	
15		•	•	•	•	•		15	
0				•		•		0	Bottom
	0	15	45	60	90	110	120		

Diameter (cm)

Thermistor positions for other tests (CS1 and CS2):

Instrumentation section: CS1

Height (cm)	0	10	40	60	90	110	120		
154		•		•		•		154	Top
135		•	•	•	•	•		135	
115		•	•	•	•	•		115	
95		•	•	•	•	•		95	
75		•	•	•	•	•		75	
55		•	•	•	•	•		55	
35		•	•	•	•	•		35	
15		•	•	•	•	•		15	
0				•		•		0	Bottom
	0	10	40	60	90	110	120		

A' Diameter (cm) A

Instrumentation section: CS2

Height (cm)	0	20	40	60	80	100	120		
154								154	Top
124		•	•		•	•		124	
93		•	•		•	•		93	
62		•	•		•	•		62	
31		•	•		•	•		31	
0								0	Bottom
	0	20	40	60	80	100	120		

B Diameter (cm) B'

• Thermistor

Convection in Empty Test Tank

Test No. 1 Top-To-Bottom **ΔT=5°C (B30-T25)**

Recorded at: 30/01/2007 11:30

Test started at: 26/01/2007 16:04

(Heating below)

Instrumentation section: CS1

Condition: Steady State Unit: °C

Height (cm)	0	15	45	60	90	110	120		
154				25.7		25.7		154	Top
135		26.3	26.4	26.4	26.4	26.3		135	
115		26.4		26.4	26.5	26.3		115	
95			26.5	26.5	26.5	26.4		95	
75		26.4		26.3	26.6	26.4		75	
55		26.4	26.5	26.5	26.5	26.6		55	
35		26.5	26.6	26.5	26.6	26.7		35	
15		26.6	26.6	26.6	26.7	26.7		15	
0				28.2		27.8		0	Bottom
	0	15	45	60	90	110	120		

Diameter (cm)

Test No. 2 Top-To-Bottom **ΔT=10°C (B30-T20)**

Recorded at: 01/02/2007 17:00

Test started at: 30/01/2007 11:37

(Cooling above; continued from Test No. 1)

Instrumentation section: CS1

Condition: Steady State Unit: °C

Height (cm)	0	15	45	60	90	110	120		
154				22.8		22.8		154	Top
135		24.6	24.6	24.7	24.6	24.6		135	
115		24.6		24.7	24.7	24.5		115	
95			24.7	24.7	24.8	24.7		95	
75		24.7		24.4	24.9	24.6		75	
55		24.8	24.8	24.8	24.7	24.8		55	
35		24.8	24.9	24.8	24.9	25.0		35	
15		24.9	24.9	24.9	25.0	25.1		15	
0				27.1		27.1		0	Bottom
	0	15	45	60	90	110	120		

Diameter (cm)

Test No. 3 Top-To-Bottom **ΔT=20°C (B35-T15)**

Recorded at: 02/02/2007 19:00

Test started at: 01/02/2007 17:36

(Heating below and cooling above; continued from Test No. 2)

Instrumentation section: CS1

Condition: Steady State Unit: °C

Height (cm)	0	15	45	60	90	110	120		
154				21.3		21.3		154	Top
135		24.8	25.0	25.0	25.0	24.9		135	
115		25.0		25.1	25.1	24.8		115	
95			25.2	25.2	25.1	25.0		95	
75		25.2		24.9	25.3	25.0		75	
55		25.3	25.2	25.3	25.1	25.2		55	
35		25.4	25.3	25.3	25.3	25.5		35	
15		25.6	25.5	25.4	25.4	25.6		15	
0				29.5		29.5		0	Bottom
	0	15	45	60	90	110	120		

Diameter (cm)

Test No. 4 Top-To-Bottom **ΔT=25°C (B35-T10)**

Recorded at: 05/02/2007 11:00

Test started at: 01/02/2007 19:30

(Cooling above; continued from Test No. 3)

Instrumentation section: CS1

Condition: Steady State Unit: °C

Height (cm)	0	15	45	60	90	110	120		
154				18.4		18.4		154	Top
135		22.8	22.9	23.0	23.0	22.9		135	
115		22.9		23.1	23.1	22.9		115	
95			23.2	23.2	23.2	23.2		95	
75		23.2		22.9	23.4	23.2		75	
55		23.3	23.3	23.3	23.2	23.4		55	
35		23.4	23.3	23.3	23.4	23.6		35	
15		23.6	23.5	23.5	23.5	23.8		15	
0				28.4		28.1		0	Bottom
	0	15	45	60	90	110	120		

Diameter (cm)

Test No. 5 Top-To-Bottom **ΔT=30°C (B40-T10)**

Recorded at: 18/01/2007 16:00

Test started at: 16/01/2007 13:00

(Heating below and cooling above)

Instrumentation section: CS1

Condition: Steady State Unit: °C

Height (cm)	0	15	45	60	90	110	120		
154				19.9		20.0		154	Top
135		25.1	25.3	25.4	25.4	25.3		135	
115		25.3		25.5	25.5	25.3		115	
95			25.5	25.6	25.7	25.6		95	
75		25.5		25.3	25.8	25.7		75	
55		25.6	25.7	25.7	25.7	25.9		55	
35		25.8	25.8	25.7	25.9	26.1		35	
15		26.2	26.0	26.0	26.1	26.3		15	
0				31.8		31.6		0	Bottom
	0	15	45	60	90	110	120		

Diameter (cm)

Conduction in Empty Test Tank

Test No. 6 Top-To-Bottom **ΔT=15°C (B25-T40)**

Recorded at: 22/01/2007 12:00

Test started at: 19/01/2007 16:20

(Heating above)

Instrumentation section: CS1

Condition: Steady State Unit: °C

Height (cm)	0	15	45	60	90	110	120		
154				35.1		35.2		154	Top
135		30.7	30.8	30.8	30.8	30.7		135	
115		30.3		30.1	30.3	30.3		115	
95			29.9	29.9	30.0	30.0		95	
75		29.7		29.6	29.5	29.7		75	
55		29.5	29.5	29.5	29.7	29.5		55	
35		29.3	29.2	29.1	29.2	29.3		35	
15		29.0	28.9	29.0	29.0	29.0		15	
0				27.0		27.1		0	Bottom
	0	15	45	60	90	110	120		

Diameter (cm)

Test No. 7 Top-To-Bottom **ΔT=30°C (B10-T40)**

Recorded at: 24/01/2007 14:30

Test started at: 22/01/2007 15:56

(Heating above)

Instrumentation section: CS1

Condition: Steady State Unit: °C

Height (cm)	0	15	45	60	90	110	120		
154				32.8		32.9		154	Top
135		25.5	25.5	25.6	25.5	25.5		135	
115		24.7		24.6	24.7	24.7		115	
95			24.1	24.1	24.2	24.2		95	
75		23.7		23.6	23.2	23.7		75	
55		23.2	23.2	23.2	23.7	23.3		55	
35		22.7	22.6	22.5	22.6	22.7		35	
15		21.9	21.9	21.9	21.9	22.0		15	
0				15.1		16.2		0	Bottom
	0	15	45	60	90	110	120		

Diameter (cm)

Convection Using Styrofoam Chips in Test Tank

Test No. 8 Top-To-Bottom **ΔT=5°C (B28-T23)**

Recorded at: 07/06/2007 20:00 (1h)

Test started at: 07/06/2007 18:54

(Heating below)

Instrumentation section: CS1

Condition: Transient Pattern Unit: °C

Height (cm)	0	15	45	60	90	110	120	
154				22.6		23.2		154 Top
135		24.3	23.6	23.8	24.0	24.5		135
115		24.5		23.9	24.2	24.2		115
95			23.9	24.0	24.1	24.2		95
75		23.5		23.5	23.5	23.4		75
55		23.1	23.5	23.6	23.7	22.4		55
35		23.0	23.9	24.1	23.7	23.0		35
15		23.5	24.8	25.2	24.5	23.2		15
0				26.3		26.2		0 Bottom
	0	15	45	60	90	110	120	

Diameter (cm)

Test No. 8 Top-To-Bottom **ΔT=5°C (B28-T23)**

Recorded at: 07/06/2007 21:00 (2h)

Test started at: 07/06/2007 18:54

(Heating below)

Instrumentation section: CS1

Condition: Transient Pattern Unit: °C

Height (cm)	0	15	45	60	90	110	120	
154				22.7		23.2		154 Top
135		24.2	23.6	23.9	23.9	24.2		135
115		24.3		24.0	24.2	24.0		115
95			24.1	24.3	24.2	24.2		95
75		23.7		24.0	24.3	23.6		75
55		23.4	24.5	24.8	24.1	22.7		55
35		23.3	25.1	25.5	24.6	23.3		35
15		23.7	25.7	26.3	25.1	23.4		15
0				27.1		26.7		0 Bottom
	0	15	45	60	90	110	120	

Diameter (cm)

Test No. 8 Top-To-Bottom **ΔT=5°C (B28-T23)**

Recorded at: 07/06/2007 22:00 (3h)

Test started at: 07/06/2007 18:54

(Heating below)

Instrumentation section: CS1

Condition: Transient Pattern Unit: °C

Height (cm)	0	15	45	60	90	110	120	
154				22.7		23.1		154 Top
135		24.0	23.7	24.0	23.9	24.0		135
115		24.3		24.2	24.3	24.0		115
95			24.4	24.6	24.4	24.2		95
75		23.8		24.6	24.6	23.7		75
55		23.6	24.9	25.3	24.4	22.8		55
35		23.5	25.4	25.9	24.9	23.4		35
15		23.9	26.0	26.6	25.3	23.5		15
0				27.3		26.8		0 Bottom
	0	15	45	60	90	110	120	

Diameter (cm)

Test No. 8 Top-To-Bottom **ΔT=5°C (B28-T23)**

Recorded at: 08/06/2007 0:00 (5h)

Test started at: 07/06/2007 18:54

(Heating below)

Instrumentation section: CS1

Condition: Transient Pattern Unit: °C

Height (cm)	0	15	45	60	90	110	120	
154				22.7		23.0		154 Top
135		23.7	23.7	24.1	23.9	23.7		135
115		24.1		24.4	24.3	23.8		115
95			24.6	24.9	24.5	24.1		95
75		23.9		24.9	24.9	23.8		75
55		23.7	25.1	25.5	24.6	23.0		55
35		23.7	25.6	26.1	25.1	23.6		35
15		24.1	26.1	26.8	25.5	23.8		15
0				27.5		27.0		0 Bottom
	0	15	45	60	90	110	120	

Diameter (cm)

Test No. 8 Top-To-Bottom **ΔT=5°C (B28-T23)**

Recorded at: 08/06/2007 5:00 (10h)

Test started at: 07/06/2007 18:54

(Heating below)

Instrumentation section: CS1

Condition: Transient Pattern Unit: °C

Height (cm)	0	15	45	60	90	110	120		
154				22.7		22.9		154	Top
135		23.3	23.7	24.1	23.6	23.2		135	
115		23.7		24.5	24.2	23.3		115	
95			24.6	25.0	24.5	23.9		95	
75		23.8		25.0	25.1	23.8		75	
55		23.8	25.2	25.7	24.7	23.1		55	
35		23.8	25.7	26.3	25.3	23.9		35	
15		24.4	26.3	27.0	25.8	24.2		15	
0				27.6		27.2		0	Bottom
	0	15	45	60	90	110	120		

Diameter (cm)

Test No. 8 Top-To-Bottom **ΔT=5°C (B28-T23)**

Recorded at: 08/06/2007 18:00 (23h)

Test started at: 07/06/2007 18:54

(Heating below)

Instrumentation section: CS1

Condition: Steady State Unit: °C

Height (cm)	0	15	45	60	90	110	120		
154				22.7		22.8		154	Top
135		22.9	23.6	24.0	23.5	22.9		135	
115		23.1		24.4	24.0	22.9		115	
95			24.4	25.0	24.3	23.5		95	
75		23.4		25.0	25.1	23.6		75	
55		23.5	25.1	25.6	24.7	23.1		55	
35		23.8	25.6	26.2	25.5	24.1		35	
15		24.5	26.2	27.0	26.1	24.6		15	
0				27.7		27.3		0	Bottom
	0	15	45	60	90	110	120		

Diameter (cm)

Test No. 9 Top-To-Bottom **ΔT=10°C (B33-T23)**

Recorded at: 09/06/2007 16:00 (1h)

Test started at: 09/06/2007 15:00

(Heating below)

Instrumentation section: CS1

Condition: Transient Pattern Unit: °C

Height (cm)	0	15	45	60	90	110	120		
154				22.6		22.8		154	Top
135		22.4	22.8	23.1	22.9	22.6		135	
115		22.4		23.0	23.0	22.4		115	
95			22.9	23.2	23.2	22.9		95	
75		22.5		23.1	23.7	22.9		75	
55		22.6	23.2	23.5	23.3	22.5		55	
35		23.1	24.2	24.5	24.5	23.7		35	
15		24.3	26.1	26.3	26.2	24.5		15	
0				29.0		29.1		0	Bottom
	0	15	45	60	90	110	120		

Diameter (cm)

Test No. 9 Top-To-Bottom **ΔT=10°C (B33-T23)**

Recorded at: 09/06/2007 16:30 (1.5h)

Test started at: 09/06/2007 15:00

(Heating below)

Instrumentation section: CS1

Condition: Transient Pattern Unit: °C

Height (cm)	0	15	45	60	90	110	120		
154				22.6		22.8		154	Top
135		22.4	22.9	23.2	22.9	22.6		135	
115		22.5		23.2	23.1	22.5		115	
95			23.3	23.8	23.5	23.0		95	
75		22.7		24.7	25.3	23.1		75	
55		22.9	25.6	26.5	24.1	22.9		55	
35		23.4	26.9	27.9	26.2	24.0		35	
15		24.2	28.0	28.9	27.3	24.5		15	
0				30.4		30.0		0	Bottom
	0	15	45	60	90	110	120		

Diameter (cm)

Test No. 9 Top-To-Bottom **ΔT=10°C (B33-T23)**
Recorded at: 09/06/2007 17:00 (2h)
Test started at: 09/06/2007 15:00
(Heating below)
Instrumentation section: CS1
Condition: Transient Pattern Unit: °C

Height (cm)	0	15	45	60	90	110	120		
154				22.6		22.8		154	Top
135		22.5	23.2	23.6	23.2	22.7		135	
115		22.7		24.8	23.9	22.7		115	
95			25.4	26.1	24.7	23.4		95	
75		23.1		26.7	26.1	23.6		75	
55		23.2	26.5	27.7	25.4	23.1		55	
35		23.5	27.3	28.6	26.7	24.1		35	
15		24.2	28.2	29.6	27.5	24.6		15	
0				31.1		30.4		0	Bottom
	0	15	45	60	90	110	120		

Diameter (cm)

Test No. 9 Top-To-Bottom **ΔT=10°C (B33-T23)**
Recorded at: 09/06/2007 18:00 (3h)
Test started at: 09/06/2007 15:00
(Heating below)
Instrumentation section: CS1
Condition: Transient Pattern Unit: °C

Height (cm)	0	15	45	60	90	110	120		
154				22.8		22.8		154	Top
135		23.1	24.9	25.5	24.4	23.2		135	
115		23.5		26.4	25.3	23.3		115	
95			26.3	27.2	25.6	23.8		95	
75		23.5		27.3	26.7	23.9		75	
55		23.5	26.9	28.2	26.1	23.4		55	
35		23.6	27.5	29.0	27.1	24.3		35	
15		24.3	28.4	30.0	27.7	24.7		15	
0				31.6		30.7		0	Bottom
	0	15	45	60	90	110	120		

Diameter (cm)

Test No. 9 Top-To-Bottom **ΔT=10°C (B33-T23)**
Recorded at: 09/06/2007 21:00 (6h)
Test started at: 09/06/2007 15:00
(Heating below)
Instrumentation section: CS1
Condition: Transient Pattern Unit: °C

Height (cm)	0	15	45	60	90	110	120		
154				23.0		22.9		154	Top
135		23.6	25.7	26.3	25.1	23.6		135	
115		24.0		27.1	26.0	23.8		115	
95			26.8	27.7	26.3	24.3		95	
75		23.9		27.8	27.2	24.4		75	
55		23.9	27.1	28.5	26.7	23.8		55	
35		24.0	27.7	29.3	27.7	24.7		35	
15		24.5	28.5	30.3	28.3	25.2		15	
0				32.1		31.1		0	Bottom
	0	15	45	60	90	110	120		

Diameter (cm)

Test No. 9 Top-To-Bottom **ΔT=10°C (B33-T23)**
Recorded at: 10/06/2007 1:00 (10h)
Test started at: 09/06/2007 15:00
(Heating below)
Instrumentation section: CS1
Condition: Transient Pattern Unit: °C

Height (cm)	0	15	45	60	90	110	120		
154				23.1		23.0		154	Top
135		23.7	25.8	26.5	25.3	23.8		135	
115		24.2		27.3	26.2	24.0		115	
95			27.0	27.9	26.6	24.6		95	
75		24.2		27.9	27.6	24.7		75	
55		24.2	27.3	28.7	27.0	24.3		55	
35		24.3	27.8	29.4	28.1	25.2		35	
15		24.8	28.6	30.4	28.7	25.7		15	
0				32.2		31.2		0	Bottom
	0	15	45	60	90	110	120		

Diameter (cm)

Test No. 9 Top-To-Bottom **ΔT=10°C (B33-T23)**

Recorded at: 10/06/2007 7:00 (16h)

Test started at: 09/06/2007 15:00

(Heating below)

Instrumentation section: CS1

Condition: Transient Pattern Unit: °C

Height (cm)	0	15	45	60	90	110	120		
154				23.1		23.0		154	Top
135		23.8	25.9	26.7	25.5	23.9		135	
115		24.3		27.4	26.4	24.2		115	
95			27.1	28.0	26.8	24.9		95	
75		24.4		28.1	27.9	25.1		75	
55		24.4	27.3	28.7	27.3	24.7		55	
35		24.5	27.8	29.5	28.4	25.7		35	
15		25.1	28.7	30.5	29.1	26.2		15	
0				32.2		31.3		0	Bottom
	0	15	45	60	90	110	120		

Diameter (cm)

Test No. 9 Top-To-Bottom **ΔT=10°C (B33-T23)**

Recorded at: 10/06/2007 11:00 (20h)

Test started at: 09/06/2007 15:00

(Heating below)

Instrumentation section: CS1

Condition: Transient Pattern Unit: °C

Height (cm)	0	15	45	60	90	110	120		
154				23.1		23.0		154	Top
135		23.8	26.0	26.7	25.6	24.0		135	
115		24.3		27.5	26.5	24.4		115	
95			27.1	28.1	26.9	25.0		95	
75		24.5		28.1	28.1	25.2		75	
55		24.5	27.3	28.7	27.4	24.9		55	
35		24.6	27.8	29.4	28.6	25.9		35	
15		25.2	28.7	30.4	29.3	26.5		15	
0				32.2		31.4		0	Bottom
	0	15	45	60	90	110	120		

Diameter (cm)

Test No. 9 Top-To-Bottom **ΔT=10°C (B33-T23)**

Recorded at: 11/06/2007 11:00 (44h)

Test started at: 09/06/2007 15:00

(Heating below)

Instrumentation section: CS1

Condition: Steady State Unit: °C

Height (cm)	0	15	45	60	90	110	120	
154				23.1		23.0		154 Top
135		23.7	26.0	26.9	26.0	24.5		135
115		24.3		27.6	27.0	25.0		115
95			27.0	28.0	27.3	25.7		95
75		24.5		27.8	28.5	26.0		75
55		24.5	26.9	28.2	27.8	25.7		55
35		24.6	27.2	28.8	29.0	26.9		35
15		25.2	28.1	29.9	29.8	27.6		15
0				32.2		31.4		0 Bottom
	0	15	45	60	90	110	120	

Diameter (cm)

Test No.10 Top-To-Bottom **ΔT=10°C (B33-T23)**

Recorded at: 12/09/2007 13:30
Test started at: 10/09/2007 16:52
(Heating below)

Instrumentation section: CS1
Condition: Steady State Unit: °C

Height (cm)	0	10	40	60	90	110	120		
154		23.0		23.0		23.2		154	Top
135		23.6	25.9	27.2	27.8	26.3		135	
115		24.0	26.5	27.7	28.6	27.2		115	
95		24.0	26.3	27.7	28.7	27.6		95	
75		24.2	26.1	27.5	28.3	26.7		75	
55		24.2	26.2	27.7	28.7	25.9		55	
35		24.3	26.9	28.5	29.4	26.9		35	
15		25.0	28.0	29.8	30.3	28.0		15	
0				32.2		31.4		0	Bottom
	0	10	40	60	90	110	120		
A'				Diameter (cm)				A	

Instrumentation section: CS2
Condition: Steady State Unit: °C

Height (cm)	0	20	40	60	80	100	120		
154								154	Top
124		25.5	27.3		26.7	25.1		124	
93		25.6	27.3		26.5	25.0		93	
62		25.4	27.3		26.6	24.8		62	
31		25.4	27.7		27.2	24.9		31	
0								0	Bottom
	0	20	40	60	80	100	120		
B				Diameter (cm)				B'	

Test No.11 Top-To-Bottom **ΔT=20°C (B43-T23)**

Recorded at: 13/09/2007 13:30

Test started at: 12/09/2007 13:40

(Heating below; continued from Test No. 10)

Instrumentation section: CS1

Condition: Steady State Unit: °C

Height (cm)	0	10	40	60	90	110	120		
154		23.4		24.2		24.2		154	Top
135		26.4	31.2	32.9	33.1	29.9		135	
115		26.9	31.7	33.3	34.1	31.3		115	
95		26.8	31.0	33.5	34.4	31.8		95	
75		26.8	30.4	33.0	34.3	31.2		75	
55		26.8	30.1	33.2	35.1	30.5		55	
35		26.7	30.6	34.4	35.8	31.8		35	
15		27.3	32.2	36.6	36.9	33.3		15	
0				41.3		39.6		0	Bottom
	0	10	40	60	90	110	120		
A'				Diameter (cm)				A	

Instrumentation section: CS2

Condition: Steady State Unit: °C

Height (cm)	0	20	40	60	80	100	120		
154								154	Top
124		29.5	32.8		32.0	29.4		124	
93		29.5	32.6		31.4	28.7		93	
62		29.2	32.3		31.0	28.0		62	
31		28.6	32.0		31.4	27.6		31	
0								0	Bottom
	0	20	40	60	80	100	120		
B				Diameter (cm)				B'	

Test No.12 Top-To-Bottom **ΔT=30°C (B53-T23)**

Recorded at: 14/09/2007 12:30

Test started at: 13/09/2007 13:40

(Heating below; continued from Test No. 11)

Instrumentation section: CS1

Condition: Steady State Unit: °C

Height (cm)	0	10	40	60	90	110	120		
154		24.2		25.5		25.7		154	Top
135		29.4	36.5	38.8	39.2	35.0		135	
115		29.9	36.4	38.8	40.2	36.5		115	
95		29.4	35.1	38.4	40.6	37.2		95	
75		29.2	33.9	37.3	40.8	37.5		75	
55		29.1	32.9	37.0	41.9	37.5		55	
35		28.8	33.1	38.4	42.7	39.2		35	
15		29.2	35.0	41.6	44.2	41.3		15	
0				50.0		47.6		0	Bottom
	0	10	40	60	90	110	120		

A' Diameter (cm) A

Instrumentation section: CS2

Condition: Steady State Unit: °C

Height (cm)	0	20	40	60	80	100	120		
154								154	Top
124		34.3	38.3		37.2	33.7		124	
93		33.8	37.4		35.8	32.2		93	
62		32.8	36.2		34.6	31.1		62	
31		31.5	34.7		34.8	30.4		31	
0								0	Bottom
	0	20	40	60	80	100	120		

B Diameter (cm) B'

Test No.13 Top-To-Bottom **ΔT=50°C (B53-T3)**

Recorded at: 16/12/2007 20:40

Test started at: 14/12/2007 16:45

(Heating below and cooling above)

Instrumentation section: CS1

Condition: Steady State Unit: °C

Height (cm)	0	10	40	60	90	110	120		
154		7.0		11.6		11.9		154	Top
135		19.2	30.5	33.0	34.1	32.4		135	
115		19.7	28.9	31.1	34.0	33.9		115	
95		19.1	26.1	29.2	33.5	34.7		95	
75		19.0	24.3	27.0	31.4	35.0		75	
55		19.1	22.2	24.5	29.2	35.5		55	
35		19.1	21.0	23.1	27.6	35.8		35	
15		19.5	21.2	29.6	27.3	35.8		15	
0				46.5		45.7		0	Bottom
	0	10	40	60	90	110	120		
A'			Diameter (cm)					A	

Instrumentation section: CS2

Condition: Steady State Unit: °C

Height (cm)	0	20	40	60	80	100	120		
154								154	Top
124		32.3	34.1		30.6	20.3		124	
93		30.4	31.1		27.4	20.2		93	
62		28.0	27.0		24.0	19.7		62	
31		28.2	24.7		21.2	18.9		31	
0								0	Bottom
	0	20	40	60	80	100	120		
B			Diameter (cm)					B'	

Test No.13 Top-To-Bottom **ΔT=50°C (B53-T3)**

Recorded at: 15/12/2007 15:10

Test started at: 14/12/2007 16:45

(Heating below and cooling above; oscillation)

Instrumentation section: CS1

Condition: Transient Pattern Unit: °C

Height (cm)	0	10	40	60	90	110	120		
154		6.9		11.4		12.1		154	Top
135		17.8	28.4	31.0	31.8	29.2		135	
115		18.2	26.6	29.0	30.9	29.6		115	
95		17.8	24.0	27.3	29.9	29.4		95	
75		18.0	22.3	24.9	27.9	28.8		75	
55		18.1	21.1	23.6	26.1	29.5		55	
35		18.3	26.0	26.5	24.9	32.5		35	
15		19.0	31.8	28.0	23.7	36.5		15	
0		46.1		46.4		46.1		0	Bottom
	0	10	40	60	90	110	120		

Diameter (cm)

Test No.13 Top-To-Bottom **ΔT=50°C (B53-T3)**

Recorded at: 15/12/2007 15:17

Test started at: 14/12/2007 16:45

(Heating below and cooling above; oscillation)

Instrumentation section: CS1

Condition: Transient Pattern Unit: °C

Height (cm)	0	10	40	60	90	110	120		
154		6.9		11.4		12.1		154	Top
135		17.8	28.4	30.9	31.7	29.2		135	
115		18.1	26.5	28.5	30.6	29.5		115	
95		17.8	23.7	26.7	29.6	29.5		95	
75		18.0	22.3	25.3	27.8	28.9		75	
55		18.1	21.5	25.7	26.2	29.4		55	
35		18.3	22.1	25.7	25.3	32.4		35	
15		18.9	23.6	24.8	24.0	36.5		15	
0				46.2		46.3		0	Bottom
	0	10	40	60	90	110	120		

Diameter (cm)

Test No.13 Top-To-Bottom **ΔT=50°C (B53-T3)**
Recorded at: 15/12/2007 15:25
Test started at: 14/12/2007 16:45
(Heating below and cooling above; oscillation)
Instrumentation section: CS1
Condition: Transient Pattern Unit: °C

Height (cm)	0	10	40	60	90	110	120		
154		7.0		11.3		12.0		154	Top
135		17.8	28.2	30.7	31.6	29.2		135	
115		18.2	26.4	28.6	30.7	29.6		115	
95		17.8	24.0	27.6	30.0	29.6		95	
75		18.0	22.6	26.1	28.1	29.0		75	
55		18.1	20.9	24.4	26.6	29.3		55	
35		18.2	20.0	22.5	25.3	32.4		35	
15		18.8	22.8	22.1	23.9	36.4		15	
0				45.9		46.2		0	Bottom
	0	10	40	60	90	110	120		

Diameter (cm)

Test No.13 Top-To-Bottom **ΔT=50°C (B53-T3)**
Recorded at: 15/12/2007 15:35
Test started at: 14/12/2007 16:45
(Heating below and cooling above; oscillation)
Instrumentation section: CS1
Condition: Transient Pattern Unit: °C

Height (cm)	0	10	40	60	90	110	120		
154		7.0		11.4		12.1		154	Top
135		17.9	28.4	31.0	31.8	29.3		135	
115		18.2	26.7	29.0	30.8	29.6		115	
95		17.8	24.0	27.3	30.0	29.6		95	
75		17.9	22.4	24.9	27.9	28.9		75	
55		18.1	21.0	23.4	26.2	29.6		55	
35		18.3	25.9	26.4	24.8	32.7		35	
15		19.0	31.8	28.1	23.6	36.3		15	
0				46.3		46.0		0	Bottom
	0	10	40	60	90	110	120		

Diameter (cm)

Test No.14 Top-To-Bottom **ΔT=60°C (B63-T3)**

Recorded at: 18/12/2007 22:00

Test started at: 17/12/2007 13:28

(Heating below and cooling above)

Instrumentation section: CS1

Condition: Steady State Unit: °C

Height (cm)	0	10	40	60	90	110	120	
154		8.1		14.1		14.4		154 Top
135		20.6	35.2	38.5	41.8	40.9		135
115		21.6	33.0	35.8	41.6	42.8		115
95		20.9	29.5	33.3	40.7	43.9		95
75		20.7	27.4	30.6	37.6	44.5		75
55		20.7	25.0	27.6	35.0	45.2		55
35		20.7	23.7	25.9	33.1	45.9		35
15		21.0	23.9	32.0	34.6	47.4		15
0				55.6		53.7		0 Bottom
	0	10	40	60	90	110	120	

A' Diameter (cm) A

Instrumentation section: CS2

Condition: Steady State Unit: °C

Height (cm)	0	20	40	60	80	100	120	
154								154 Top
124		34.6	38.7		36.1	24.4		124
93		33.0	35.0		31.6	24.5		93
62		29.6	30.2		27.5	23.5		62
31		27.8	29.2		24.5	22.2		31
0								0 Bottom
	0	20	40	60	80	100	120	

B Diameter (cm) B'

Test No. 15 Top-To-Bottom **ΔT=10°C (B33-T23)**
Recorded at: 07/09/2007 17:00 (1h)
Test started at: 07/09/2007 16:00
(Cooling above)
Instrumentation section: CS1
Condition: Transient Pattern Unit: °C

Height (cm)	0	15	45	60	90	110	120	
154				16.5		16.7		154 Top
135		20.2	20.5	21.8	23.2	22.9		135
115		21.3		22.8	24.0	23.4		115
95			22.2	22.8	24.0	23.8		95
75		22.0		22.6	23.1	22.7		75
55		21.8	22.0	22.2	22.4	21.5		55
35		21.8	22.0	22.1	22.3	21.9		35
15		22.0	22.1	22.2	22.4	21.9		15
0				22.7		22.7		0 Bottom
	0	15	45	60	90	110	120	

Diameter (cm)

Test No. 15 Top-To-Bottom **ΔT=10°C (B33-T23)**
Recorded at: 07/09/2007 19:00 (3h)
Test started at: 07/09/2007 16:00
(Cooling above)
Instrumentation section: CS1
Condition: Transient Pattern Unit: °C

Height (cm)	0	15	45	60	90	110	120	
154				14.1		14.5		154 Top
135		17.6	17.1	20.7	23.0	23.0		135
115		18.6		21.1	23.3	23.2		115
95			18.8	20.8	23.0	23.2		95
75		20.5		20.3	22.0	22.2		75
55		20.8	19.5	20.2	21.7	21.2		55
35		21.2	19.9	20.4	21.9	21.9		35
15		21.8	20.9	21.1	22.3	22.0		15
0				22.8		22.7		0 Bottom
	0	15	45	60	90	110	120	

Diameter (cm)

Test No. 15 Top-To-Bottom **ΔT=10°C (B33-T23)**
Recorded at: 07/09/2007 21:00 (5h)
Test started at: 07/09/2007 16:00
(Cooling above)
Instrumentation section: CS1
Condition: Transient Pattern Unit: °C

Height (cm)	0	15	45	60	90	110	120		
154				13.9		14.2		154	Top
135		16.8	16.8	20.2	22.5	22.8		135	
115		18.1		20.7	22.9	22.8		115	
95			18.2	20.2	22.5	22.8		95	
75		20.1		19.8	21.0	21.8		75	
55		20.5	18.9	19.5	21.5	20.9		55	
35		20.9	19.3	19.5	21.1	21.7		35	
15		21.5	20.0	20.0	21.6	21.9		15	
0				22.8		22.8		0	Bottom
	0	15	45	60	90	110	120		

Diameter (cm)

Test No. 15 Top-To-Bottom **ΔT=10°C (B33-T23)**
Recorded at: 07/09/2007 23:00 (7h)
Test started at: 07/09/2007 16:00
(Cooling above)
Instrumentation section: CS1
Condition: Transient Pattern Unit: °C

Height (cm)	0	15	45	60	90	110	120		
154				13.8		14.0		154	Top
135		16.4	16.7	20.1	22.4	22.5		135	
115		17.6		20.5	22.6	22.6		115	
95			18.1	20.1	22.3	22.6		95	
75		19.7		19.5	20.9	21.6		75	
55		20.3	18.6	19.4	21.3	20.7		55	
35		20.7	19.0	19.3	21.0	21.6		35	
15		21.4	19.7	19.8	21.4	21.9		15	
0				22.7		22.7		0	Bottom
	0	15	45	60	90	110	120		

Diameter (cm)

Test No. 15 Top-To-Bottom **ΔT=10°C (B33-T23)**

Recorded at: 08/09/2007 2:00 (10h)

Test started at: 07/09/2007 16:00

(Cooling above)

Instrumentation section: CS1

Condition: Transient Pattern Unit: °C

Height (cm)	0	15	45	60	90	110	120	
154				13.8		13.9		154 Top
135		15.8	17.0	20.0	22.1	22.3		135
115		17.0		20.4	22.4	22.3		115
95			18.1	20.0	22.1	22.2		95
75		19.3		19.5	20.7	21.3		75
55		20.0	18.4	19.2	21.1	20.5		55
35		20.6	18.8	19.1	20.8	21.5		35
15		21.3	19.6	19.6	21.3	21.8		15
0				22.7		22.7		0 Bottom
	0	15	45	60	90	110	120	

Diameter (cm)

Test No. 15 Top-To-Bottom **ΔT=10°C (B33-T23)**

Recorded at: 08/09/2007 4:00 (12h)

Test started at: 07/09/2007 16:00

(Cooling above)

Instrumentation section: CS1

Condition: Transient Pattern Unit: °C

Height (cm)	0	15	45	60	90	110	120	
154				13.7		13.9		154 Top
135		15.5	17.1	20.0	22.0	22.2		135
115		16.7		20.4	22.3	22.1		115
95			18.1	19.8	21.9	22.1		95
75		19.0		19.4	20.6	21.3		75
55		19.8	18.3	19.0	21.0	20.5		55
35		20.4	18.7	19.0	20.7	21.4		35
15		21.1	19.4	19.4	21.3	21.8		15
0				22.7		22.8		0 Bottom
	0	15	45	60	90	110	120	

Diameter (cm)

Test No. 15 Top-To-Bottom **ΔT=10°C (B33-T23)**

Recorded at: 08/09/2007 16:00 (24h)

Test started at: 07/09/2007 16:00

(Cooling above)

Instrumentation section: CS1

Condition: Transient Pattern Unit: °C

Height (cm)	0	15	45	60	90	110	120		
154				13.8		13.8		154	Top
135		15.0	17.6	19.9	21.6	21.6		135	
115		15.8		20.2	21.9	21.6		115	
95			18.2	19.8	21.6	21.6		95	
75		17.5		19.2	20.3	20.8		75	
55		18.5	17.9	18.7	20.6	20.1		55	
35		19.5	18.1	18.6	20.4	21.2		35	
15		20.6	18.8	18.8	20.8	21.7		15	
0				22.6		22.6		0	Bottom
	0	15	45	60	90	110	120		

Diameter (cm)

Test No. 15 Top-To-Bottom **ΔT=10°C (B33-T23)**

Recorded at: 09/09/2007 4:00 (36h)

Test started at: 07/09/2007 16:00

(Cooling above)

Instrumentation section: CS1

Condition: Transient Pattern Unit: °C

Height (cm)	0	15	45	60	90	110	120		
154				13.7		13.7		154	Top
135		15.0	17.6	19.9	21.5	21.4		135	
115		15.7		20.1	21.8	21.4		115	
95			18.2	19.7	21.4	21.3		95	
75		17.0		19.1	20.2	20.6		75	
55		17.7	17.7	18.5	20.5	20.0		55	
35		18.8	17.8	18.3	20.1	21.1		35	
15		20.1	18.4	18.5	20.6	21.6		15	
0				22.4		22.6		0	Bottom
	0	15	45	60	90	110	120		

Diameter (cm)

Test No. 15 Top-To-Bottom **ΔT=10°C (B33-T23)**

Recorded at: 09/09/2007 15:00 (47h)

Test started at: 07/09/2007 16:00

(Cooling above)

Instrumentation section: CS1

Condition: Steady State Unit: °C

Height (cm)	0	15	45	60	90	110	120	
154				13.7		13.8		154 Top
135		14.9	17.6	19.7	21.3	21.3		135
115		15.7		20.0	21.6	21.2		115
95			18.2	19.5	21.3	21.2		95
75		16.7		19.0	20.1	20.6		75
55		17.3	17.6	18.4	20.4	20.0		55
35		18.2	17.7	18.1	20.0	21.1		35
15		19.6	18.2	18.4	20.5	21.7		15
0				22.5		22.6		0 Bottom
	0	15	45	60	90	110	120	

Diameter (cm)

Test No. 16 Top-To-Bottom **ΔT=20°C (B30-T10)**

Recorded at: 15/05/2007 8:00

Test started at: 09/05/2007 9:10

(Cooling above; continued from Test No. 18)

Instrumentation section: CS1

Condition: Steady State Unit: °C

Height (cm)	0	15	45	60	90	110	120		
154				12.4		12.5		154	Top
135		13.2	20.6	22.7	23.7	23.6		135	
115		14.5		22.8	24.1	23.9		115	
95			21.0	22.5	24.0	24.5		95	
75		15.2		21.5	23.3	24.6		75	
55		15.4	19.1	20.4	23.6	24.5		55	
35		15.7	18.4	19.5	22.4	25.8		35	
15		16.2	17.9	19.2	22.3	26.6		15	
0				27.8		27.4		0	Bottom
	0	15	45	60	90	110	120		

Diameter (cm)

Test No. 17 Top-To-Bottom **ΔT=30°C (B40-T10)**

Recorded at: 02/05/2007 8:00

Test started at: 26/04/2007 9:45

(Cooling above)

Instrumentation section: CS1

Condition: Steady State Unit: °C

Height (cm)	0	15	45	60	90	110	120		
154				13.5		14.4		154	Top
135		16.0	26.0	28.1	29.5	29.2		135	
115		17.9		27.7	29.6	29.5		115	
95			25.2	26.8	29.0	29.9		95	
75		17.6		24.7	27.4	30.2		75	
55		17.6	22.4	23.7	28.1	30.5		55	
35		17.8	21.2	22.3	25.9	32.2		35	
15		18.0	20.4	21.9	26.0	33.6		15	
0				36.2		35.7		0	Bottom
	0	15	45	60	90	110	120		

Diameter (cm)

Test No. 18 Top-To-Bottom **ΔT=40°C (B50-T10)**

Recorded at: 09/05/2007 3:30

Test started at: 02/05/2007 10:20

(Cooling above; continued from Test No. 17)

Instrumentation section: CS1

Condition: Steady State Unit: °C

Height (cm)	0	15	45	60	90	110	120		
154				15.6		16.1		154	Top
135		19.4	31.9	34.2	36.3	35.8		135	
115		21.4		33.2	35.9	36.2		115	
95			29.8	31.7	34.9	36.6		95	
75		19.9		28.7	32.3	36.9		75	
55		19.7	26.0	27.5	33.5	37.5		55	
35		19.7	24.4	25.7	30.5	39.6		35	
15		19.9	23.2	25.1	31.3	41.6		15	
0				44.4		43.5		0	Bottom
	0	15	45	60	90	110	120		

Diameter (cm)

Test No. 19 Top-To-Bottom **ΔT=40°C (B53-T13)**

Recorded at: 15/09/2007 13:30

Test started at: 14/09/2007 14:00

(Cooling above)

Instrumentation section: CS1

Condition: Steady State Unit: °C

Height (cm)	0	10	40	60	90	110	120	
154		15.8		17.2		19.0		154 Top
135		23.7	33.5	35.9	37.9	36.3		135
115		24.1	33.7	35.5	38.4	37.8		115
95		23.6	31.6	33.9	37.8	39.1		95
75		23.1	29.7	31.7	36.1	39.6		75
55		22.8	27.7	29.4	34.4	39.5		55
35		22.5	26.4	27.9	32.3	41.2		35
15		22.6	25.0	26.8	30.9	42.3		15
0				47.4		46.2		0 Bottom
	0	10	40	60	90	110	120	

A' Diameter (cm) A

Instrumentation section: CS2

Condition: Steady State Unit: °C

Height (cm)	0	20	40	60	80	100	120	
154								154 Top
124		31.9	35.4		36.2	34.4		124
93		30.6	32.8		34.0	32.5		93
62		28.5	29.6		31.7	30.7		62
31		26.5	26.9		30.9	29.9		31
0								0 Bottom
	0	20	40	60	80	100	120	

B Diameter (cm) B'

Test No.20 Top-To-Bottom **ΔT=10°C (B22.5-T12.5)**

Recorded at: 25/09/2007 15:30

Test started at: 23/09/2007 17:50

(Rotation check; cooling above)

Instrumentation section: CS1

Condition: Steady State Unit: °C

Height (cm)	0	10	40	60	90	110	120	Height (cm)	
154		13.3		14.1		14.3		154	Top
135		15.2	17.3	19.3	19.6	19.1		135	
115		16.1	17.8	19.0	19.6	19.1		115	
95		16.6	17.3	18.7	19.5	19.5		95	
75		16.7	16.9	18.1	19.0	19.4		75	
55		16.8	16.5	17.3	18.7	18.8		55	
35		17.2	16.5	17.0	18.5	20.0		35	
15		18.3	17.2	17.5	18.8	20.7		15	
0				21.7		21.9		0	Bottom
	0	10	40	60	90	110	120		
A'				Diameter (cm)				A	

Instrumentation section: CS2

Condition: Steady State Unit: °C

Height (cm)	0	20	40	60	80	100	120	Height (cm)	
154								154	Top
124		20.2	20.5		17.7	14.8		124	
93		19.6	19.5		17.4	15.7		93	
62		19.5	18.4		16.6	15.9		62	
31		19.9	17.9		16.3	16.4		31	
0								0	Bottom
	0	20	40	60	80	100	120		
B				Diameter (cm)				B'	

Test No.21 Top-To-Bottom **ΔT=40°C (B52.5-T12.5)**

Recorded at: 27/09/2007 12:30

Test started at: 25/09/2007 17:51

(Rotation check; continued from Test No. 20)

Instrumentation section: CS1

Condition: Steady State Unit: °C

Height (cm)	0	10	40	60	90	110	120	
154		15.7		19.4		19.9		154 Top
135		19.9	29.2	32.0	33.2	31.7		135
115		20.9	28.1	30.2	32.6	31.9		115
95		21.4	26.1	28.5	31.4	32.1		95
75		21.3	24.6	26.6	29.6	31.3		75
55		21.0	22.9	25.0	28.1	31.0		55
35		20.7	22.1	25.2	27.3	32.3		35
15		20.7	22.1	32.8	26.8	35.4		15
0				46.2		45.8		0 Bottom
	0	10	40	60	90	110	120	

A' Diameter (cm) A

Instrumentation section: CS2

Condition: Steady State Unit: °C

Height (cm)	0	20	40	60	80	100	120	
154								154 Top
124		32.5	33.8		29.4	20.2		124
93		30.9	30.6		26.5	20.9		93
62		30.3	27.7		23.9	20.3		62
31		32.9	26.8		21.9	19.8		31
0								0 Bottom
	0	20	40	60	80	100	120	

B Diameter (cm) B'

Test No. 22 Top-To-Bottom **ΔT=10°C (LB32-T22)**
Recorded at: 29/10/2007 16:10 (1h)
Test started at: 29/10/2007 15:08
(Localized heating below)
Instrumentation section: CS1
Condition: Transient Pattern Unit: °C

Height (cm)	0	10	40	60	90	110	120		
154		21.6		21.5		21.7		154	Top
135		20.9	21.8	22.6	22.7	21.8		135	
115		20.9	21.7	22.5	22.7	22.1		115	
95		20.8	21.4	22.3	22.5	22.1		95	
75		20.7	21.2	22.0	22.1	21.8		75	
55		20.7	21.2	21.8	21.9	21.5		55	
35		20.7	21.9	23.1	22.3	21.5		35	
15		20.9	23.3	25.3	23.2	21.5		15	
0				28.3		22.0		0	Bottom
	0	10	40	60	90	110	120		

Diameter (cm)

Test No. 22 Top-To-Bottom **ΔT=10°C (LB32-T22)**
Recorded at: 29/10/2007 17:10 (2h)
Test started at: 29/10/2007 15:08
(Localized heating below)
Instrumentation section: CS1
Condition: Transient Pattern Unit: °C

Height (cm)	0	10	40	60	90	110	120		
154		21.8		21.8		21.9		154	Top
135		21.1	22.2	23.0	22.9	22.0		135	
115		21.0	22.3	23.2	23.1	22.3		115	
95		21.0	22.2	23.6	23.2	22.4		95	
75		20.9	22.2	23.8	23.1	22.2		75	
55		20.9	22.6	24.5	23.2	21.8		55	
35		20.9	23.2	25.6	23.4	21.7		35	
15		21.0	23.9	27.1	23.7	21.7		15	
0				29.6		22.3		0	Bottom
	0	10	40	60	90	110	120		

Diameter (cm)

Test No. 22 Top-To-Bottom **ΔT=10°C (LB32-T22)**

Recorded at: 29/10/2007 19:10 (4h)

Test started at: 29/10/2007 15:08

(Localized heating below)

Instrumentation section: CS1

Condition: Transient Pattern Unit: °C

Height (cm)	0	10	40	60	90	110	120		
154		21.9		22.1		22.0		154	Top
135		21.4	23.0	23.9	23.6	22.3		135	
115		21.4	23.1	24.0	23.8	22.7		115	
95		21.3	22.9	24.3	23.7	22.8		95	
75		21.3	22.8	24.3	23.6	22.5		75	
55		21.1	23.1	25.0	23.5	22.1		55	
35		21.1	23.5	25.9	23.7	22.0		35	
15		21.3	24.1	27.5	23.9	21.9		15	
0				30.1		22.4		0	Bottom
	0	10	40	60	90	110	120		

Diameter (cm)

Test No. 22 Top-To-Bottom **ΔT=10°C (LB32-T22)**

Recorded at: 30/10/2007 3:10 (12h)

Test started at: 29/10/2007 15:08

(Localized heating below)

Instrumentation section: CS1

Condition: Transient Pattern Unit: °C

Height (cm)	0	10	40	60	90	110	120		
154		21.9		22.1		22.0		154	Top
135		21.4	23.0	23.9	23.6	22.3		135	
115		21.4	23.1	24.0	23.8	22.7		115	
95		21.3	22.9	24.3	23.7	22.8		95	
75		21.3	22.8	24.3	23.6	22.5		75	
55		21.1	23.1	25.0	23.5	22.1		55	
35		21.1	23.5	25.9	23.7	22.0		35	
15		21.3	24.1	27.5	23.9	21.9		15	
0				30.1		22.4		0	Bottom
	0	10	40	60	90	110	120		

Diameter (cm)

Test No. 22 Top-To-Bottom **ΔT=10°C (LB32-T22)**
Recorded at: 30/10/2007 15:10 (24h)
Test started at: 29/10/2007 15:08
(Localized heating below)
Instrumentation section: CS1
Condition: Transient Pattern Unit: °C

Height (cm)	0	10	40	60	90	110	120	
154		22.0		22.2		22.1		154 Top
135		22.0	23.7	24.6	24.2	22.9		135
115		22.3	23.8	24.8	24.6	23.4		115
95		22.3	23.6	24.9	24.5	23.6		95
75		22.3	23.6	24.9	24.4	23.5		75
55		22.2	23.8	25.4	24.3	23.1		55
35		22.1	24.3	26.3	24.3	22.9		35
15		22.2	24.9	27.8	24.5	22.7		15
0				30.3		22.7		0 Bottom
	0	10	40	60	90	110	120	

Diameter (cm)

Test No. 22 Top-To-Bottom **ΔT=10°C (LB32-T22)**
Recorded at: 31/10/2007 17:10 (50h)
Test started at: 29/10/2007 15:08
(Localized heating below)
Instrumentation section: CS1
Condition: Steady State Unit: °C

Height (cm)	0	10	40	60	90	110	120	
154		22.0		22.1		22.2		154 Top
135		22.2	23.7	24.7	24.5	23.1		135
115		22.5	23.9	25.0	24.8	23.6		115
95		22.5	23.8	25.1	24.7	23.9		95
75		22.5	23.7	25.1	24.6	23.8		75
55		22.5	24.0	25.5	24.5	23.4		55
35		22.5	24.5	26.5	24.5	23.2		35
15		22.6	25.1	27.9	24.7	22.9		15
0				30.4		22.7		0 Bottom
	0	10	40	60	90	110	120	

Diameter (cm)

Test No.22 Top-To-Bottom **ΔT=10°C (LB32-T22)**

Recorded at: 01/11/2007 19:40

Test started at: 29/10/2007 15:08

(Localized heating below)

Instrumentation section: CS1

Condition: Steady State Unit: °C

Height (cm)	0	10	40	60	90	110	120		
154		21.9		22.3		22.2		154	Top
135		22.3	23.8	24.9	24.6	23.2		135	
115		22.6	24.0	25.0	24.9	23.8		115	
95		22.6	23.8	25.2	24.9	24.0		95	
75		22.6	23.8	25.2	24.7	23.8		75	
55		22.6	24.1	25.6	24.6	23.5		55	
35		22.7	24.6	26.5	24.7	23.3		35	
15		22.8	25.2	27.9	24.8	23.0		15	
0				30.4		22.6		0	Bottom
	0	10	40	60	90	110	120		
A'	Diameter (cm)							A	

Instrumentation section: CS2

Condition: Steady State Unit: °C

Height (cm)	0	20	40	60	80	100	120		
154								154	Top
124		24.6	25.5		24.0	22.4		124	
93		24.8	25.5		24.0	22.6		93	
62		24.0	25.2		24.1	22.5		62	
31		23.6	25.9		24.7	22.5		31	
0								0	Bottom
	0	20	40	60	80	100	120		
B	Diameter (cm)							B'	

Test No.23 Top-To-Bottom **ΔT=20°C (LB42-T22)**

Recorded at: 03/11/2007 23:00

Test started at: 01/11/2007 19:45

(Localized heating below; continued from Test No. 22)

Instrumentation section: CS1

Condition: Steady State Unit: °C

Height (cm)	0	10	40	60	90	110	120	Height (cm)	
154		22.1		22.9		22.5		154	Top
135		23.3	26.7	28.1	27.1	24.5		135	
115		24.0	27.1	28.5	27.5	25.5		115	
95		24.2	26.8	29.1	27.6	25.9		95	
75		24.2	26.8	29.3	27.5	25.9		75	
55		24.3	27.2	30.6	27.3	25.4		55	
35		24.2	27.7	32.0	27.0	25.0		35	
15		24.3	28.0	34.3	26.6	24.4		15	
0				38.4		23.5		0	Bottom
	0	10	40	60	90	110	120		

A' Diameter (cm) A

Instrumentation section: CS2

Condition: Steady State Unit: °C

Height (cm)	0	20	40	60	80	100	120	Height (cm)	
154								154	Top
124		26.2	28.4		27.1	23.7		124	
93		26.9	28.9		27.2	24.2		93	
62		26.3	29.2		27.3	24.2		62	
31		25.4	29.7		27.7	24.1		31	
0								0	Bottom
	0	20	40	60	80	100	120		

B Diameter (cm) B'

Test No.24 Top-To-Bottom **ΔT=30°C (LB52-T22)**

Recorded at: 05/11/2007 21:30

Test started at: 03/11/2007 23:02

(Localized heating below; continued from Test No. 23)

Instrumentation section: CS1

Condition: Steady State Unit: °C

Height (cm)	0	10	40	60	90	110	120		
154		22.5		23.8		22.8		154	Top
135		25.0	30.3	31.7	29.6	25.4		135	
115		25.8	30.5	32.5	29.9	26.5		115	
95		26.0	30.1	33.3	29.8	27.2		95	
75		26.1	30.0	33.8	29.8	27.4		75	
55		26.0	30.6	35.7	29.3	26.9		55	
35		25.9	31.0	37.7	28.7	26.4		35	
15		26.1	31.1	41.0	28.0	25.7		15	
0				46.2		24.3		0	Bottom
	0	10	40	60	90	110	120		
A'				Diameter (cm)				A	

Instrumentation section: CS2

Condition: Steady State Unit: °C

Height (cm)	0	20	40	60	80	100	120		
154								154	Top
124		26.8	31.3		30.6	25.6		124	
93		28.0	31.9		30.7	26.1		93	
62		27.8	32.3		30.6	26.0		62	
31		27.0	32.5		30.8	25.8		31	
0								0	Bottom
	0	20	40	60	80	100	120		
B				Diameter (cm)				B'	

Test No. 25 Top-To-Bottom **ΔT=60°C (LB63-T3)**

Recorded at: 01/12/2007 15:30

Test started at: 30/11/2007 11:24

(Localized heating below)

Instrumentation section: CS1

Condition: Steady State Unit: °C

Height (cm)	0	10	40	60	90	110	120		
154		6.2		10.1		8.1		154	Top
135		15.4	24.7	27.0	24.2	19.4		135	
115		15.8	23.5	27.8	23.7	20.9		115	
95		16.0	21.3	28.9	22.9	20.9		95	
75		16.3	20.0	29.1	21.9	20.0		75	
55		16.5	19.8	32.0	20.9	19.0		55	
35		16.8	20.0	34.1	20.3	18.4		35	
15		17.3	20.2	39.3	19.2	17.1		15	
0				51.2		8.8		0	Bottom
	0	10	40	60	90	110	120		
A'				Diameter (cm)				A	

Instrumentation section: CS2

Condition: Steady State Unit: °C

Height (cm)	0	20	40	60	80	100	120		
154								154	Top
124		22.9	26.7		24.2	15.0		124	
93		22.6	27.9		21.7	15.2		93	
62		21.1	29.7		19.6	15.5		62	
31		19.6	30.4		19.3	15.8		31	
0								0	Bottom
	0	20	40	60	80	100	120		
B				Diameter (cm)				B'	

Test No. 26 Top-To-Bottom **ΔT=10°C (B20.5-LT10.5)**
Recorded at: 05/10/2007 23:00 (1h)
Test started at: 05/10/2007 22:00
(Localized cooling above)
Instrumentation section: CS1
Condition: Transient Pattern Unit: °C

Height (cm)	0	10	40	60	90	110	120		
154		19.9		17.1		20.5		154	Top
135		20.1	20.4	21.4	21.7	21.0		135	
115		20.1	20.9	21.7	21.9	21.2		115	
95		20.1	20.7	21.6	21.7	21.3		95	
75		20.1	20.5	21.3	21.4	21.0		75	
55		20.0	20.3	20.7	21.0	20.7		55	
35		20.1	20.3	20.5	20.9	20.8		35	
15		20.2	20.4	20.5	21.0	20.9		15	
0				20.5		20.6		0	Bottom
	0	10	40	60	90	110	120		

Diameter (cm)

Test No. 26 Top-To-Bottom **ΔT=10°C (B20.5-LT10.5)**
Recorded at: 06/10/2007 0:00 (2h)
Test started at: 05/10/2007 22:00
(Localized cooling above)
Instrumentation section: CS1
Condition: Transient Pattern Unit: °C

Height (cm)	0	10	40	60	90	110	120		
154		19.6		13.5		20.5		154	Top
135		19.8	17.7	19.9	21.5	21.1		135	
115		19.8	19.3	20.8	21.6	21.2		115	
95		19.9	19.9	20.9	21.6	21.3		95	
75		20.0	20.3	21.0	21.2	21.0		75	
55		20.0	20.2	20.6	20.9	20.8		55	
35		20.0	20.3	20.5	20.8	20.8		35	
15		20.2	20.4	20.5	21.0	20.9		15	
0				20.6		20.6		0	Bottom
	0	10	40	60	90	110	120		

Diameter (cm)

Test No. 26 Top-To-Bottom **ΔT=10°C (B20.5-LT10.5)**
Recorded at: 06/10/2007 2:00 (4h)
Test started at: 05/10/2007 22:00
(Localized cooling above)
Instrumentation section: CS1
Condition: Transient Pattern Unit: °C

Height (cm)	0	10	40	60	90	110	120		
154		19.6		12.7		20.5		154	Top
135		19.7	17.0	19.2	21.2	21.1		135	
115		19.6	18.2	19.9	21.2	21.1		115	
95		19.5	18.7	19.7	21.1	21.1		95	
75		19.7	18.8	19.8	20.6	20.8		75	
55		19.7	19.1	19.5	20.4	20.6		55	
35		19.9	19.5	19.7	20.4	20.7		35	
15		20.1	20.0	20.1	20.7	20.9		15	
0				20.7		20.6		0	Bottom
	0	10	40	60	90	110	120		

Diameter (cm)

Test No. 26 Top-To-Bottom **ΔT=10°C (B20.5-LT10.5)**
Recorded at: 06/10/2007 10:00 (12h)
Test started at: 05/10/2007 22:00
(Localized cooling above)
Instrumentation section: CS1
Condition: Transient Pattern Unit: °C

Height (cm)	0	10	40	60	90	110	120		
154		19.5		12.6		20.4		154	Top
135		19.5	16.8	18.8	21.0	20.9		135	
115		19.4	18.0	19.6	21.0	20.9		115	
95		19.3	18.4	19.5	20.8	20.8		95	
75		19.4	18.6	19.6	20.4	20.5		75	
55		19.4	18.8	19.2	20.1	20.3		55	
35		19.7	19.2	19.3	20.2	20.5		35	
15		20.1	19.8	19.9	20.5	20.7		15	
0				20.6		20.6		0	Bottom
	0	10	40	60	90	110	120		

Diameter (cm)

Test No. 26 Top-To-Bottom **ΔT=10°C (B20.5-LT10.5)**

Recorded at: 06/10/2007 22:00 (24h)

Test started at: 05/10/2007 22:00

(Localized cooling above)

Instrumentation section: CS1

Condition: Transient Pattern Unit: °C

Height (cm)	0	10	40	60	90	110	120		
154		19.5		12.4		20.4		154	Top
135		19.4	16.7	18.8	20.9	20.9		135	
115		19.3	17.9	19.5	20.9	20.8		115	
95		19.1	18.3	19.4	20.7	20.7		95	
75		19.1	18.5	19.5	20.3	20.4		75	
55		19.2	18.7	19.1	20.0	20.2		55	
35		19.5	19.0	19.2	20.1	20.4		35	
15		19.9	19.7	19.7	20.5	20.7		15	
0				20.5		20.6		0	Bottom
	0	10	40	60	90	110	120		

Diameter (cm)

Test No. 26 Top-To-Bottom **ΔT=10°C (B20.5-LT10.5)**

Recorded at: 07/10/2007 15:00 (41h)

Test started at: 05/10/2007 22:00

(Localized cooling above)

Instrumentation section: CS1

Condition: Steady State Unit: °C

Height (cm)	0	10	40	60	90	110	120		
154		19.4		12.5		20.4		154	Top
135		19.4	16.7	18.8	20.9	20.8		135	
115		19.3	18.0	19.6	20.8	20.7		115	
95		19.1	18.3	19.4	20.7	20.6		95	
75		19.0	18.5	19.5	20.3	20.3		75	
55		19.2	18.6	19.1	20.0	20.2		55	
35		19.4	19.0	19.2	20.0	20.4		35	
15		19.8	19.6	19.7	20.4	20.6		15	
0				20.5		20.6		0	Bottom
	0	10	40	60	90	110	120		

Diameter (cm)

Test No.26 Top-To-Bottom **ΔT=10°C (B20.5-LT10.5)**

Recorded at: 07/10/2007 15:30

Test started at: 05/10/2007 22:00

(Localized cooling above)

Instrumentation section: CS1

Condition: Steady State Unit: °C

Height (cm)	0	10	40	60	90	110	120		
154		19.6		12.3		20.4		154	Top
135		19.4	16.8	18.9	20.9	20.9		135	
115		19.2	18.0	19.6	20.9	20.4		115	
95		19.1	18.4	19.4	20.6	20.6		95	
75		19.1	18.5	19.5	20.2	20.4		75	
55		19.2	18.7	19.0	20.0	20.2		55	
35		19.4	19.1	19.2	20.0	20.3		35	
15		19.8	19.7	19.7	20.4	20.7		15	
0				20.6		20.6		0	Bottom
	0	10	40	60	90	110	120		

A' Diameter (cm) A

Instrumentation section: CS2

Condition: Steady State Unit: °C

Height (cm)	0	20	40	60	80	100	120		
154								154	Top
124		21.5	21.2		17.0	18.9		124	
93		21.0	20.7		18.2	18.7		93	
62		20.1	19.8		18.5	18.9		62	
31		20.1	19.7		19.1	19.5		31	
0								0	Bottom
	0	20	40	60	80	100	120		

B Diameter (cm) B'

Test No. 27 Top-To-Bottom **ΔT=15°C (B20.5-LT5.5)**

Recorded at: 09/10/2007 13:25

Test started at: 07/10/2007 15:47

(Localized cooling above; continued from Test No. 26)

Instrumentation section: CS1

Condition: Steady State Unit: °C

Height (cm)	0	10	40	60	90	110	120		
154		19.1		8.7		20.3		154	Top
135		18.9	14.7	17.0	20.2	20.5		135	
115		18.5	16.0	18.0	20.0	20.1		115	
95		18.3	16.5	17.7	19.7	19.9		95	
75		18.2	16.6	17.7	19.2	19.6		75	
55		18.3	16.8	17.1	18.7	19.5		55	
35		18.7	17.1	17.1	18.7	19.8		35	
15		19.3	17.9	17.7	19.0	20.2		15	
0				20.4		20.5		0	Bottom
	0	10	40	60	90	110	120		

A' Diameter (cm) A

Instrumentation section: CS2

Condition: Steady State Unit: °C

Height (cm)	0	20	40	60	80	100	120		
154								154	Top
124		20.8	20.3		14.5	18.4		124	
93		20.1	19.5		16.0	17.8		93	
62		19.4	18.4		16.4	17.7		62	
31		19.5	18.1		17.0	18.5		31	
0								0	Bottom
	0	20	40	60	80	100	120		

B Diameter (cm) B'

Test No. 28 Top-To-Bottom **ΔT=20°C (B21-LT1)**

Recorded at: 10/10/2007 21:00

Test started at: 09/10/2007 13:26

(Localized cooling above; continued from Test No. 27)

Instrumentation section: CS1

Condition: Steady State Unit: °C

Height (cm)	0	10	40	60	90	110	120		
154		18.8		6.4		20.2		154	Top
135		18.7	13.6	15.8	19.8	20.2		135	
115		18.2	14.8	16.9	19.6	19.7		115	
95		17.8	15.4	16.7	19.2	19.5		95	
75		17.8	15.5	16.7	18.7	19.2		75	
55		17.9	15.7	15.9	18.1	19.1		55	
35		18.3	16.0	15.9	17.9	19.5		35	
15		18.9	16.8	16.5	18.1	19.9		15	
0				20.2		20.4		0	Bottom
	0	10	40	60	90	110	120		
A'				Diameter (cm)				A	

Instrumentation section: CS2

Condition: Steady State Unit: °C

Height (cm)	0	20	40	60	80	100	120		
154								154	Top
124		20.4	19.8		13.2	18.1		124	
93		19.6	18.9		14.7	17.4		93	
62		18.9	17.7		15.2	17.3		62	
31		19.0	17.1		15.9	18.1		31	
0								0	Bottom
	0	20	40	60	80	100	120		
B				Diameter (cm)				B'	

Conduction Using Styrofoam Chips in Test Tank

Test No. 29 Top-To-Bottom **ΔT=20°C (B23-T43)**

Recorded at: 27/11/2007 17:00

Test started at: 24/11/2007 16:45

(Heating above)

Instrumentation section: CS1

Condition: Steady State Unit: °C

Height (cm)	0	10	40	60	90	110	120		
154		41.4		40.8		40.9		154	Top
135		33.4	33.5	33.3	33.2	32.6		135	
115		30.4	30.4	30.1	30.5	30.2		115	
95		28.0	28.2	28.7	28.8	28.6		95	
75		26.4	26.6	27.1	27.2	26.8		75	
55		25.0	25.2	25.4	25.5	25.2		55	
35		24.1	24.2	24.3	24.5	24.1		35	
15		23.3	23.5	23.7	23.9	23.5		15	
0				23.0		22.9		0	Bottom
	0	10	40	60	90	110	120		

Diameter (cm)

Test No. 30 Top-To-Bottom **ΔT=20°C (B15-T35)**

Recorded at: 26/05/2007 15:00

Test started at: 24/05/2007 18:45

(Cooling below and heating above)

Instrumentation section: CS1

Condition: Steady State Unit: °C

Height (cm)	0	15	45	60	90	110	120		
154				33.1		33.1		154	Top
135		27.8	28.4	28.4	28.0	27.3		135	
115		25.7		25.4	25.7	25.1		115	
95			23.7	23.9	23.9	23.7		95	
75		22.3		22.0	21.1	22.1		75	
55		21.1	20.9	21.0	22.4	20.3		55	
35		19.7	19.6	19.6	19.8	19.9		35	
15		18.2	17.9	18.1	18.3	18.4		15	
0				15.6		15.6		0	Bottom
	0	15	45	60	90	110	120		

Diameter (cm)